(MDHS) just below the boundary with the Dunite-harzburgite suite with remarkable layering (DHSRL) and is frequently found in the central part of the area where Lugu i Batres and Ahu i Vetem are located.

(4) Visible Feature and Texture of Chromitite

Chromitite from this area is always olivine-chromitite composed of chromian spinel and olivine. Pyroxene, mostly of orthopyroxene, is absent or is rarely recognized in chromitite and its enclosing dunite. Olivine is generally serpentinized, however, sometimes relatively fresh one can be found in chromitite. Chromian spinel is relatively fresh and has been partly or completely altered to ferrit-chromite or magnetite.

The boundary between the dunite and the harzburgite is very sharp in the Dunite-harzburgite suite with remarkable layering. In the Massive dunite-harzburgite suite where chromitite occurs, however, pyroxene is recognized not only in harzburgite but also in the margin of the dunite ranging its widths of several centimeters to several meters.

The strike of dunite lenses by which chromitite is enclosed is concordant or discordant with the general structural trend, NW-SE, of the Shebenik ultrabasic massif as shown in Fig. 2-1-6 (2). At some outcrops, however, the long axis of elliptic nodules of chromian spinel in nodular chromitite is aligned concordant with the boundary between dunite and harzburgite (see Fig. 2-1-6(3)). This evidence suggests some influence of deformation after the concentration of chromitite in dunite.

2-1-4 Results of Laboratory Test

(1) Microscopic Observation

The results of microscopic observation of polished-thin sections and thin sections are given in Table 2-1-2. Twenty polished-thin sections were prepared, of which fifteen are for chromitite and five for dunite with relatively high concentrations of chromian spinel. Twenty eight rock thin sections were also prepared, of which eleven are for dunite, fifteen for harzburgite and two for pyroxenite.

[Harzburgite]

Harzburgite consists mainly of olivine and orthopyroxene and rarely with chromian spinel and clinopyroxene. Harzburgite usually has a protogranular texture and sometimes shows a porphyroclastic texture with foliation.

Olivine (1.0 - 0.1 mm in size) and pyroxene (orthopyroxene; 5.0 - 0.1 mm, clinopyroxene; 1.0 - less than 0.1 mm in size) are partly or totally replaced by serpentine (chrysotile/lizardite), which sometimes has a mesh texture. Kink band structure sometimes occurs in orthopyroxene.

Chromian spinel (1.0 - 0.1 mm in size) is reddish brown to opaque and is altered to ferrit-chromite or magnetite along cracks and grain boundaries but mostly remains unaltered in the core. Olivine, pyroxene and pargasite are found as inclusions in chromian spinel .

Talc, tremolite and carbonates are recognized as secondary minerals in harzburgite. Olivine and pyroxene are replaced by talc and tremolite. Chlorite is sometimes recognized as a decomposed product of talc and also found as a alteration halo around chromian spinel. Carbonates of calcite and dolomite are rarely found as veinlets filling small cracks.

[Dunite]

Dunite consists entirely of olivine and is accompanied by chromian spinel. The mode of

Table 2-1-2 Results of microscopic observation on polished-thin sections

No.	Sample No.	Rock type	primary minerals							secondary minerals										Note
			ol	opx	cpx	sp	par	pl	mi	ser	tc	chl	bru	mt	f.c	tre	ca	di	cl	
1	IM002Cr	Olivine chromitite	◎			○				◎	·	·								Olivine chromitite (orbicular texture)
2	IM002Du	Dunite	◎			△				◎				·						Relic fluid inclusion in olivine is rich
3	IM002Hz	Harzburgite	◎	○	·	△				◎	·	·								Porphyroclastic texture
4	IM003Cr	Olivine chromitite	△			◎				△		△								Inclusions (altered)
5	IM003Du	Dunite	◎			△				◎										Strongly serpentinized
6	IM003Hz	Harzburgite	◎	○		△				◎	○	△				△				Strongly serpentinized
7	IM005Cr	Chromitite	○			◎				△	△	·								Spinel has inclusion
8	IM005Du	Dunite	◎		·	△				◎										
9	IM005Hz	Harzburgite	◎	○	·	△				◎										
10	IM007Cr	Olivine chromitite	○			◎				○	△	△								brecciated
11	IM007Du	Dunite	◎		△	△				◎										Strongly serpentinized
12	IM007Hz	Harzburgite	◎	○	△	△				◎										
13	IM009Cr	Chromitite + Dunite	○			◎	·			○		△								Pargasite is inclusion in spinel
14	IM009Du	Dunite	◎		·	△				◎										
15	IM009Hz	opx poor harzburgite	◎	△		△				◎	·						·			Pyroxene is completely altered (dun. or wehr.?)
16	IM011Cr	Olivine chromitite	○	○		◎				○	△									
17	IM011Du	Dunite	◎			○				◎		·								Spinel rich dunite
18	IM011Hz	Harzburgite	◎	○	·	·				◎	○					·				
19	IM013Cr1	Olivine chromitite	△			◎				△		△								Brecciated
20	IM013Cr2	Olivine chromitite	△			◎				△		△								Brecciated and cracked
21	IM013Du	Dunite	◎			·				◎										
22	IM013Hz	Harzburgite	◎	○	·	·				◎										Porphyroclastic texture
23	IM014Cr1	Olivine chromitite	○			◎				○		△								Relatively fine grain
24	IM014Du1	Dunite	◎			△				◎				·						Spinel has inclusion
25	IM014Cr2	Olivine chromitite	○			◎				○		○								
26	IM014Du2	Dunite	◎			△				◎										Spinel is fine grain
27	IM014Hz	Harzburgite	◎	○	·	·				◎										Foliation; porphyroclastic texture
28	IM017Cr	Dunite (sp. rich)	◎			○				◎										Spinel concentration (seam form)
29	IM017Du	Dunite	◎		·	△				◎										It has spinel-rich seam
30	IM017Hz	Harzburgite	◎	○	·	·				◎										Protogranular texture
31	IM020Cr	Olivine chromitite	○			◎				◎										
32	IM020Px	Orthopyroxenite	·	◎	△	△				·	·					·				OPX is crushed and kinked
33	IM021Hz	Harzburgite	◎	○	△	△				◎										Porphyroclastic texture
34	IM022Du	Dunite	◎	·	·	△				◎										
35	IM023Du	Dunite	◎	·		△				◎										Relic fluid inclusion in olivine are relatively rich
36	IM023Hz	Harzburgite	◎	○	·	△				◎										
37	NN006Cr	Spinel-rich Dunite	◎			◎				◎		·								Anti-nodular texture, strongly serpentinized
38	NN006Du	Dunite	◎			△				◎		·								Strongly serpentinized
39	NN006Hz	Orthopyroxenite		◎		·				○	△					△				Porphyroclastic texture
40	NN008Hz	Harzburgite	◎	○	·	△				◎										Porphyroclastic texture
41	NN009Cr	Olivine chromitite	◎			◎				◎										Dunitic part is anti nodular-like texture
42	NN009Du	Dunite	◎			△				◎										
43	NN009Hz	Harzburgite	◎	○	·	△				◎	△									Protogranular texture
44	NN010Du	Harzburgite	◎	○	·	△				◎										Porphyroclastic texture
45	NN010Hz	Harzburgite	◎	○		△				◎										Relatively OPX-poor
46	NN011Hz	Harzburgite	◎	○	·	·				◎										

Legend; ◎,abundant; ○, common; △, minor; · rare

ol:olivine, opx:ortho pyroxene, cpx:clino pyroxene, sp:chromian spinel, par: pargasite, pl: plagioclase, mi:mica,
ser: serpentine (chrysotile/lizardite), tc: talc, chl: chlorite, bru: brucite, mt: magnetite,
f.t.: ferrit chromite, tre: tremolite, di: diopside, ca: carbonate, cl: clay minerals

chromian spinel is relatively variable, that is, scarcely with chromian spinel and resembling chromitite with the chromian spinel-mode of more than 20 %. Chromian spinel sometimes is concentrated as seams. Orthopyroxene and clinopyroxene are rarely associated with dunite.

Dunite usually has a protogranular texture. Olivine (1.0 to 0.1 mm in size) and pyroxene (orthopyroxene; 5.0 to 0.1 mm clinopyroxene; 1.0 to less than 0.1 mm in size) are usually replaced in part or all by serpentine (chrysotile/lizardite or antigorite), which sometimes has a mesh texture.

Chromian spinel (1.0 to 0.1 mm in size) is reddish brown to opaque and is altered to ferrit-chromite or magnetite along cracks and grain boundaries but mostly remains unaltered in the core. Olivine, pyroxene and pargasite are found as inclusions (less than 0.2 mm in size).

As mentioned above, there are two main strikes of dunite lenses, one is concordant and the other discordant with the general structural trend, NW-SE, of the Shebenik-Pogradec ultrabasic massif. A comparison of both types of dunite under microscope is as follows.

Samples for the comparison are taken from the outcrop of IM014 (see Fig. 2-1-6(2)) where they coexist. Some inclusions are found in chromian spinel of discordant dunite (IM014, Du 2). On the other hand, concordant dunite (IM014, Du 1) is fine- to medium-grained (1.0 to less than 0.1 mm in size) and lacks inclusions in spinel. These differences are very important for a discussion about the genesis of chromitite.

[Chromitite]

Chromitite consists mainly of olivine and chromian spinel. The mode of chromian spinel and olivine is quite variable even in one single polished-thin section. Some part has a lithology like dunite and other part like chromitite due to the small difference of a position at which the thin section was prepared. This characteristic is found frequently in nodular and banded ores. Orbicular structure is recognized in chromitite in addition to the other five ore-types of massive, nodular, anti-nodular, banded and disseminated ores observed in field.

All chromitites are of olivine chromitite. Olivine (5.0 to 0.1mm in size) is usually altered to serpentine (chrysotile/lizardite or antigorite). Some spinel and olivine which are free from alteration coexist together with serpentinized ones in single polished-thin sections of chromitite. This fact is important for discussing the genetic environment, especially regarding tectonic setting of chromitite.

Chlorite filling interstices between spinel grains is found in some chromitite with high mode of chromian spinel. Chromian spinel is often altered to ferrit-chromite or magnetite along cracks and grain boundaries. Spinel inclusions are sometimes found and many of them are replaced by chlorite or serpentine.

[Clinopyroxenite]

Clinopyroxenite occurs in the area in small scale. Two types of it are distinguished under the microscope . One is from a outcrop IM020 where clinopyroxenite occurs as a dike. Orthopyroxene is dominant and clinopyroxene is common in this clinopyroxenite. Small amounts of olivine and patch-like concentration of chromian spinel are also recognized in this rock. The other type is from that of NN060 where the mode of occurrence is unclear due to poor exposure. This clinopyroxenite consists mainly of orthopyroxene with a small amount of chromian spinel. Both types of clinopyroxenite have porphyroclastic texture. Serpentine, talc and tremolite are common as secondary minerals.

(2) Chemical analysis of rocks and ore samples

Twenty four elements were analyzed on harzburgite, dunite, chromitite and clinopyroxenite

Table 2-1-3 Results of chemical analysis of 24 elements for whole rock

No.	SAMPLE DESCRIPTION	Ag ppm	Al %	Ba ppm	Be ppm	Bi ppm	Ca %	Cd ppm	Co ppm	Cr ppm	Cu ppm	Fe %	K %	Mg %	Mn ppm	Mo ppm	Na %	Ni ppm	P ppm	Pb ppm	Sr ppm	Ti %	V ppm	W ppm	Zn ppm	Cr2O3 %
1	IM001Cr	–	–	–	–	–	–	–	–	–	–	–	–	–	–	–	–	–	–	–	–	–	–	–	–	55.7
2	IM002Cr	<.2	0.39	10	<.5	Intf*	0.06	<.5	33	>10000	24	1.92	<.01	10.55	415	Intf*	0.03	1380	100	<2	1	0.01	44	Intf*	50	37.4
3	IM002Du	<.2	0.12	<10	<.5	Intf*	0.07	<.5	73	530	<1	4.16	0.01	>15.00	700	<1	0.12	2300	Intf*	<2	<1	<.01	18	<10	22	–
4	IM002Hz	<.2	0.24	<10	<.5	Intf*	0.29	<.5	71	2060	18	4.34	<.01	>15.00	760	<1	0.05	1775	Intf*	<2	<1	<.01	35	<10	28	–
5	IM003Cr	<.2	0.88	<10	<.5	Intf*	0.15	<.5	44	>10000	4	2.6	<.01	6.41	410	Intf*	0.04	539	120	<2	1	<.01	113	Intf*	38	51.6
6	IM003Cr2	–	–	–	–	–	–	–	–	–	–	–	–	–	–	–	–	–	–	–	–	–	–	–	–	50
7	IM003Du	<.2	0.1	<10	<.5	Intf*	0.1	<.5	78	892	<1	4.48	<.01	>15.00	710	<1	0.07	1995	Intf*	<2	1	<.01	19	<10	26	–
8	IM003Hz	<.2	0.21	<10	<.5	Intf*	0.15	<.5	80	3060	<1	4.84	<.01	>15.00	780	<1	0.06	1880	Intf*	<2	1	<.01	34	<10	34	–
9	IM004Cr	–	–	–	–	–	–	–	–	–	–	–	–	–	–	–	–	–	–	–	–	–	–	–	–	51.8
10	IM005Cr	<.2	4.51	<10	<.5	Intf*	0.94	<.5	195	>10000	1	10.05	<.01	9.18	1140	Intf*	0.01	1045	390	<2	3	0.03	899	Intf*	276	52.6
11	IM005Du	<.2	0.1	<10	<.5	Intf*	0.11	<.5	80	720	<1	4.87	<.01	>15.00	745	<1	0.1	2180	Intf*	<2	3	<.01	19	<10	26	–
12	IM005Hz	<.2	0.28	<10	<.5	Intf*	0.19	<.5	82	8270	5	4.99	<.01	>15.00	845	<1	0.01	1925	Intf*	<2	3	<.01	55	<10	38	–
13	IM006Cr	–	–	–	–	–	–	–	–	–	–	–	–	–	–	–	–	–	–	–	–	–	–	–	–	30.3
14	IM007Cr	<.2	1.06	<10	<.5	Intf*	0.35	<.5	101	>10000	3	4.57	<.01	8.83	715	Intf*	0.01	1050	200	<2	<1	<.01	205	Intf*	108	49.7
15	IM007Du	<.2	0.06	<10	<.5	Intf*	0.11	<.5	76	786	<1	3.94	<.01	>15.00	620	<1	0.03	2200	Intf*	<2	1	<.01	18	<10	22	–
16	IM007Hz	<.2	0.17	<10	<.5	Intf*	0.26	<.5	83	2950	5	5.55	<.01	>15.00	910	<1	0.03	1945	Intf*	<2	3	<.01	35	<10	38	–
17	IM008Cr	–	–	–	–	–	–	–	–	–	–	–	–	–	–	–	–	–	–	–	–	–	–	–	–	32.2
18	IM009Cr	<.2	0.19	<10	<.5	Intf*	0.15	<.5	74	>10000	3	4.03	<.01	>15.00	605	Intf*	0.01	2390	Intf*	<2	2	<.01	39	Intf*	30	27.7
19	IM009Du	<.2	0.08	<10	<.5	Intf*	0.12	<.5	76	472	8	4.13	<.01	>15.00	645	<1	0.05	2430	Intf*	<2	3	<.01	17	<10	24	–
20	IM009Hz	<.2	0.11	<10	<.5	Intf*	0.14	<.5	75	753	16	4.55	<.01	>15.00	710	<1	0.03	1980	Intf*	<2	3	<.01	19	<10	28	–
21	IM010Cr	–	–	–	–	–	–	–	–	–	–	–	–	–	–	–	–	–	–	–	–	–	–	–	–	37.9
22	IM011Cr	<.2	1.5	10	<.5	Intf*	0.37	<.5	92	>10000	6	4.65	<.01	9.93	630	Intf*	0.06	1120	140	<2	6	<.01	249	Intf*	72	38.9
23	IM011Du	<.2	0.28	<10	<.5	Intf*	0.12	<.5	66	>10000	1	4.12	<.01	>15.00	620	Intf*	0.04	1940	Intf*	<2	3	<.01	39	Intf*	26	6.57
24	IM011Hz	<.2	0.14	<10	<.5	Intf*	0.1	<.5	78	2130	1	4.71	<.01	>15.00	730	<1	0.03	2130	Intf*	<2	1	<.01	21	<10	26	–
25	IM012Cr	–	–	–	–	–	–	–	–	–	–	–	–	–	–	–	–	–	–	–	–	–	–	–	–	12.5
26	IM013Cr	<.2	3.48	<10	<.5	Intf*	0.63	<.5	150	>10000	<1	6.96	<.01	7.82	855	Intf*	0.04	890	210	<2	1	0.01	486	Intf*	166	50.9
27	IM013Cr2	<.2	2.67	<10	<.5	Intf*	0.52	<.5	133	>10000	<1	6.6	<.01	6.45	905	Intf*	0.04	954	250	<2	<1	<.01	454	Intf*	220	47
28	IM013Du	<.2	0.16	<10	<.5	Intf*	0.12	<.5	76	5060	3	4.44	<.01	>15.00	680	<1	0.07	2050	Intf*	<2	<1	<.01	27	<10	30	–
29	IM013Hz	<.2	0.34	<10	<.5	Intf*	0.29	<.5	78	>10000	7	5.18	<.01	>15.00	830	Intf*	0.04	1940	Intf*	<2	<1	<.01	55	Intf*	44	–
30	IM014Cr1	<.2	1.78	<10	<.5	Intf*	0.45	<.5	109	>10000	<1	5	<.01	8.79	555	Intf*	0.04	1240	210	<2	<1	<.01	277	Intf*	76	50.3
31	IM014Du1	<.2	0.11	<10	<.5	Intf*	0.09	<.5	80	1745	1	4.94	<.01	>15.00	735	<1	0.05	2060	Intf*	<2	1	<.01	22	<10	34	–
32	IM014Cr2	<.2	2.45	<10	<.5	Intf*	0.51	<.5	154	>10000	<1	6.26	<.01	8.87	840	Intf*	0.04	845	200	<2	<1	<.01	405	Intf*	170	45.3
33	IM014Du2	<.2	0.14	<10	<.5	Intf*	0.1	<.5	71	3770	4	4.16	<.01	>15.00	620	<1	0.07	2410	Intf*	<2	1	<.01	23	<10	24	–
34	IM014Hz	<.2	0.29	<10	<.5	Intf*	0.26	<.5	68	7150	1	4.35	<.01	>15.00	710	<1	0.04	1690	Intf*	<2	<1	<.01	46	<10	34	–
35	IM015Cr	–	–	–	–	–	–	–	–	–	–	–	–	–	–	–	–	–	–	–	–	–	–	–	–	33.7
36	IM016Cr	–	–	–	–	–	–	–	–	–	–	–	–	–	–	–	–	–	–	–	–	–	–	–	–	17.7
37	IM017Cr	–	–	–	–	–	–	–	–	–	–	–	–	–	–	–	–	–	–	–	–	–	–	–	–	20.8
38	IM018Cr	–	–	–	–	–	–	–	–	–	–	–	–	–	–	–	–	–	–	–	–	–	–	–	–	27.6
39	IM020Cr	<.2	2.38	<10	<.5	Intf*	0.32	<.5	98	>10000	<1	4.66	<.01	9.84	560	Intf*	0.04	1295	100	<2	<1	<.01	280	Intf*	74	36
40	IM020Px	<.2	0.39	<10	<.5	Intf*	0.65	<.5	72	>10000	<1	5.05	<.01	>15.00	1105	Intf*	0.06	910	Intf*	<2	<1	<.01	104	Intf*	58	–
41	NN002Cr	<.2	0.77	<10	<.5	Intf*	0.25	<.5	77	>10000	<1	3.88	<.01	9.16	590	Intf*	0.03	895	80	<2	<1	<.01	183	Intf*	56	30.1
42	NN002Du	<.2	0.08	<10	<.5	Intf*	0.1	<.5	75	1715	1	4.28	<.01	>15.00	645	<1	0.02	2030	Intf*	<2	1	<.01	22	10	26	–
43	NN002Hz	<.2	0.14	<10	<.5	Intf*	0.2	<.5	73	5050	1	4.49	<.01	>15.00	720	<1	0.02	1810	Intf*	<2	4	<.01	34	<10	30	–
44	NN004Cr	–	–	–	–	–	–	–	–	–	–	–	–	–	–	–	–	–	–	–	–	–	–	–	–	37.5
45	NN005Cr	–	–	–	–	–	–	–	–	–	–	–	–	–	–	–	–	–	–	–	–	–	–	–	–	42.6
46	NN006Cr	<.2	1.06	<10	<.5	Intf*	0.21	<.5	98	>10000	<1	4.79	<.01	>15.00	740	Intf*	0.04	1940	Intf*	<2	<1	<.01	172	Intf*	58	28.4
47	NN006Du	<.2	0.22	<10	<.5	Intf*	0.22	<.5	72	902	3	3.99	0.04	>15.00	630	<1	0.09	2310	Intf*	<2	8	<.01	21	<10	26	–
48	NN006Hz	<.2	1.37	<10	<.5	Intf*	0.27	<.5	52	4420	<1	3.7	<.01	>15.00	840	<1	0.01	1230	Intf*	<2	4	<.01	46	<10	30	–
49	NN007Cr	–	–	–	–	–	–	–	–	–	–	–	–	–	–	–	–	–	–	–	–	–	–	–	–	25.4
50	NN009Cr	<.2	1.2	<10	<.5	Intf*	0.1	<.5	74	>10000	<1	3.8	<.01	9.2	540	Intf*	<.01	930	10	<2	3	<.01	184	Intf*	72	36.4
51	NN010Du	–	–	–	–	–	–	–	–	–	–	–	–	–	–	–	–	–	–	–	–	–	–	–	–	0.66
52	NN011Hz	<.2	0.31	<10	<.5	Intf*	0.41	<.5	76	1565	4	5.05	0.01	>15.00	830	<1	0.07	1850	Intf*	<2	<1	<.01	42	<10	34	–
53	N1005Cr1	–	–	–	–	–	–	–	–	–	–	–	–	–	–	–	–	–	–	–	–	–	–	–	–	34.1
	maximum	<.2	4.51	10	<.5	–	0.94	<.5	195	>10000	24	10.05	0.04	>15.00	1140	–	0.12	2430	–	–	8	0.03	899	–	276	55.7
	Average	–	0.804	–	–	–	0.257	–	84.95	–	–	4.71	–	–	719.5	–	–	1662	–	–	–	–	128.6	–	58.22	35.5
	minimum	<.2	0.06	<10	<.5	–	0.07	<.5	33	472	<1	1.92	<.01	6.41	410	–	<.01	539	–	–	<1	<.01	17	–	22	0.7
	Standard Dev.	–	1.064	–	–	–	0.194	–	30.19	–	–	1.282	–	–	153.9	–	–	546.8	–	–	–	–	183.1	–	58.12	14.0

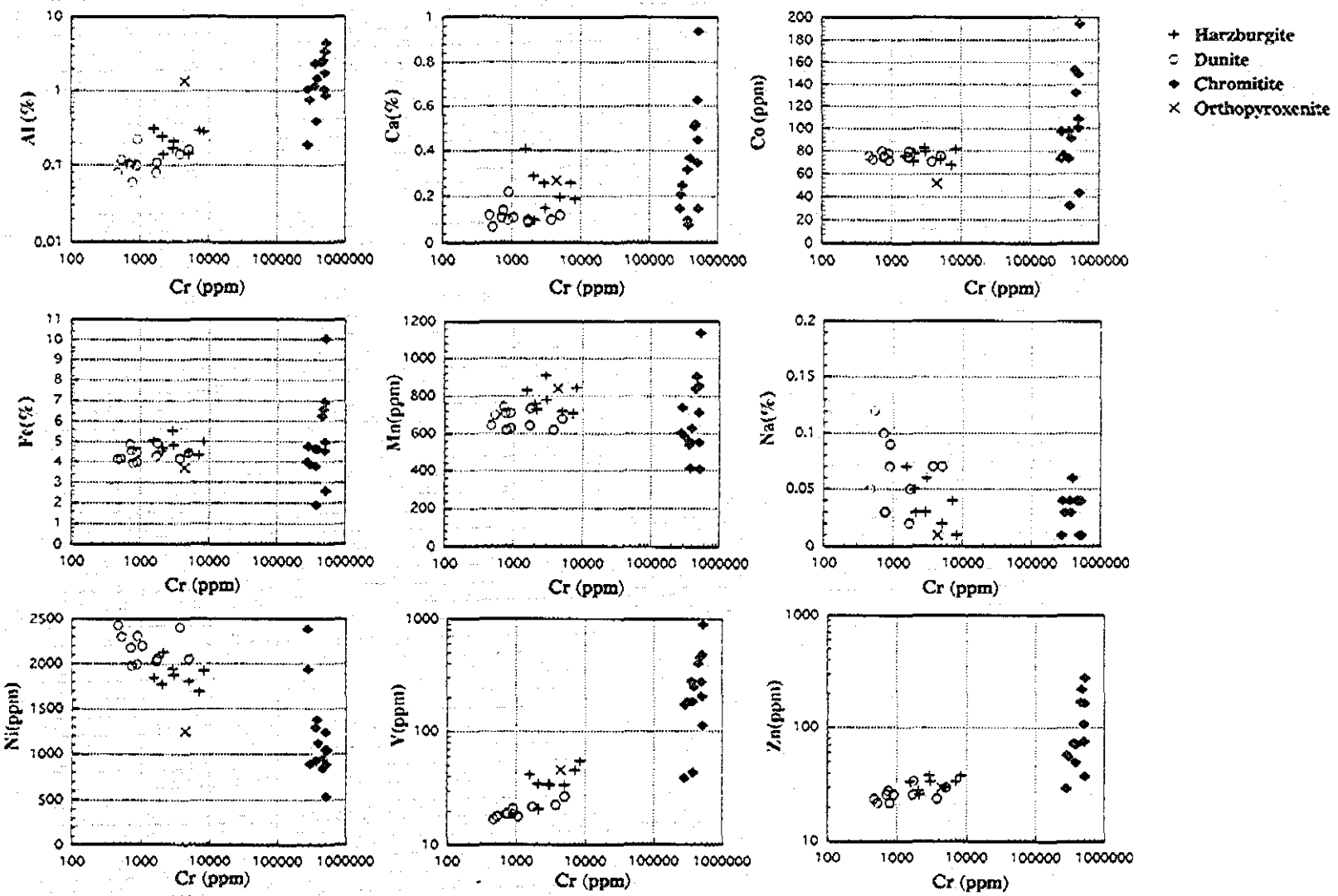

Figure 2-1-7 Variation diagrams of Al, Ca, Co, Fe, Mn, Na, Ni, V, Zn, and Cr contents

samples. They are Ag, Ba, Be, Bi, Cd, Co, Cu, Mn, Mo, Ni, Sr, V, Zn, Al, Ca, Fe, K, Mg, Na, Ti, Pb and Cr. The analytical results are shown in Table 2-1-3.

The values of eleven elements, i.e. Ba, Be, Bi, Cd, Cu, Mo, Sr, K, Mg, Ti and Pb are under the detection limits so that it is impossible to examine differences among lithofacies of harzburgite, dunite, chromitite and clinopyroxenite. Each rock contains characteristic values of Al, Ca, Co, Fe, Mn, Na, Ni, V, Zn and Cr. Values of each element are plotted in variation diagrams (Fig. 2-1-7) with the X axis of Cr and Y axis of other elements. The chemical characteristics of each rock-type are controlled by content ratios of chromian spinel, olivine, orthopyroxene and clinopyroxene.

Chromitite usually has a much larger value of Cr content, ranging from 12 to 56 % (average; 38 %), than dunite and harzburgite because chromitite consists mainly of chromian spinel. On the other hand, harzburgite shows a higher average content of Cr (3,665 ppm) than dunite (1,659 ppm). This may indicate that clinopyroxene contains larger quantities of Cr than olivine. This is also concordant with a difference in the clinopyroxene content ratio between dunite and harzburgite.

It is noteworthy that two samples of dunite from IM013 and IM014 have relatively higher Cr content than other dunite samples and the Cr content of these two samples is nearly equal to that of harzburgite. These high ratios of Cr content may be controlled by the mode of chromian spinel and clinopyroxene. In any case, the dunite which has a higher Cr content is one characteristic "lithology" (spinel-rich dunite or clinopyroxene-rich dunite) and may be a good indicator for chromitite exploration. The sampling points of IM013 and IM014 are at Lugu i Batres and Ahu i Vetem where many ore bodies of massive chromitite were recognized on the surface.

Content ratios of Al, Ca, Mn and V in each lithology show similar trends to that of Cr because orthopyroxene contains larger quantities of these elements than olivine.

On the other hand, the content ratio of Ni indicates a different manner from the other elements. The average Ni content of dunite (2,173 ppm) is higher than that of harzburgite (1,893 ppm) because olivine contains larger quantities of Ni than clinopyroxene. Dunite and harzburgite have their own range of chemical compositions which are easily read on Fig. 2-1-7.

There is little or no difference in Co, Fe and Zn content between dunite and harzburgite. This may indicate that orthopyroxene and olivine contain equal quantities of these elements.

(3) EPMA analysis of chromian spinel

The purpose of the EPMA analysis is to detect favorable host rocks for relatively large chromitite deposits by analyzing the chemical composition of chromian spinel. The following four indices are important EPMA anomalies which indicate some possibility for the existence of relatively large chromitite deposits.

1. Relatively low Cr# (Cr/(Cr+Al) atomic ratio, 0.4 to 0.6) of chromian spinel of harzburgite
2. Relatively high TiO_2 content of chromian spinel of harzburgite
3. Relatively high Fe^{3+}# (Fe^{3+}/(Cr+Al+Fe^{+3}) atomic ratio) of chromian spinel of harzburgite or dunite
4. Relatively high Cr# and low V_2O_3 content of chromian spinel of dunite or harzburgite

These four indices are based on the genetic model of podiform type chromitite, which has been recently proposed by Arai (1992), Arai and Yurimoto (1994 and 1995), Matsumoto et al. (1995) and Matsumoto (1996) etc. This model explains podiform chromitite genesis as follows. Interaction between harzburgite wall and primitive melt makes a secondary melt. Mixing of the secondary melt with a subsequently supplied primitive melt forms a concentration of chromian spinel. The model also indicates that a model for stratiform chromitite genesis proposed by Irvine (1975) could apply

basically to podiform chromitite. The first index mentioned above is based on the fact that Cr# of chromian spinel of harzburgite in relatively large chromitite deposits of the world usually show low values, ranging from 0.4 to 0.6. The indices from the second to the last indicate that a large amount of secondary melt are produced in the host rock by interaction with melt.

The test conditions for EPMA analysis are as follows:

-Test apparatus: Model JAX-733 (wavelength dispersion) of Nihondenshi Co., Ltd.
-Acc. Voltage: 15 kV
-X-ray angle: 40 Å
-Probe current: 12 nA (12×10^{-9}A)
-Probe diameter: 1 μ
-Elements tested: Cr, Al, Fe, Mg, Ti, Mn, V
-Standard sample: Chromite (Acoje Mine), $MnSiO_4$ (Mn-Olivine), V_2O_3, Al_2O_3, Fe_2O_3, MgO, TiO_2

The EPMA quantitative analysis was carried out on chromian spinels in chromitite and their host rocks, harzburgite and dunite. Analysis is performed only on unaltered core of chromian spinel grains. Twelve chromitite, fourteen dunite, sixteen harzburgite and two clinopyroxenite samples were tested by EPMA analysis.

The results of EPMA analysis are given in Table 2-1-4. Cr-Al-Fe^{3+} proportions of chromian spinel are shown in Fig. 2-1-8 and relationships between; Cr# and TiO_2content, Mg# and Cr#, Cr# and Fe^{3+}#, Cr# and V_2O_3 content are also shown in Figs. 2-1-9 to 2-1-10, Fig. 2-1-11 to 2-1-12, Fig. 2-1-13 to 2-1-14 and Fig. 2-1-15 to 2-1-16 respectively. The purpose of these diagrams is to examine differences in each characteristic between the Massive dunite-harzburgite suite and the Dunite-harzburgite suite with remarkable layering and between dunite, harzburgite and chromitite.

a) Cr#; Cr/(Cr+Al) atomic ratio

The Cr# of spinel varies from 0.55 to 0.85 and is different in harzburgite, dunite and chromitite as shown in Fig. 2-1-9 and Fig. 2-1-10. The Cr# of spinel in chromitite is relatively high, ranging from 0.759 to 0.855 with an average of 0.809. On the other hand, the Cr# of spinel in harzburgite is varies from 0.559 to 0.823 and the average is 0.697. The Cr# of spinel in dunite is lower than that in chromitite, ranging from 0.707 to 0.833 with an average of 0.762.

The Cr# of spinel in the harzburgite surrounding relatively large scale chromitite deposits of the world is usually from 0.4 to 0.6 (Arai, 1994). This evidence shows that a harzburgite which has chromian spinel with a lower Cr# is a more suitable host for large-scale podiform chromitite. Therefore, a harzburgite with a Cr# lower than 0.6 is considered as an EPMA anomaly in this report.

Harzburgite samples with Cr# of spinel lower than 0.6 were obtained from IM002 and NN008 which are located in the Massive dunite-harzburgite suite.

b) TiO_2 wt%

The TiO_2 content of spinel is lower than 0.2 wt% in all samples as shown in Fig. 2-1-9. The content of spinels in dunite and chromitite, are higher than that in harzburgite and the average is 0.082 in chromitite, 0.080 in dunite and 0.033 in harzburgite. It is easy to distinguish dunite and chromitite from harzburgite by consideration of the TiO_2 content (Fig. 2-1-9).

Differences in TiO_2 content among these three kinds of rock are usually recognized in the ultramafic rocks from other areas (for example Arai, 1994). Matsumoto et al. (1995) and Matsumoto (1996) indicate that a harzburgite with relatively high TiO_2 content may be more strongly influenced by the melt-rock interaction, that is, mineralization.

A harzburgite with TiO_2 content higher than 0.05 wt.% was defined as an EPMA anomaly in

Table 2-1-4 Results of EPMA analysis

No.	Sample No.	Rock type	TiO2	Al2O3	Cr2O3	FeO*	V2O3	MnO	MgO	Total	Ti	Al	Cr	Fe	V	Mn	Mg	total	Fe2+	Fe3+	Cr#	Mg#	Fe3+#
1	IM002 Cr	Ol-chromitite	0.12	8.96	62.36	13.67	0.09	0.21	15.02	100.42	0.003	0.337	1.573	0.365	0.002	0.006	0.714	3.000	0.283	0.082	0.824	0.718	0.0412
2	IM002 Du	Dunite	0.10	12.41	57.64	18.02	0.15	0.33	11.24	99.89	0.003	0.474	1.478	0.489	0.004	0.009	0.544	3.000	0.450	0.039	0.757	0.547	0.0195
3	IM002 Hz	Harzburgite	0.03	21.55	46.95	18.01	0.29	0.30	11.77	98.91	0.001	0.797	1.164	0.473	0.007	0.008	0.550	3.000	0.442	0.030	0.594	0.554	0.0151
4	IM003 Cr	Ol-chromitite	0.07	12.18	59.31	14.32	0.13	0.25	13.61	99.87	0.002	0.459	1.499	0.383	0.003	0.007	0.648	3.000	0.346	0.036	0.766	0.652	0.0182
5	IM003 Du	Dunite	0.09	14.79	54.18	17.46	0.19	0.33	11.36	98.39	0.002	0.567	1.393	0.475	0.005	0.009	0.550	3.000	0.443	0.032	0.711	0.554	0.0159
6	IM003 Hz	Harzburgite	0.06	13.42	55.92	20.11	0.30	0.33	9.92	100.06	0.002	0.515	1.439	0.547	0.008	0.009	0.481	3.000	0.511	0.036	0.737	0.485	0.0180
7	IM005 Cr	Chromitite	0.07	10.75	60.41	15.32	0.13	0.26	13.25	100.19	0.002	0.407	1.535	0.412	0.003	0.007	0.635	3.000	0.360	0.052	0.790	0.638	0.0259
8	IM005 Du	Dunite	0.08	11.54	56.42	20.61	0.17	0.36	10.37	99.53	0.002	0.447	1.464	0.566	0.005	0.010	0.507	3.000	0.485	0.081	0.766	0.511	0.0406
9	IM005 Hz	Harzburgite	0.01	15.30	54.64	17.82	0.31	0.29	11.49	99.85	0.000	0.577	1.382	0.477	0.008	0.008	0.548	3.000	0.445	0.032	0.706	0.551	0.0162
10	IM007 Cr	Ol-chromitite	0.08	7.49	64.18	15.56	0.08	0.28	12.44	100.11	0.002	0.289	1.664	0.427	0.002	0.008	0.608	3.000	0.386	0.041	0.852	0.611	0.0204
11	IM007 Du	Dunite	0.11	9.46	60.08	18.38	0.13	0.33	10.87	99.35	0.003	0.369	1.571	0.509	0.004	0.009	0.536	3.000	0.458	0.051	0.810	0.540	0.0256
12	IM007 Hz	Harzburgite	0.01	13.84	54.61	19.12	0.31	0.33	10.34	98.57	0.000	0.535	1.417	0.525	0.008	0.009	0.506	3.000	0.485	0.040	0.726	0.509	0.0198
13	IM009 Cr	Chr+Dun	0.03	8.20	63.19	14.65	0.12	0.28	13.12	99.59	0.001	0.316	1.633	0.400	0.003	0.008	0.639	3.000	0.354	0.047	0.838	0.642	0.0233
14	IM009 Du	Dunite	0.06	12.41	56.28	18.22	0.22	0.30	11.32	98.81	0.002	0.478	1.456	0.498	0.006	0.008	0.552	3.000	0.441	0.057	0.753	0.555	0.0287
15	IM009 Hz	OPX poor harz.	0.03	9.93	57.10	19.37	0.22	0.34	9.04	96.03	0.001	0.404	1.557	0.559	0.006	0.010	0.464	3.000	0.526	0.032	0.794	0.467	0.0162
16	IM011 Cr	Ol-chromitite	0.06	10.47	60.21	15.01	0.15	0.24	12.64	98.79	0.002	0.404	1.557	0.411	0.004	0.007	0.616	3.000	0.379	0.032	0.794	0.620	0.0161
17	IM011 Du	Dunite	0.07	11.11	57.87	19.10	0.13	0.34	10.39	99.02	0.002	0.433	1.512	0.528	0.004	0.010	0.512	3.000	0.480	0.048	0.778	0.515	0.0240
18	IM011 Hz	Harzburgite	0.05	13.74	55.67	18.69	0.16	0.32	10.54	99.16	0.001	0.528	1.436	0.510	0.004	0.009	0.512	3.000	0.480	0.030	0.731	0.515	0.0150
19	IM013 Cr	Ol-chromitite	0.08	12.50	58.65	14.35	0.12	0.24	14.33	100.26	0.002	0.466	1.467	0.380	0.003	0.006	0.676	3.000	0.320	0.060	0.759	0.679	0.0300
20	IM013 Cr2	Ol-chromitite	0.09	11.30	59.61	15.15	0.16	0.26	13.58	100.15	0.002	0.426	1.508	0.405	0.004	0.007	0.647	3.000	0.348	0.058	0.780	0.651	0.0290
21	IM013 Du	Dunite	0.08	13.42	56.16	17.77	0.16	0.31	11.76	99.66	0.002	0.510	1.431	0.479	0.004	0.009	0.565	3.000	0.428	0.051	0.737	0.569	0.0255
22	IM013 Hz	Harzburgite	0.00	16.85	52.81	17.10	0.27	0.28	11.87	99.17	0.000	0.633	1.332	0.456	0.007	0.008	0.565	3.000	0.428	0.028	0.678	0.567	0.0140
23	IM014 Cr1	Ol-chromitite	0.09	9.22	62.34	13.83	0.11	0.21	14.48	100.28	0.002	0.348	1.579	0.371	0.003	0.006	0.691	3.000	0.305	0.065	0.819	0.695	0.0328
24	IM014 Du1	Dunite	0.06	14.98	53.82	18.60	0.20	0.32	11.55	99.51	0.001	0.567	1.366	0.499	0.005	0.009	0.553	3.000	0.440	0.059	0.707	0.556	0.0298
25	IM014 Cr2	Ol-chromitite	0.08	10.77	60.49	15.08	0.14	0.27	13.17	100.00	0.002	0.409	1.540	0.406	0.004	0.007	0.632	3.000	0.362	0.044	0.790	0.636	0.0220
26	IM014 Du2	Dunite	0.08	12.73	54.12	20.12	0.16	0.32	10.21	97.73	0.002	0.498	1.422	0.559	0.004	0.009	0.506	3.000	0.488	0.072	0.740	0.509	0.0359
27	IM014 Hz	Harzburgite	0.03	18.93	50.02	19.08	0.31	0.31	11.02	99.70	0.001	0.706	1.252	0.505	0.008	0.008	0.520	3.000	0.472	0.033	0.639	0.523	0.0163
28	IM017 Cr	Dun with so. conc.	0.12	9.94	59.43	16.85	0.11	0.31	11.79	98.54	0.003	0.387	1.553	0.466	0.003	0.009	0.581	3.000	0.414	0.052	0.801	0.585	0.0260
29	IM017 Du	Dunite	0.12	10.92	56.46	17.54	0.15	0.34	11.63	99.15	0.003	0.422	1.514	0.481	0.004	0.009	0.568	3.000	0.426	0.055	0.782	0.572	0.0274
30	IM017 Hz	Harzburgite	0.03	10.60	57.81	19.35	0.38	0.33	9.87	98.36	0.001	0.418	1.529	0.541	0.010	0.009	0.492	3.000	0.499	0.042	0.785	0.496	0.0210
31	IM021 Hz	Harzburgite	0.03	18.79	50.46	16.91	0.28	0.27	11.81	98.54	0.001	0.705	1.270	0.450	0.007	0.007	0.560	3.000	0.433	0.017	0.643	0.563	0.0085
32	IM022 Du	Dunite	0.04	8.72	60.56	19.57	0.23	0.37	9.64	99.13	0.001	0.345	1.606	0.549	0.006	0.010	0.482	3.000	0.509	0.040	0.823	0.485	0.0203
33	IM023 Du	Dunite	0.07	11.61	57.67	17.70	0.24	0.33	11.00	98.62	0.002	0.451	1.503	0.488	0.006	0.009	0.540	3.000	0.452	0.036	0.769	0.544	0.0180
34	IM023 Hz	Harzburgite	0.03	17.49	52.44	17.88	0.30	0.31	11.38	99.84	0.001	0.654	1.316	0.475	0.008	0.008	0.539	3.000	0.454	0.021	0.668	0.542	0.0104
35	NN006 Cr	Sp-rich dunite	0.07	7.27	63.38	16.19	0.11	0.28	12.64	99.93	0.002	0.281	1.644	0.444	0.003	0.008	0.618	3.000	0.376	0.069	0.854	0.621	0.0344
36	NN006 Du	Dunite	0.07	8.27	61.45	19.39	0.18	0.35	10.14	99.86	0.002	0.324	1.617	0.540	0.005	0.010	0.503	3.000	0.489	0.051	0.833	0.506	0.0254
37	NN006 Hz	Orthopyroxenite	0.08	8.58	59.24	23.09	0.32	0.36	8.33	99.99	0.002	0.339	1.574	0.649	0.009	0.010	0.417	2.999	0.575	0.074	0.823	0.421	0.0373
38	NN008 Hz	Harzburgite	0.01	23.92	45.21	17.05	0.22	0.24	12.79	99.44	0.000	0.866	1.098	0.438	0.006	0.006	0.586	3.000	0.408	0.030	0.559	0.588	0.0150
39	NN009 Cr	Ol-chromitite	0.08	7.32	64.11	14.68	0.13	0.25	13.49	100.06	0.002	0.281	1.651	0.400	0.003	0.007	0.655	3.000	0.340	0.060	0.855	0.659	0.0303
40	NN009 Du	Dunite	0.08	12.11	57.40	17.44	0.21	0.31	11.41	98.95	0.002	0.467	1.484	0.477	0.006	0.008	0.556	3.000	0.438	0.040	0.761	0.560	0.0199
41	NN009 Hz	Harzburgite	0.05	17.74	52.11	16.70	0.22	0.28	12.22	99.31	0.001	0.662	1.305	0.442	0.006	0.008	0.577	3.000	0.417	0.025	0.663	0.580	0.0126
42	NN010 Du	Harzburgite	0.04	14.64	54.18	18.73	0.24	0.31	10.70	98.84	0.001	0.562	1.394	0.510	0.006	0.009	0.519	3.000	0.473	0.036	0.713	0.522	0.0182
43	NN010 Hz	Harzburgite	0.05	12.18	56.28	18.24	0.24	0.32	10.21	97.51	0.001	0.479	1.486	0.509	0.007	0.009	0.508	3.000	0.484	0.025	0.756	0.512	0.0128
44	NN011 Hz	Harzburgite	0.03	18.52	50.96	18.13	0.30	0.27	11.56	99.77	0.001	0.689	1.272	0.479	0.008	0.007	0.544	3.000	0.449	0.030	0.649	0.547	0.0148

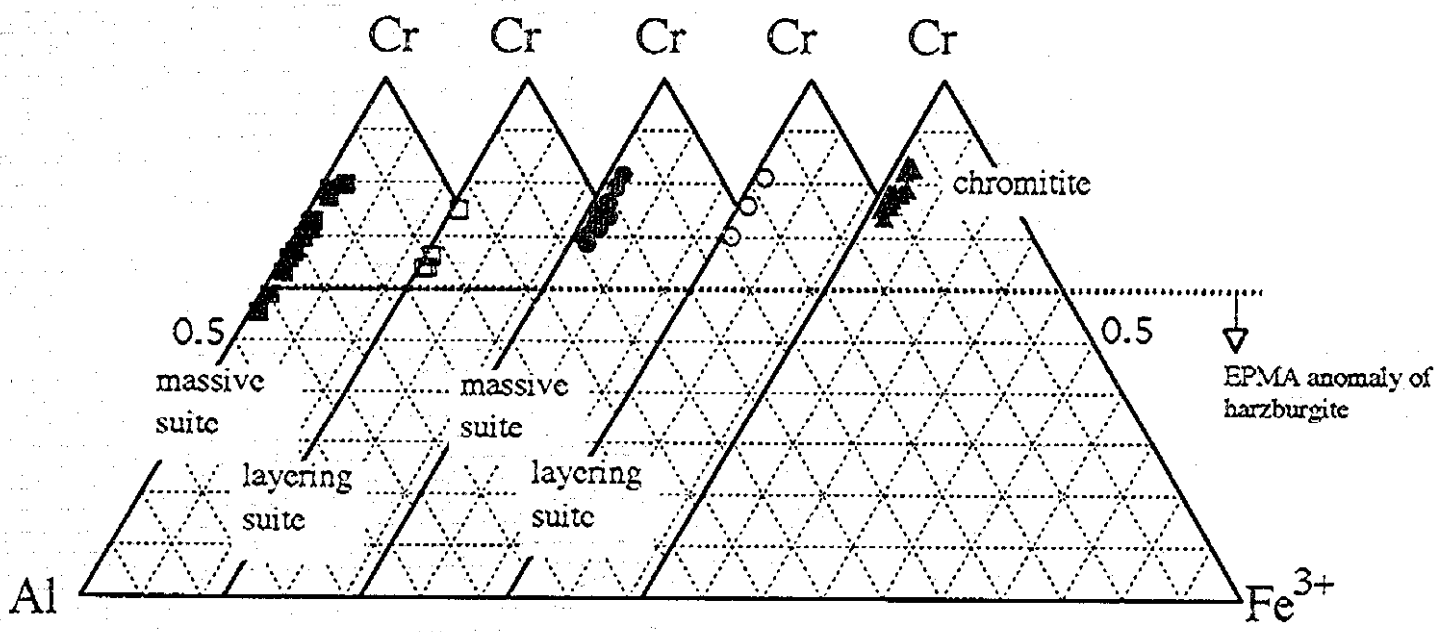

■ Harzburgite from massive dunite-harzburgite suite

□ Harzburgite from dunite-harzburgite suite with remarkable layering

● Dunite from massive dunite-harzburgite suite

○ Dunite from dunite-harzburgite suite with remarkable layering

▲ Chromitite from massive dunite-harzburgite area

Figure 2-1-8 Cr-Al-Fe3+ proportion of chromian spinel

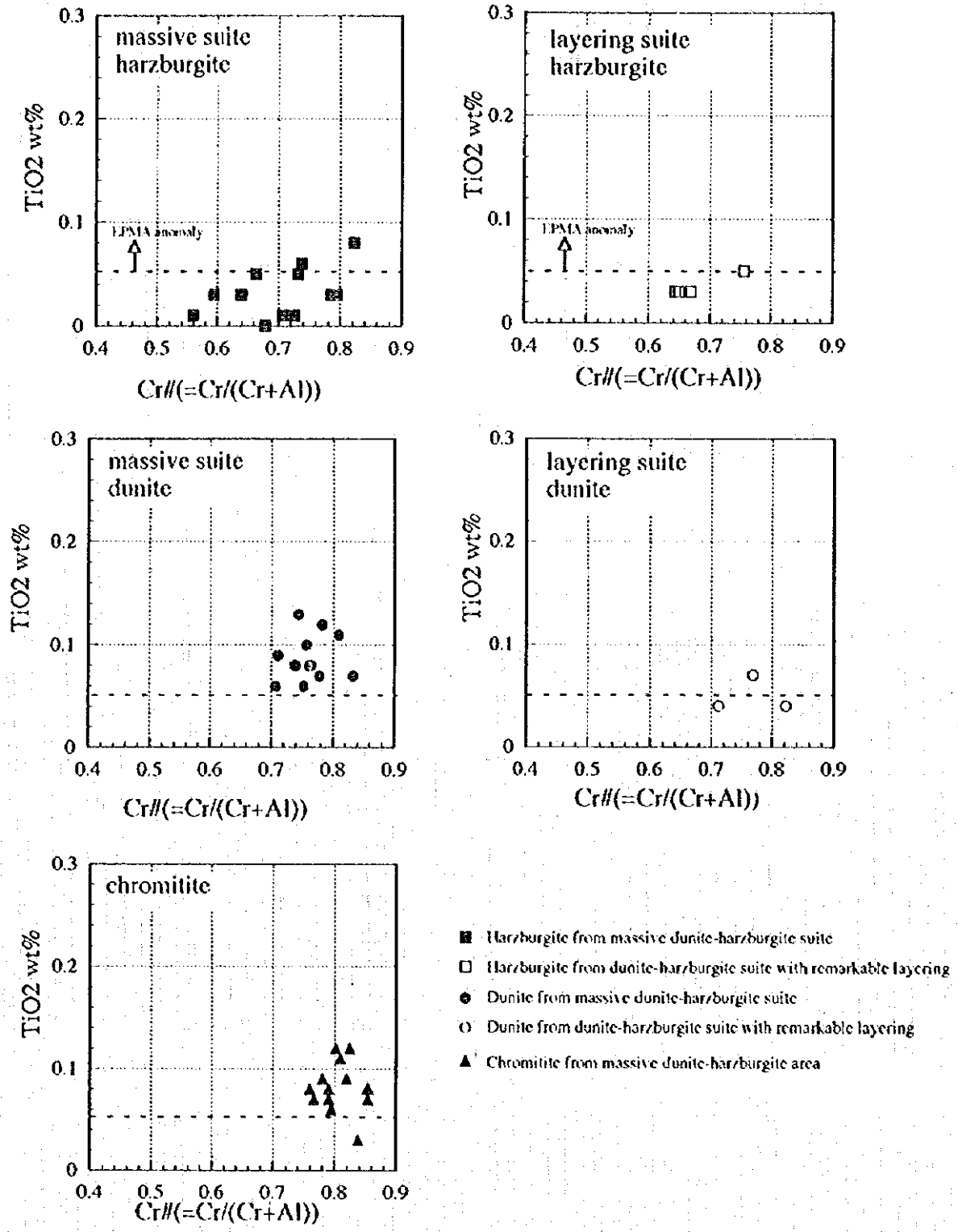

Figure 2-1-9 Relationships between Cr # and TiO2 wt% in chromian spinel

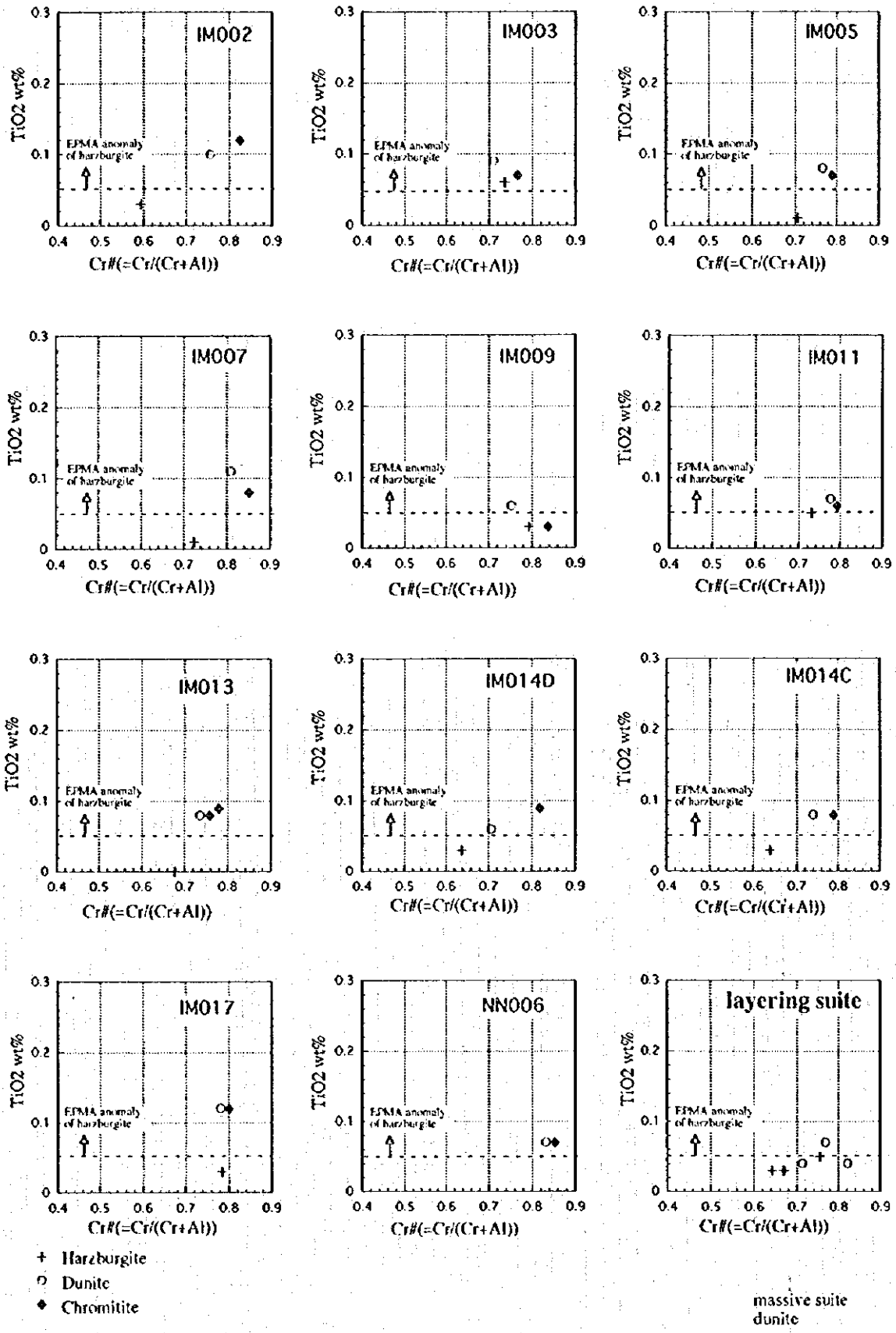

Figure 2-1-10 Relationships between Cr# and TiO2 wt% in chromian spinel in each location

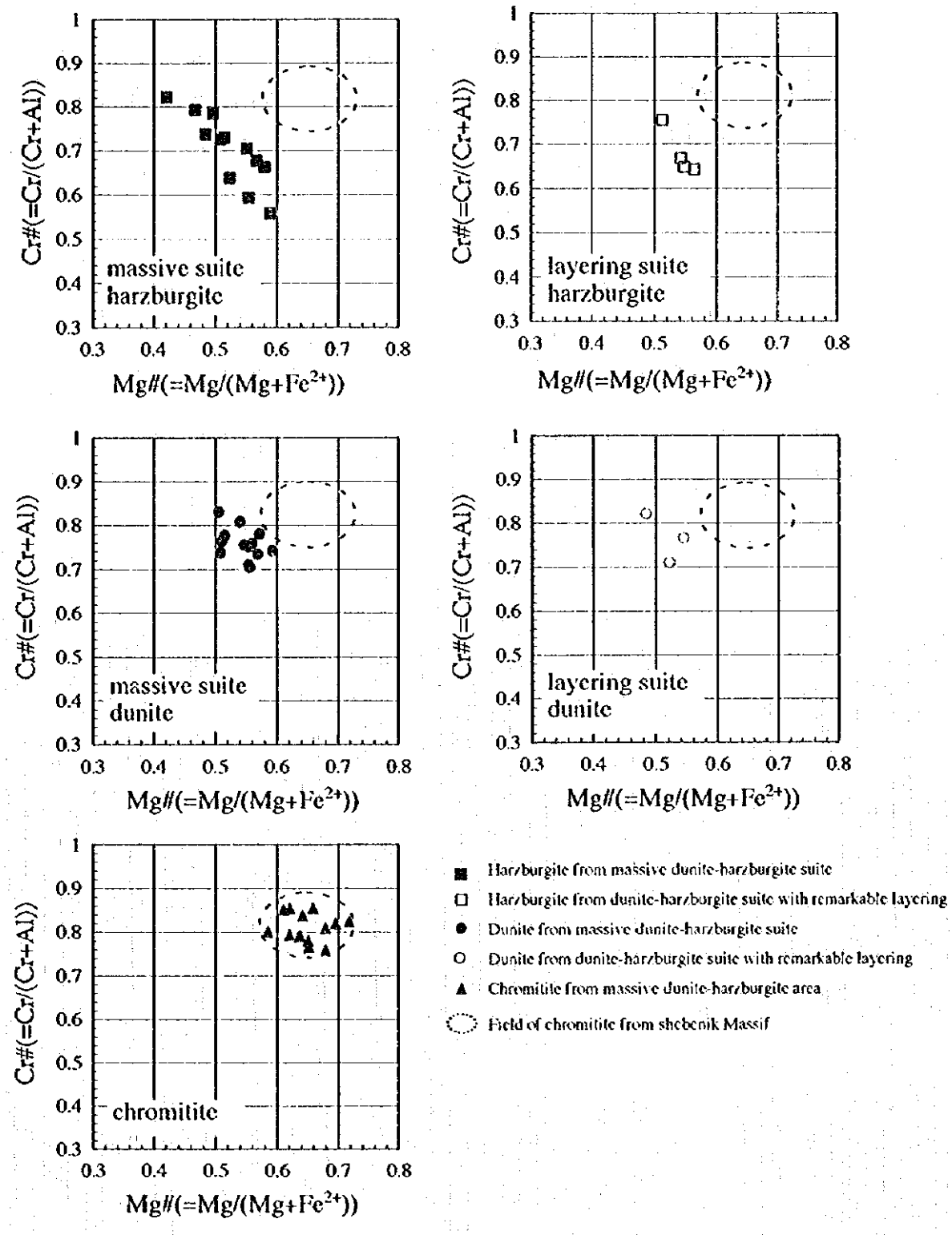

Figure 2-1-11 Relationships between Cr# and Mg# in chromian spinel

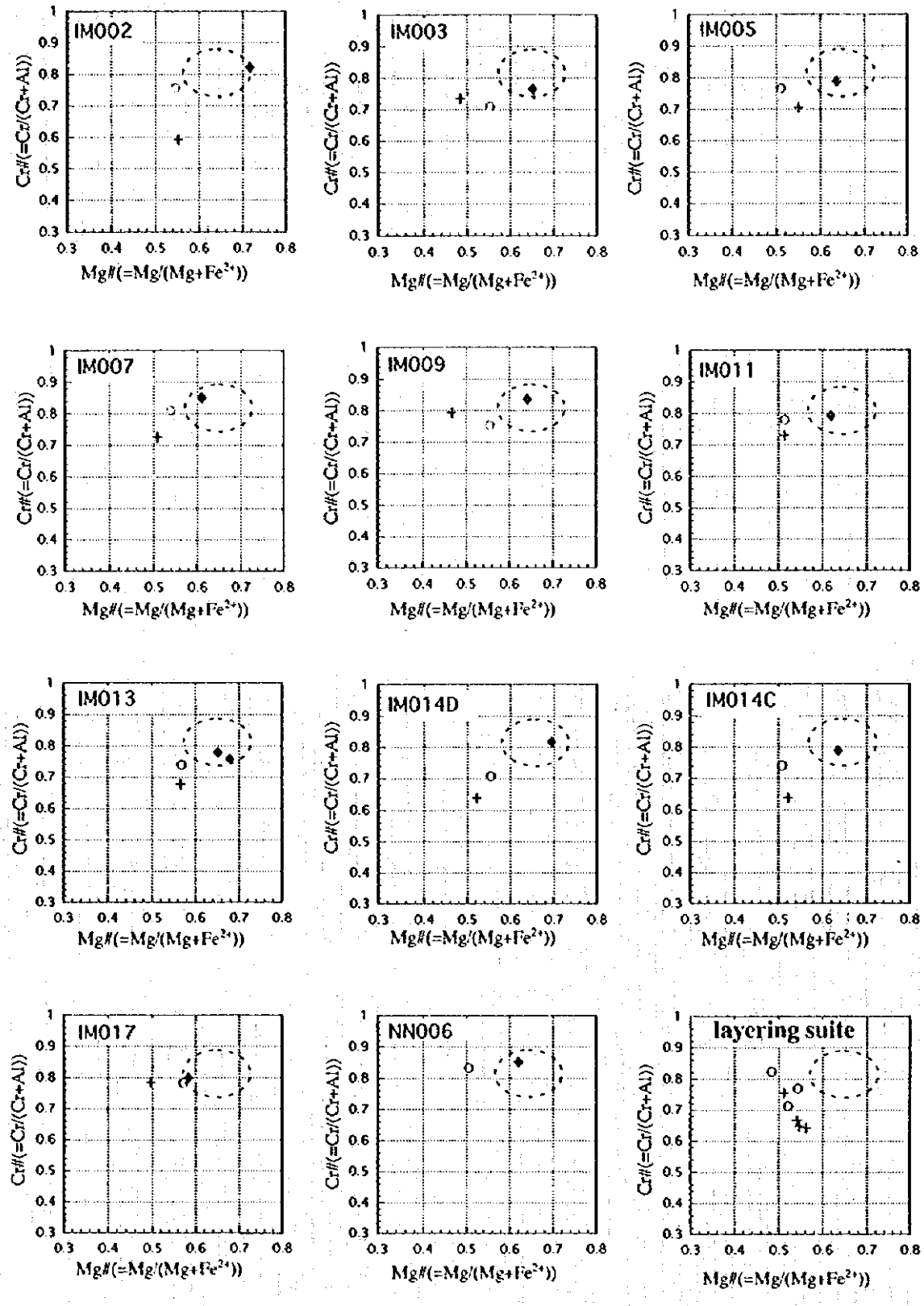

Figure 2-1-12 Relationships between Cr# and Mg# in chromian spinel in each location

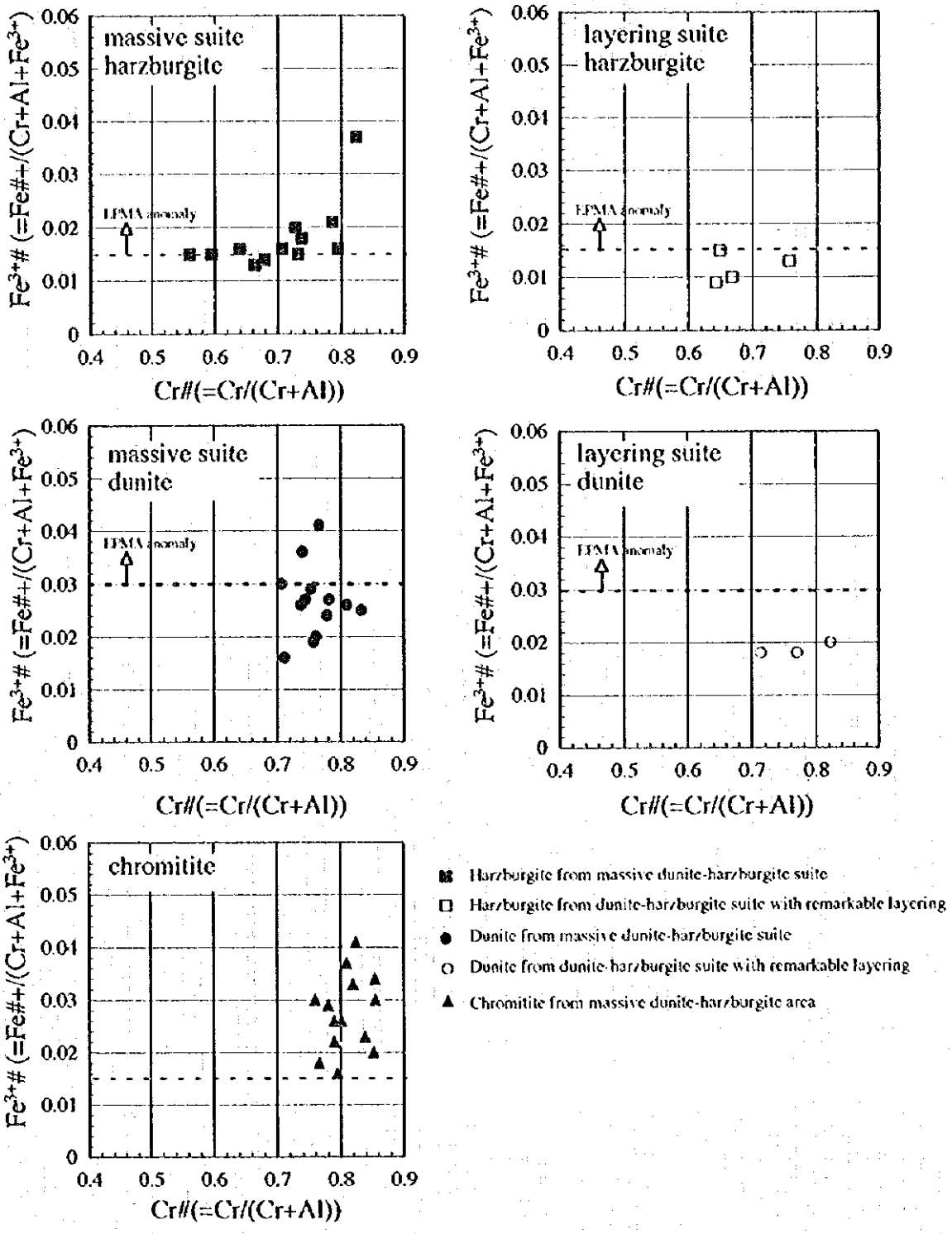

Figuer 2-1-13 Relationships between Cr# and Fe3+# in chromian spinel

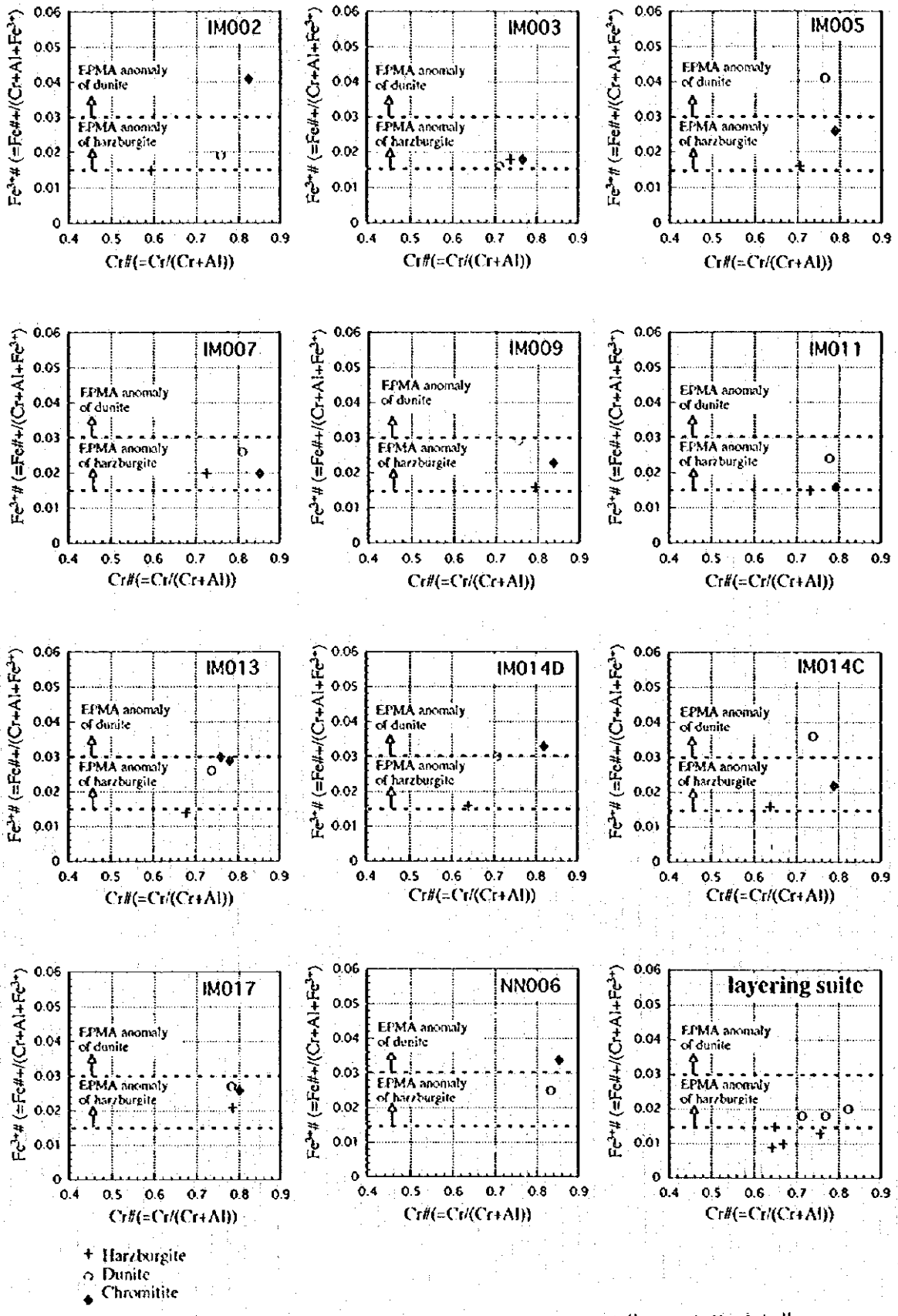

Figure 2-1-14 Relationships between Cr# and Fe3+# in chromian spinel in each location

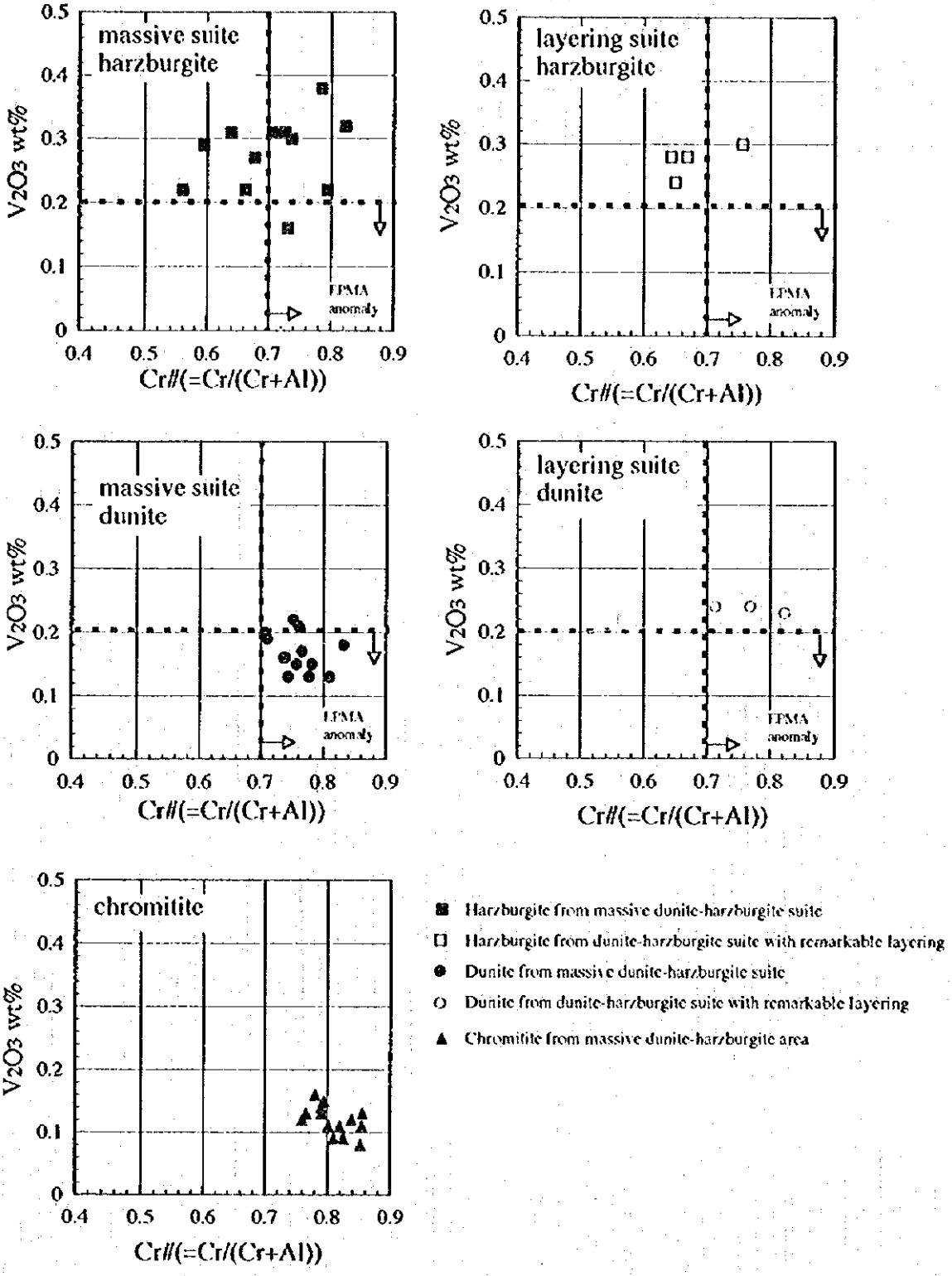

Figure 2-1-15 Relationships between Cr # and V2O3 wt% in chromian spinel

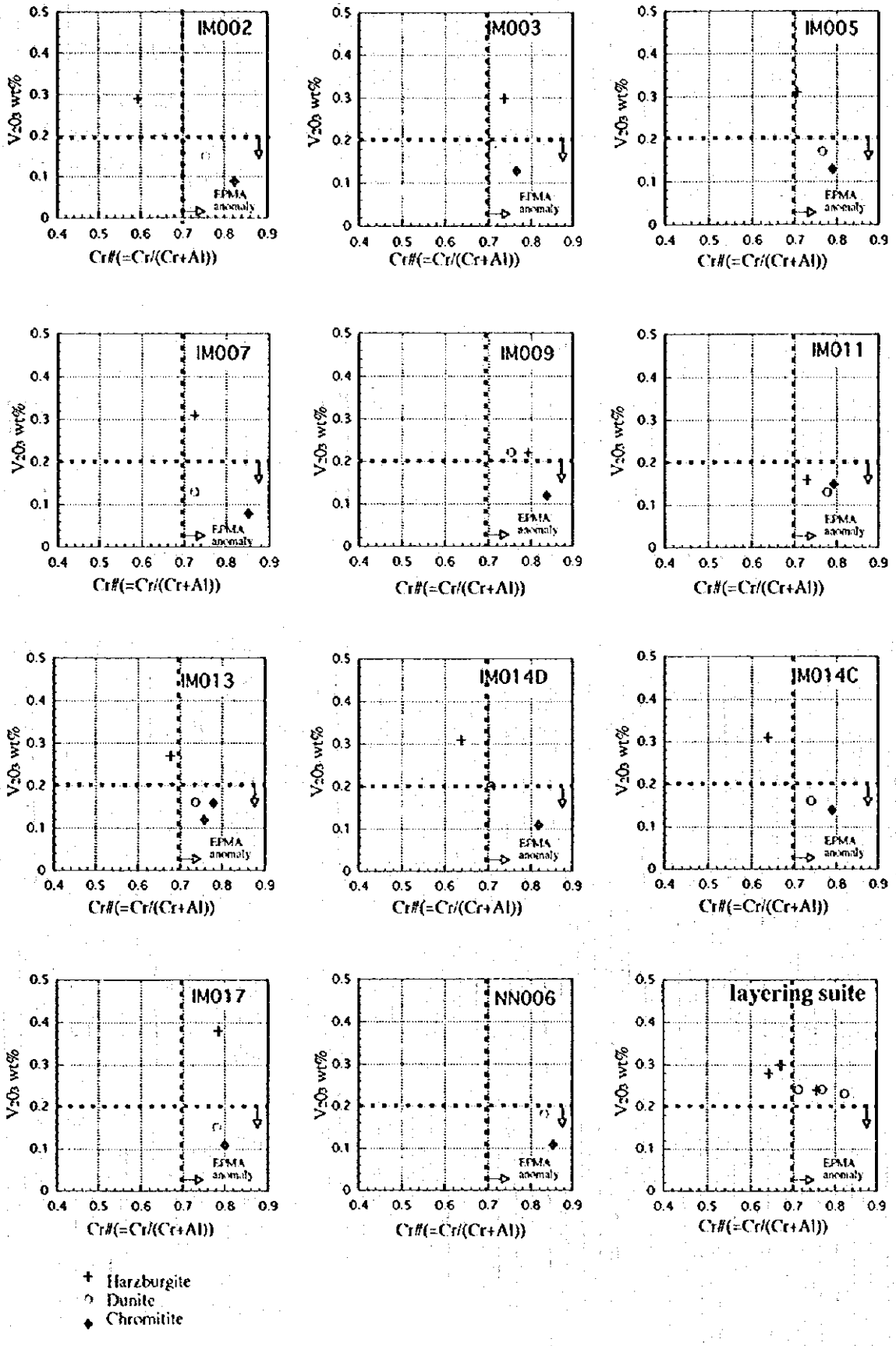

Figure 2-1-16 Relationships between Cr # and V2O3 wt% in chromian spinel in each location

this report for the reasons mentioned above. The TiO_2 content of spinel in dunite from the Dunite-harzburgite suite with remarkable layering is lower than that in harzburgite. This fact makes interpretation so complicated that the TiO_2 content of spinel in dunite is not discussed further.

Harzburgites with TiO_2 content higher than 0.05 wt.% were obtained from three localities, IM003, IM011 and NN009, of the Massive dunite-harzburgite suite and one locality, NN010, of the Dunite-harzburgite suite with remarkable layering.

c) Fe^{3+}#; $Fe^{3+}/(Cr+Al+Fe^{3+})$ atomic ratio

The Fe^{3+}# of spinel is lower than 0.05 in all samples. The ratio of spinels in dunite and chromitite are relatively higher than that in harzburgite and the average is 0.028 in chromitite, 0.025 in dunite and 0.016 in harzburgite (Figs. 2-1-13 and 2-1-14).

These differences of the Fe^{3+}# among the three kinds of rock are also usually recognized in other regions (for example, Arai, 1994). It is noteworthy that a dunite and a harzburgite with relatively high Fe^{3+}# of spinel may be influenced more strongly by the melt-rock interaction. A harzburgite with a ratio higher than 0.015 and a dunite with a ratio higher than 0.030 were defined as EPMA anomalies in this report. The samples from the Central Shebenik Area generally have relatively higher Fe^{3+}# of spinel than those from other area surveyed in 1995. This shows that the Massive dunite-harzburgite suite in the area may be strongly influenced by the melt-rock interaction and may have a relatively high potential for chromitite.

A harzburgite and a dunite with high Fe^{3+}# of spinel were detected in twelve samples from nine localities, IM002, IM003, IM005, IM007, IM009, IM011, IM014 , IM017 and NN008. These localities are all in the Massive dunite-harzburgite suite.

d) V_2O_3 wt.%

The V_2O_3 content of spinel is lower than 0.4 wt.% in all samples (Figs. 2-1-15 and 2-1-16). The content of spinel in harzburgite is the highest with an average of 0.277 wt.% and is lower in dunite, with an average of 0.181 wt%, and in chromitite, with an average of 0.119 wt%.

The behavior of spinel in ultramafic rocks is not examined in detail but Matsumoto (1995 and 1996) indicates that a peridotite with relatively high Cr# and low V_2O_3 wt% may be correlated to a halo of chromitite mineralization. This assumption could be explained by orthopyroxene chemistry as follows (Arai and Yurimoto, 1995., Matsumoto et al., 1995). Orthopyroxene preferentially dissolved into the melt is rich in Cr and scarcely includes V_2O_3.

A dunite and a harzburgite with V_2O_3 content lower than 0.2 wt% and Cr# higher than 0.7 are considered as EPMA anomalies (Fig. 2-1-16). The samples with anomalous V_2O_3 content and Cr# are detected in 11 samples from 9 localities which are all located in the Massive dunite-harzburgite suite. They are IM002, IM003, IM005, IM007, IM011, IM013, IM014, IM017 and NN006.

e) Mg#; $Mg/(Mg+Fe^{2+})$ atomic ratio

The Mg# of spinel in chromitite is plotted in an area with high values in Fig. 2-1-11 and those in dunite and harzburgite have low values. The average is 0.649 in chromitite, 0.540 in dunite and 0.526 in harzburgite.

The Mg# is controlled by the ratio of modal composition between chromian spinel and olivine because Mg is redistributed between spinel and surrounding olivine under subsolidus conditions (Arai, 1980). In other words, as the mode of spinel becomes higher then the Mg# increases.

The Mg# of spinel in stream sediments is very useful in examining the lithology of ultrabasic rocks and the distribution of chromitite deposits along a drainage basin (Arai and Okada, 1991, Arai ,

1992). However, the validity of the Mg# as an indicator of primary chromitite deposition in areas like this has not yet been examined in detail.

f) MnO wt%

The MnO content is lower than 0.4 wt% in all samples. There are some differences of the content among the three kinds of rocks. The average is 0.256 wt% in chromitite, 0.330 wt% in dunite and 0.305 wt% in harzburgite.

g) Estimation of Chrome Potentiality

The potentiality for chromitite deposit in each locality is estimated by the following equation :

Potentiality = Number $_{\text{of detected EPMA anomaly}}$ /Number $_{\text{of index for EPMA anomaly}}$ ..... (1)

where index for EPMA anomaly are follows:

1) The Cr# of spinel in harzburgite
2) The TiO_2 content of spinel in harzburgite
3) The Fe^{3+}# of spinel in harzburgite
4) The relationship between V_2O_3 and Cr# of spinel in harzburgite
5) The Fe^{3+}# of spinel in dunite
6) The relationship between V_2O_3 and Cr# of spinel in dunite

Remarks; For example, if a dunite and a harzburgite are both tested in one locality, the denominator in equation (1), number of index for EPMA anomalies, is six.

Table 2-1-5 Potentiality of EPMA anomaly

Locality Number and Locality	Frequency of EPMA Anomaly by Equation(1)	Geology of the Locality
IM011	4/6=0.666	Massive harzburgite-dunite suite
IM014 (Ahu i Vetem)	5/8=0.625	Massive harzburgite-dunite suite
IM002 (Gobille)	3/6=0.500	Massive harzburgite-dunite suite
IM003 (No.115)	3/6=0.500	Massive harzburgite-dunite suite
IM005 (Buzgare)	3/6=0.500	Massive harzburgite-dunite suite
IM007 (Qerroi i Qukut)	2/6=0.333	Massive harzburgite-dunite suite
IM017	2/6=0.333	Massive harzburgite-dunite suite
IM009 (Buzgare)	1/6=0.167	Massive harzburgite-dunite suite
IM013 (Lugu i Batres)	1/6=0.167	Massive harzburgite-dunite suite
NN008	1/4=0.250	Massive harzburgite-dunite suite
NN009 (Stanet e Vecanit)	1/6=0.167	Massive harzburgite-dunite suite
NN010	1/4=0.250	Dunite-harzburgite suite with romarkable layering

EPMA anomalies are densely distributed in the Massive dunite-harzburgite suite and only one anomaly is obtained from a harzburgite in the Dunite-harzburgite suite with remarkable layering. This fact suggests that a relatively large chromitite deposit may be formed in the Massive dunite-harzburgite suite. As for each locality, IM002, IM003, IM005, IM011 and IM014 have relatively high potentialities and it is noteworthy that IM014 and IM011 have the highest values of these five localities.

(4) Platinum Group Elements (PGE) analysis

Eleven chromitite and one clinopyroxenite were analyzed for platinum group elements (PGE). The results of analysis are shown in Table 2-1-6.

Platinum group elements are of six elements, ruthenium (Ru), rhodium (Rh), palladium (Pd), osmium (Os), iridium (Ir) and platinum (Pt). These elements are divided into two groups based upon

similarities of their physical properties; the Ir group (Os, Ir and Ru) and Pt group (Rh, Pt and Pd).

Table 2-1-6 Platinum Group Elements in the Shebenik Ultrabasic Massif

No.	Sample No.	Rock Type	Os (ppb)	Ir (ppb)	Ru (ppb)	Rh (ppb)	Pt (ppb)	Pd (ppb)	Au (ppb)	Re (ppb)
1	IM002Cr	Chromitite	18	20.0	61	9.6	< 5	< 2	4.0	< 5
2	IM003Cr	Chromitite	62	66.0	130	19.4	69	38	4.7	< 5
3	IM005Cr	Chromitite	140	110.0	240	14.5	67	33	2.4	< 5
4	IM007Cr	Chromitite	120	170.0	250	22.9	28	24	11.0	< 5
5	IM009Cr	Chromitite	12	25.0	20	1.8	< 5	< 2	3.2	< 5
6	IM013Cr	Chromitite	44	39.0	94	4.9	< 5	< 2	1.6	< 5
7	IM013Cr2	Chromitite	27	30.0	95	9.8	79	28	1.3	< 5
8	IM014Cr1	Chromitite	45	51.0	110	14.1	27	10	1.2	< 5
9	IM020Cr	Chromitite	43	60.0	110	10.7	38	10	0.8	< 5
10	IM020Px	Pyroxenite	< 2	0.2	8	0.3	6	6	< 0.5	< 5
11	NN002Cr	Chromitite	20	26.0	77	9.9	19	10	2.0	< 5
12	NN006Cr	Chromitite	2	2.6	26	4.7	< 5	< 2	< 0.5	< 5
	last year result	(chromitite)								
	Buliqiza	Average (N2)	62	54.0	94	9.0	11	10	7.0	< 5
	West korce	Average (N11)	60	70.0	120	48.0	555	733	70.0	< 5

Chondrite-normalized concentrations are usually used for discussion of relationships among these 6 elements. The results of Pt analysis in the project area and in other areas of Albania (Bulqiza Mine and the Western Zone, data obtained from 1995 survey) are compared with those from the Bushveld Complex in the Republic of South Africa and some ophiolitic rocks (Fig. 2-1-17). The Bulqiza mine is the largest chromitite deposit in Albania. The data of the Bushveld Complex are from the Merensky Reef, the largest platinum mine in South Africa and from LG-5 and LG-6 chromitite layers in the Lower Zone of the complex.

Ir group elements are usually more concentrated than Pt group elements in ophiolitic rocks and a connected line on the diagram is located to the lower-right. On the other hand, Pt group elements are densely concentrated in an ore zone like the Merensky Reef associated to a layered intrusive body.

The results from the project area show characteristics of ophiolitic rocks and the connected lines are all in the lower-right region of the diagram (Fig. 2-1-17). It is thought that the potential for the existence relatively large Pt concentrations is low in the Eastern Zone. The chromitite from the Bulqiza Mine has a similar pattern of condrite-normalized concentrations as that from the Lower Zone of the Bushveld Complex.

2-1-5 Discussion

(1) The relationship between mineralization, geochemical anomalies and geology

The ultrabasic rocks in the project area consist mainly of dunite and harzburgite. These rocks are divided into the Massive dunite-harzburgite suite (MDHS) and the Dunite-harzburgite suite with remarkable layering (DHSRL) in ascending order. Chromitite deposits are densely distributed in the lower suite, the MDHS, and only few deposits are distributed in the upper suite, the DHSRL. Furthermore, a more dense distribution of chromitite deposits is recognized in the MDHS just below the boundary of the DHSRL. Chromitite is always enclosed by dunite and many chromitite deposits are concentrated into the Dunite rich zone of the lower suite where many dunite lenses are

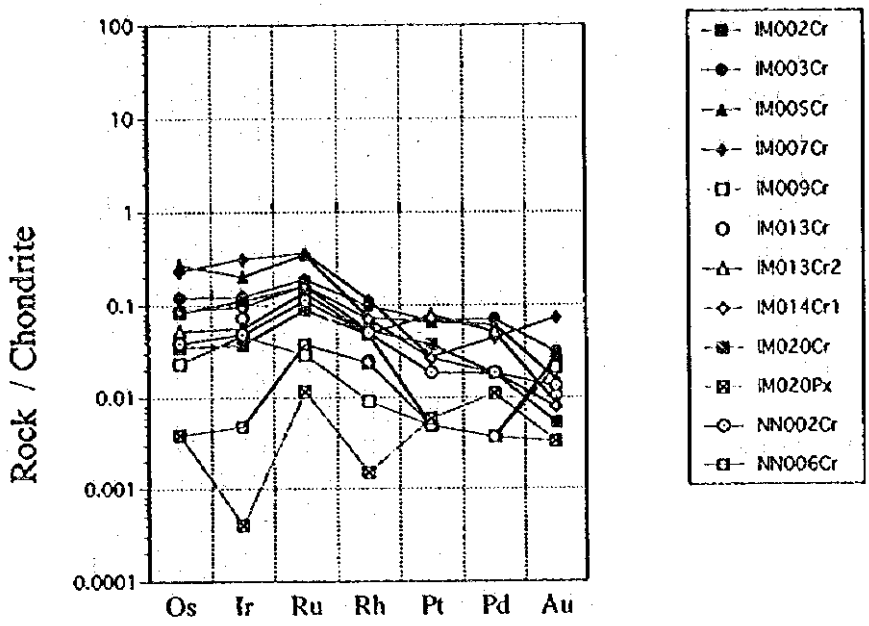

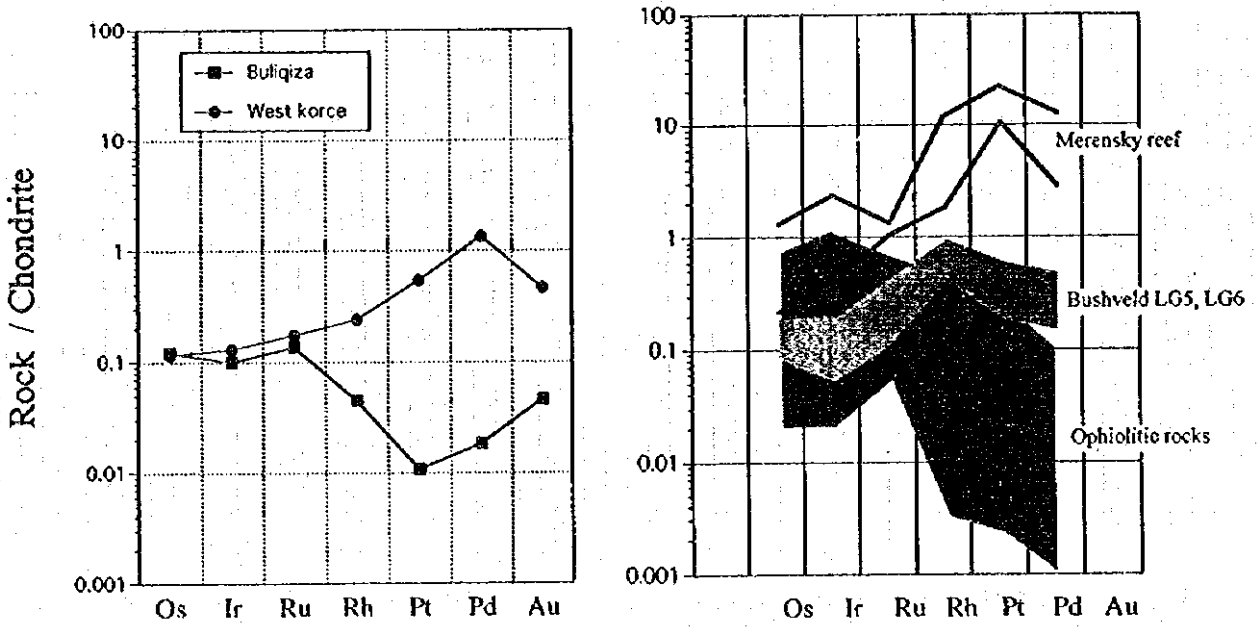

Figure 2-1-17 Chondrite-normalized PGE patterns
Data sources;
Merensky reef: Lee (1983)
Bushveld LG5, LG6: Lee and Parry (1988)
Ophiolitic rocks: Talkington and Watkinson (1986)

distributed.

This evidence suggests that chromitite-mineralization in this area is stratigraphically controlled by particular horizons of the Shebenik-Pogradec ultrabasic massif. The Dunite-rich zone of the MDHS, especially the zone located just below the boundary with the DHSRL has a relatively high potential for large sized chromitite deposits.

The particular relationship between chromitite-mineralization and geology such as that proposed in this area is also recognized in other ophiolitic complexes of the world (for example, Nicolas and Prinzhofer, 1983). The stratigraphical horizon control of mineralization believed to exist in this area could be explained without conflict with a genetic hypothesis of the podiform chrome deposit supported by a magma-mixing model (Arai and Yurimoto, 1994, 1995; Zhou et al., 1994; Matsumoto, 1996, Fig. 2-1-18).

The method of the estimation for the potentiality of chromitite deposit by the EPMA anomaly of chromian spinel is based on the above mentioned hypothesis of the origin of podiform chromitite. This method has led to the detailed examination of the chemistry of chromian spinel in dunite, harzburgite and chromitite (MITI, 1994, 1995; Matsumoto et al., 1995; Matsumoto, 1996, Fig. 2-1-19). Lithology with intermediate chemical composition between dunite and harzburgite is detected as EPMA anomalies which have higher potential for chromitite deposit. This intermediate lithology is called the transitional lithology and is a good indicator for chromitite exploration.

The EPMA anomalies are concentrated in the MDHS. Based upon the hypothesis of the origin of podiform chromitite, it is interpreted that the MDHS is the favorable horizon where the melt-rock interaction and magma mixing occur effectively. The localities which have many EPMA anomalies are IM002(Gobille), IM003(No.115), IM005(Buzgare), IM011 and IM014(Ahu i Vetem). In particular IM014(Ahu i Vetem) shows an extraordinary number of EPMA anomalies. Massive chromitite deposits are densely distributed at these localities. The EPMA anomalies are concordant with density of distribution of chromitite deposits.

(2) Comparison between chromitites deposits in the Shebenik area and those in other regions of the world.

Fig. 2-1-20 indicates a comparison between the chemical composition of chromian spinel of chromitite deposits in the main ophiolitic complexes of the world and those in the project area.

The ultrabasic rocks in Albania are divided into the Eastern and the Western zones (for example, Cina et al., 1996). The Shebenik massif belongs to the Eastern zone. The Eastern zone comprises highly depleted dunite and harzburgite. On the other hand, the Western Zone consists of poorly depleted lherzolite and harzburgite. Depletion is a term showing degree of extraction of melted components in the mantle. The difference of degree of depletion between the Eastern and Western zones is easily read in the chemical composition of chromian spinel in Fig. 2-1-20.

The Kempirsai body in the Republic of Kazakhstan where there occurs one of the largest podiform chrome deposits in the world consists of poorly depleted harzburgite with Cr# of 0.4 to 0.6. On the other hand, the northern zone of the Kamuikotan Belt in North Japan consists of highly depleted harzburgite (Cr#; 0.8 - 0.9) and is rarely accompanied by chromitite deposits. Low depleted lherzolite (Cr# is lower than 0.4) generally do not contain chromitite. The chemical composition of chromian spinel in harzburgite from the Eastern zone of Albania shows an intermediate level between that of Kazakhstan and the northern zone of the Kamuikotan Belt in North Japan. The degree of depletion of the harzburgite from the Western zone of Albania is lower than those from the Sangun zone in Southwest Japan and the Coto block in the Philippines.

The degree of concentration of chromitite and depletion of ultrabasic rocks are controlled by the genetic environment of those rocks. The chemical composition of spinel and peridotite and the lithology of peridotite from the Eastern zone of Albania are typical of an island arc environment and those from the Western zone show an oceanic or back arc environment.

(3) Potential of chromitite deposit

Not only is the chemical composition of harzburgite important in determining the potential of chromitite deposits but also the composition of melt interacting with harzburgite that affects to characteristics such as the size and grade of chromitite ore deposits. The chemical composition of harzburgite is able to be estimated from the Cr# of spinel for example but estimation of the chemical composition of the other important element, the melt, have been studied by trial and error. Arai (1995) and Arai (1996) indicate that a harzburgite which has chromian spinel with an intermediate Cr# from 0.4 to 0.6 is the most suitable host for large-scale podiform chromitite.

Some harzburgites have chromian spinel with Cr# lower than 0.6 in the project area and many surface indications of chromitite are obtained from these harzburgites. The project area possibly has a potentiality of relatively large chromitite deposits of which ore reserves of several tens to hundreds of thousands of tons can be concluded according to the chemical compositions of harzburgite, the distribution of chromitite deposits in the project area and by comparison those with large-scale chromitite deposits of the world (Fig. 2-1-20).

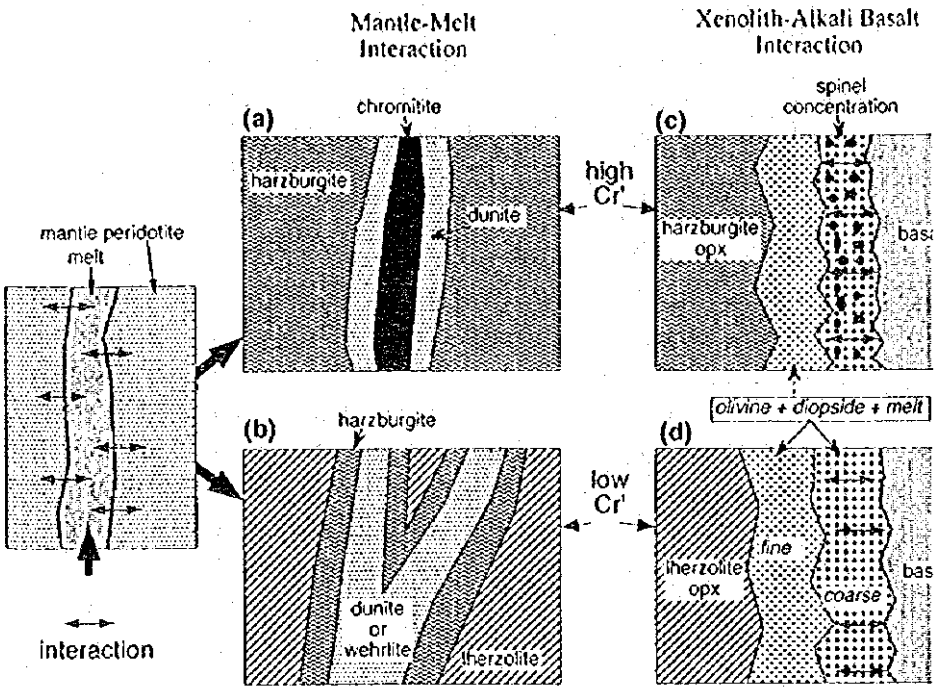

Fig. 5. Correlation of orthopyroxene–alkali-basalt interaction products with mantle-melt interaction products. During the mantle interaction, the podiform chromitite with dunite envelope could be formed in the harzburgitic mantle (a), whereas (or wehrlite) with a harzburgitic aureole may be formed in the lherzolitic mantle (b). The products of mantle-melt interact and b, are analogous, respectively, to the products of xenolith-alkali basalt, c and d. Reconstructed from descriptions by (1981a, 1981b), Nicolas (1989), and Takahashi (1992).

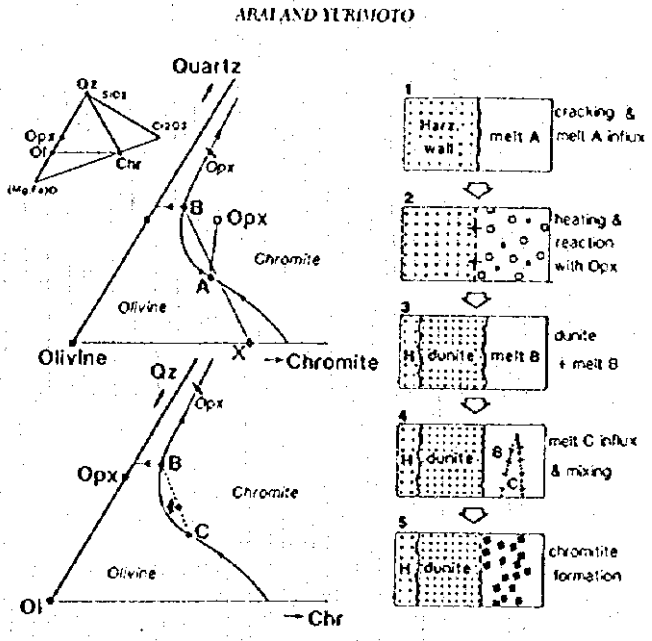

FIG. 6. A magma-mixing model for the genesis of podiform chromitite. At the first stage a melt (A) of deep origin is intruded into shallow mantle harzburgite (stage 1). Melt A reacts with orthopyroxene (open squares) in the harzburgite (stages 2 and 3) to produce olivine (+ spinel) and a secondary Si-rich melt (B), which may precipitate spinel only if mixed with successively supplied relatively primitive melt (C) (stages 4 and 5). Thin straight lines in the upper left panel indicate pairs of reactants (Opx and melt A) and products (crystal mixture X—olivine + spinel—and melt B) of the interaction. The thin dotted line in the lower left panel denotes the mixing of B (secondary silica-rich melt) and C (primitive melt). Primary liquidus fields are indicated by italicized minerals. Chr = chromite, Ol = olivine, Opx = orthopyroxene, Qz = quartz. Phase diagrams modified from Irvine (1977).

Figure 2-1-18 Magma mixing model for the genesis of Podiform chromitite (Fig.6 of Arai and Yurimoto (1994) and Fig.5 of Arai and Abe (1995)).

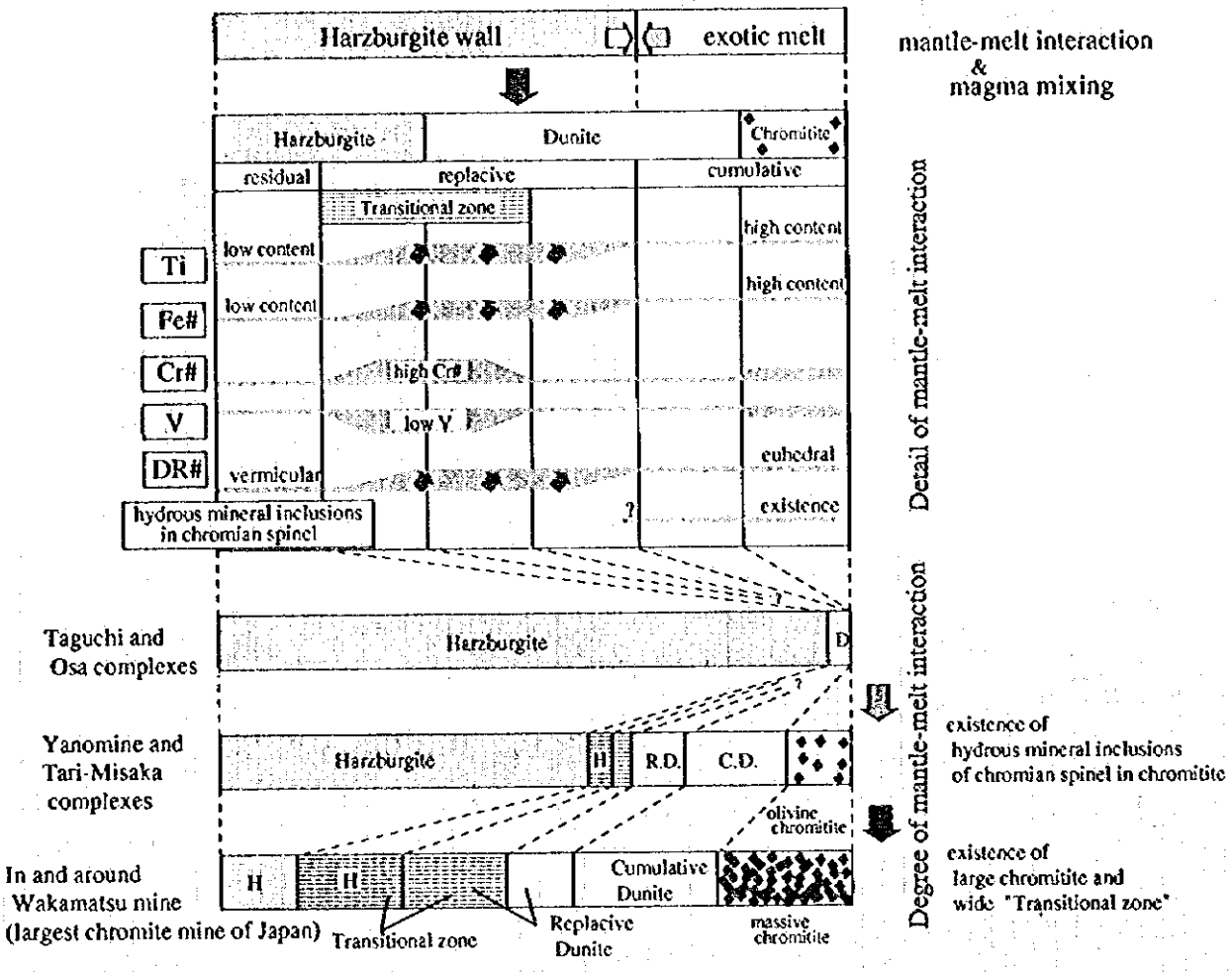

Figure 2-1-19 Correlation between degree of mantle-melt interaction and chromite concentration from the Sangun zone of SW Japan (Fig 34 of Matsumoto (1995)).

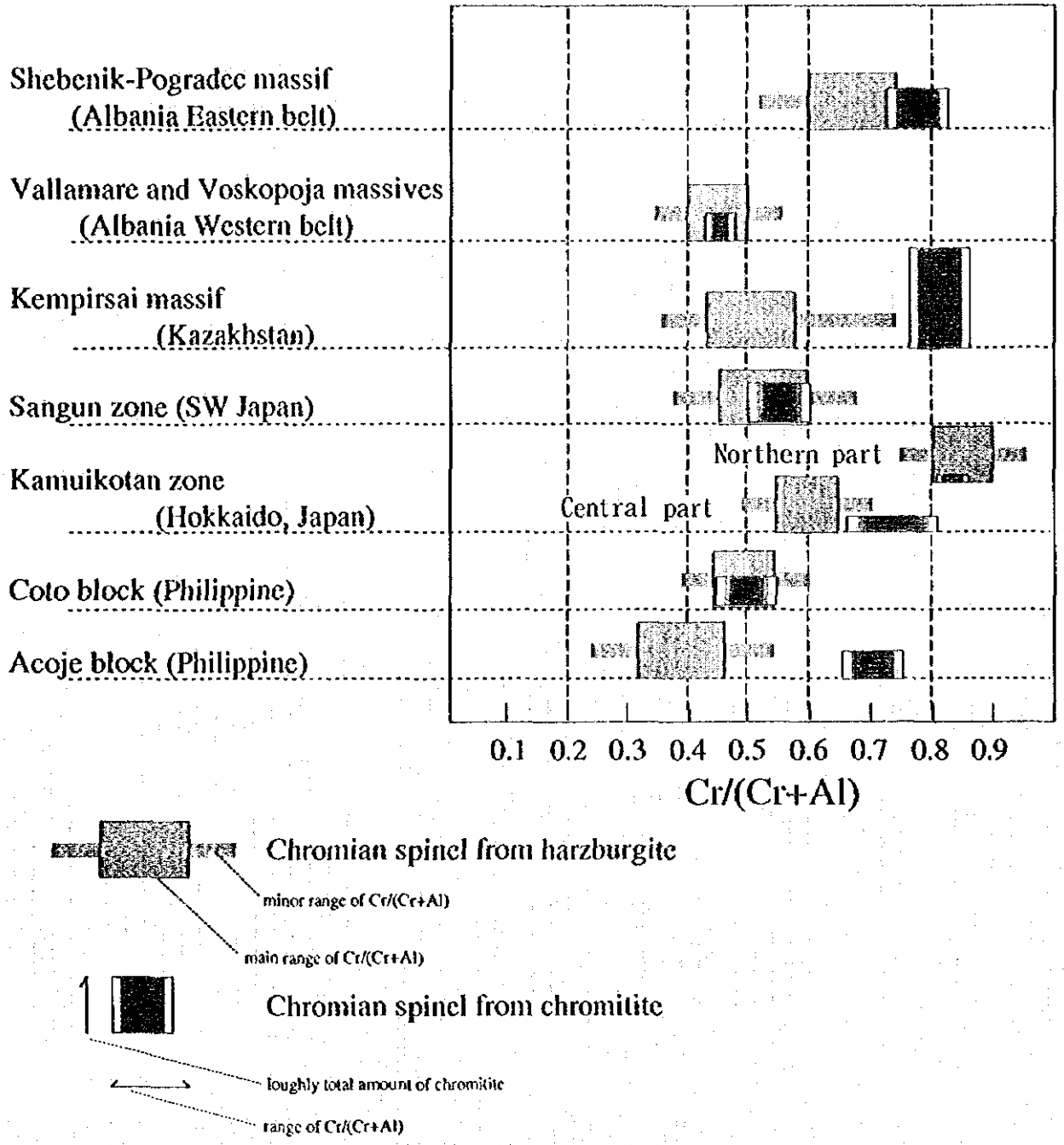

Figure 2-1-20 Comparison of Cr# of chromian spinel in the world

Data sources;
Shebenik-Pogradec, Vallamare and Voskopoja massives: This survey.
Kempisai massif: Kravchenko and Grigoryeva (1986), Melcher et al. (1994).
Sangun zone: Arai (1980), MITI(1993), Matsumoto et al., (1995).
Kamuikotan zone: Arai (1978), MITI(1994).
Coto and Acoje blocks: Leblanc (1983), Yumul (1994) .

2-2 Geophysical Survey (Magnetic Survey)

2-2-1 Location of Survey Area

As a part of the phase II survey, geophysical surveys (magnetic survey) were carried out in two areas: the Central Shebenik area and the Katjel area. The locations are indicated in Fig. 1-1-1.

The Central Shebenik area, with an area of 10.00 km², represents the western half of the geological survey area and was identified in the geological survey as having geological conditions favorable to chromitite deposits. The purpose of the survey in this area was to detect chromitite and/or dunite with chromitite by magnetic survey.

The other area, the Katjel area, has an area of 0.52 km² and covers the entire Katjel deposit, the largest chrome deposit in the Shebenik-Pogradec ultrabasic massif. The purpose of the survey in this area was to verify the effectiveness of magnetic survey over a known chrome deposit.

2-2-2 Survey Method

(1) Setting of Survey Lines

Figs. 2-2-1 and 2-2-2 indicate the survey line layout of the Central Shebenik and the Katjel areas, respectively.

In the Central Shebenik area the survey lines were set in the E-W direction after considering the geological structure of the ultrabasic rocks and terrain conditions. In the Katjel area most survey lines were set in the direction N60°E, perpendicular to the known ore body. A further four lines were set perpendicular to these, i.e. in the direction N30°W.

In both zones, in principle, the interval between the survey lines was taken as 100 m, and the interval between the survey points as 20 m, the survey lines and survey points being set by transit survey with elevation bench marks in each area and its vicinity as base points.

(2) Measurement Method

In accordance with the size of the known chromite deposit, geomagnetic measurements were made with at an interval of 20 m along survey lines. However, in cases where anomalous values were noted in the field measurements, supplementary survey points were set so as to decrease the measurement interval to 10 m.

At all of the survey points total magnetic intensity was measured at least twice, and the average of those values was taken as the true value. However, in cases where the difference between the two measured values was greater than 5 nT, the number of readings was increased until stable values were obtained, and the average of the values obtained after the readings became stable was taken as the true value.

For the sake of correction of geomagnetic diurnal variation and monitoring of magnetic storms that might affect the measured values, total magnetic intensities were measured at 5-minute intervals at fixed observation points in both study areas throughout the period of measurement. The fixed observation points were set, respectively, in an orchard in Vehcan village in the southwest part of the Central Shebenik area and in a field south of Prrenjas in the Katjel area. No magnetic storms were observed during the period of measurement.

Besides measurement of total magnetic intensity on the survey lines, measurement of magnetic susceptibility on outcrops and oriented rock sampling for the sake of measurement of natural remanent magnetization were undertaken in the Central Shebenik area, and measurement of magnetic susceptibility on outcrops was undertaken in the Katjel area.

The number of measurements carried out in the two study areas have already been given in

Table 1-1-1

Table 2-2-1 indicates the instruments used for measurement of total magnetic intensity, magnetic susceptibility and remanent magnetization.

Table 2-2-1 Table of instruments for magnetic survey

Item	Type/Model	Specification
Magnetic survey	Proton magnetometer (Scintrex, Canada)	MP-2Resolution : 1 (nT) Total field accuracy : ±1 (nT) Range : 20,000 to 100,000 in 25 overlapping steps Gradient tolerance: Up to 5, 000 (nT/meter)
Susceptibility	Kappameter KT-5 (Geofyzika Brno, Czechoslovakia)	Sensitivity : 1×10^{-5} (SI) Measuring ranges: 9.99,99.9,999$\times10^{-3}$ (SI), automatically switched Operating frequency : 10 (kHz)
	Bartington SM2 (Bartington,G.B.)	
Remnant magnetism	Spinner magnetometer SSM-85 (Natsuhara Giken, Japan) AC Demagnetizer DEM-8601 (Natsuhara Giken, Japan)	

(3) Data Processing and Analysis Methods

a) Correction of Diurnal Variation in Measured Values

On July 26 in the Central Shebenik area and on August 10 in the Katjel area the average total magnetic intensity at the respective fixed observation points was found, and each of them was used as a standard for obtaining the respective diurnal variation in each area. The correction of diurnal variation at each point was performed to map the total magnetic intensity distribution in each area.

b) Terrain Correction of Total Magnetic Intensity

Since the total magnetic intensity after diurnal variation correction was still affected by the terrain,(i.e. magnetic rock bodies in the vicinity of the survey points), such effects had to be eliminated by terrain correction in order to plot a "total magnetic intensity map after terrain correction." The specific method of terrain correction is indicated in Appendix 2-2-1.

After the total magnetic intensity underwent correction of diurnal variation, it was used in filter analyses and 2D profile simulation, in order to consider chrome deposits. Hereinafter total magnetic intensity map means the map produced after terrain corrections had been applied.

c) Filter Analyses

A reduction-to-the-pole filter and an upward-continuation filter were applied.

Reduction-to-the-pole filter analysis is an analytical method whereby the total magnetic intensity for the study region, which has an inclination of 57°, is converted to that which would have been measured at the north pole, which has 90° inclination. After such conversion, magnetic anomalies are expressed directly above the magnetic rock bodies making it easier to compare them with geology and/or geological structure.

Upward-continuation analysis is a method used for the purpose of analyzing variations due to differences in depth of the magnetic rock bodies. Thus, an analysis of depth was undertaken by

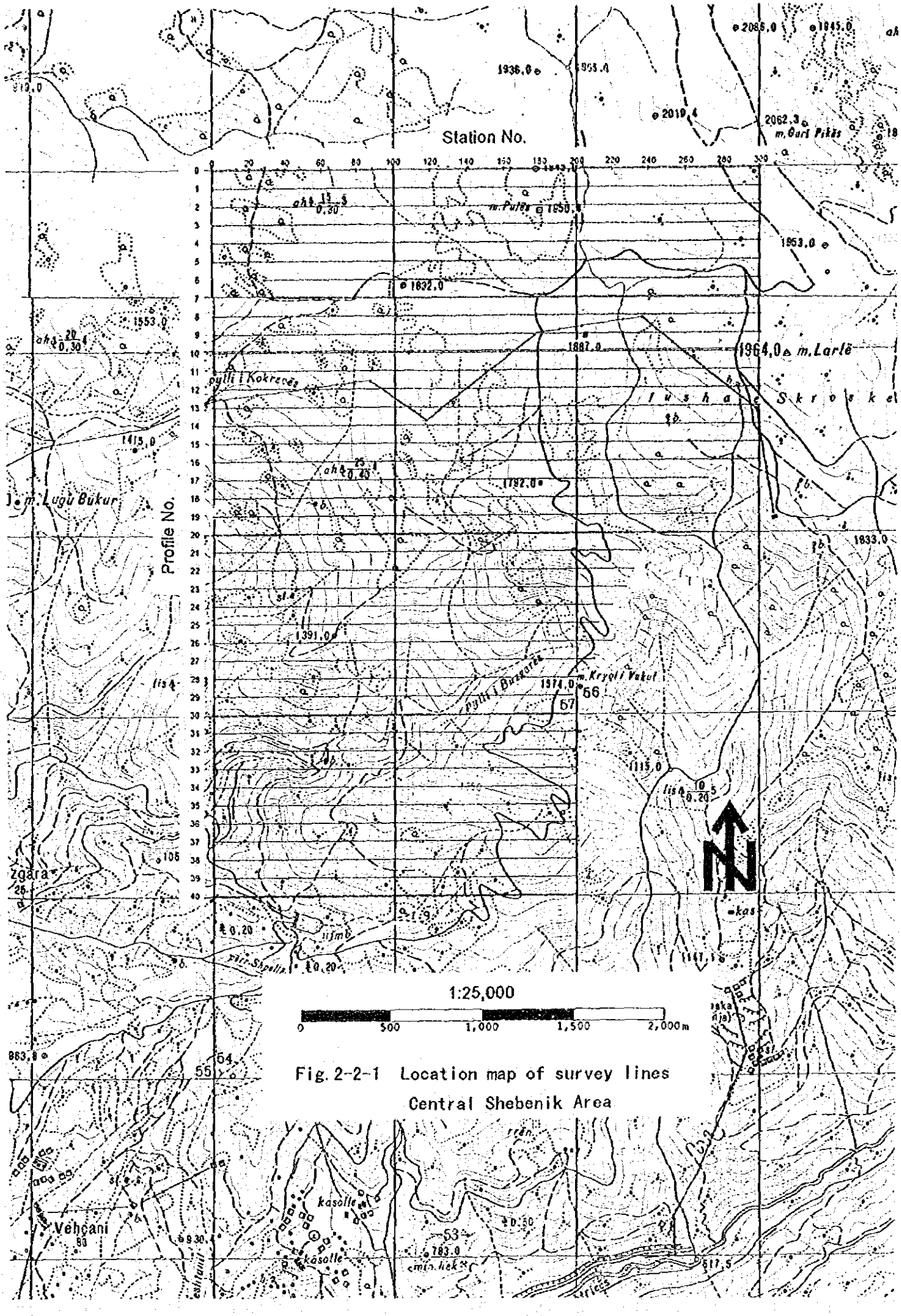

Fig. 2-2-1 Location map of survey lines
Central Shebenik Area

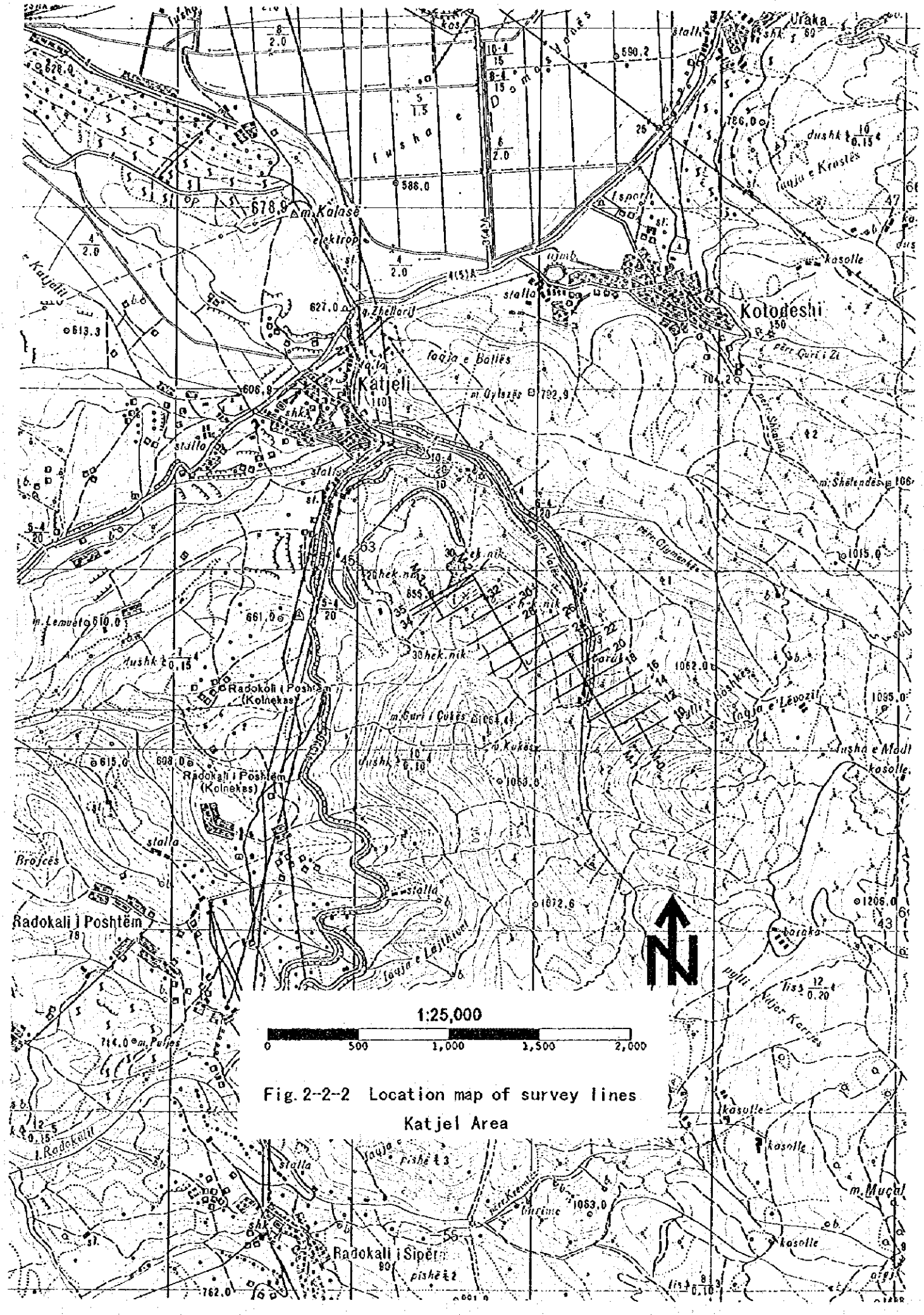

Fig. 2-2-2 Location map of survey lines
Katjel Area

power spectrum with respect to change in frequency obtained from the total magnetic intensity map, and reduction-to-the pole maps were plotted for several depths as a basis for study of magnetic anomalies.

d) 2D Simulation on Profile

2D simulation on profiles is an analytical method whereby simulation is carried out to obtain optimum solutions, with the values of size and magnetic susceptibility of the magnetic rock bodies in the magnetic profiles obtained from the total magnetic intensity map as the parameters.

Changing the parameters by trial and error was repeated with respect to two representative profiles passing through the chrome deposit in the Central Shebenik and Katjel areas, respectively, until an optimum simulation solution was obtained.

2-2-3 Results (Central Shebenik Area)

(1) Distribution of Total Magnetic Intensity

Fig. 2-2-3 gives the total magnetic intensity map after diurnal variation correction, Fig. 2-2-4 the magnetic profiles, and Fig. 2-2-5 the total magnetic intensity map after terrain correction.

Fig. 2-2-3 shows a concentrated distribution of low magnetic anomaly in the ENE-WSW direction along the valley in the southern part of the area and high magnetic anomalies in the same direction to the north and south sides of this low magnetic anomaly. These magnetic anomalies with long wavelength are accompanied and intersected by additional anomalies with medium wavelength that trend in the N15°E direction. As a whole, the northern part of the area has comparatively low values of total magnetic intensity, except for the northwestern sector where there are some high magnetic anomalies strewn in the N15°E direction. In the northeastern sector there are no conspicuous magnetic anomalies, and as a whole the values of total magnetic intensity are low.

In Fig. 2-2-5 not only has terrain correction slightly reduced the difference between maximum and minimum values of total magnetic intensity, but also the color gradation has been reduced from 19 to 18 grades, which makes for a somewhat less clear contrast of magnetic anomalies than in the total magnetic intensity map before terrain correction. Nevertheless, the overall trend of magnetic anomalies is almost the same as that expressed before correction. However, low magnetic anomalies along the valley in the southern part of the area are more strongly expressed after terrain correction.

Of the magnetic lineaments considered as directions of alignment of magnetic anomalies, those with short wavelength have a direction of N15°E throughout the area, which is different from the general direction of N30°W of the foliated structure seen in the ultrabasic rocks of the larger area. Most of those with medium wavelength also have a direction of N15°E, although some have a direction of N30°W in the eastern half of the northern part of the area.

(2) Filter Analyses

a) Reduction-to-the-Pole

Fig. 2-2-6 gives the reduction-to-the-pole map, in which the values of total magnetic intensity after terrain correction have been converted to what they would be at the north pole.

Since the color gradation has been reduced to 16 grades, the pattern of magnetic anomalies in the reduction-to-the pole map has a somewhat different appearance from that of the above-mentioned total magnetic intensity map, but the basic pattern of distribution of magnetic anomalies is very similar. It includes: the low magnetic anomalies in the ENE-WSW direction along the valley in the

southern part of the area and the high magnetic anomalies to the south of that; the high magnetic anomalies seen as somewhat concentrated within the generally low magnetic intensity in the western half of the northern part of the area; and the low magnetic anomalies of the eastern half of the northern part of the area. However, the distribution of the high magnetic anomalies to the north of the low magnetic anomalies in the ENE-WSW direction is somewhat reduced, with wider expression of low magnetic anomalies. The trend of the magnetic anomalies with short and medium wavelength is about the same as in the total magnetic intensity map.

b) Upward Continuation Analysis

As a result of depth analysis carried out on the basis of the power spectrum given in Fig. 2-2-7, obtained from frequency analysis of the total magnetic intensity map, the spatial geomagnetic waves of the area were broken down into three constituents: a short-wavelength constituent with an average depth of 20 m, a medium-wavelength constituent with an average depth of 50 m and a long-wavelength constituent with an average depth of 250 m. The boundary depths between those three constituents were set as 35 m and 150 m on the basis of the medians of the respective average depths.

Fig. 2-2-8 gives the reduction-to-the-pole map obtained by extracting the shallow component with a depth to 35 m on the basis of the above-mentioned depth analysis, Fig. 2-2-9 gives the reduction-to-the-pole map obtained by extracting the medium-deep component with a depth from 35 m to 150 m, and Fig. 2-2-10 gives the reduction-to-the-pole map obtained by extracting the deep component with a depth greater than 150 m.

b-1) Reduction-to-the-Pole Map with Extraction of the Shallow Component

Many low magnetic anomalies and weak high magnetic anomalies in the direction N10°W - N15°E can be seen in the reduction-to-the-pole map with extraction of the shallow component (Fig. 2-2-8). In particular, in the southern half of the area there is an alternating distribution of rather concentrated low magnetic anomalies and weak high magnetic anomalies, and there is a distribution of low magnetic anomalies trending in the ENE-WSW direction along the valley. In the northern half of the area the number of magnetic anomalies is less than in the southern half, and the prevailing orientation is in the NS to N15°E direction. In addition, along the eastern edge of the area there are sporadic high magnetic anomalies with principal axes in the N10°W direction.

Although the magnetic anomalies in this depth range (from surface to depth of 35 m) of the reduction-to-the-pole map with extraction of the shallow component can be considered to reflect the magnetic properties of the rocks near the surface, a clear correspondence with the geological map given in Fig. 2-1-1 is not to be seen. That may be because of migration of magnetic rock bodies due, for example, to faults developed in the area and because of change in the magnetic properties of the rocks due to difference in the degree of weathering.

b-2) Reduction-to-the-Pole Map with Extraction of the Medium-Deep Component

In the reduction-to-the-pole map with extraction of the medium-deep component (Fig. 2-2-9) there are low-contrast high and low magnetic anomalies in the northern half of the area that trend in the N15°E direction as revealed by shadow effects used in this map. A secondary trend of anomalies in the N30°W direction can be seen in the northeast corner of the zone. In the southern half of the area, besides the distribution of high and low magnetic anomalies repeating with a characteristic wavelength of 150-300 m in the N15°E direction, there are also: low magnetic anomalies in the ENE-WNW direction along the valley; high magnetic anomalies running in the same direction on both the

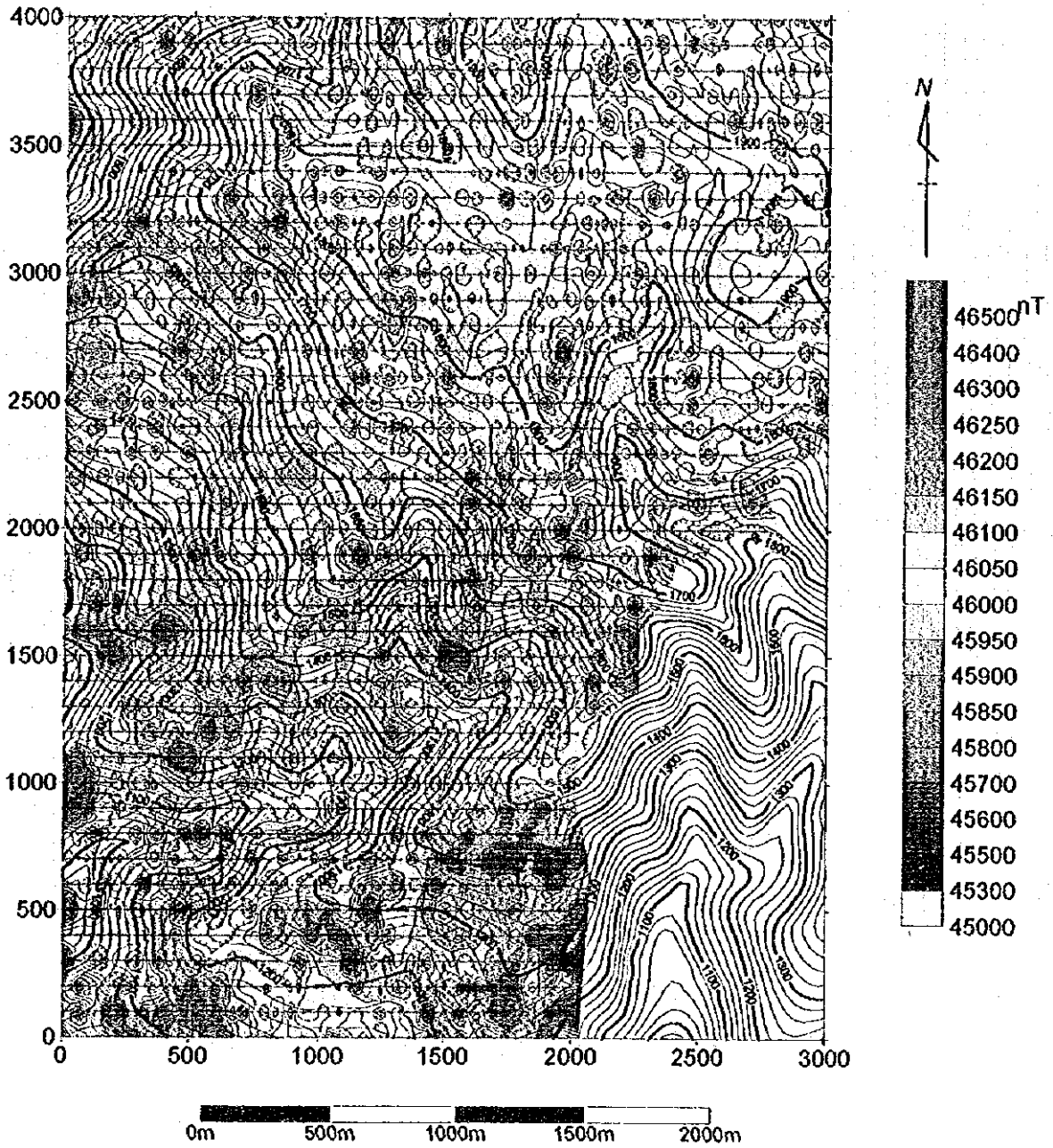

Fig. 2-2-3 Total magnetic intensity map, Central Shebenik Area

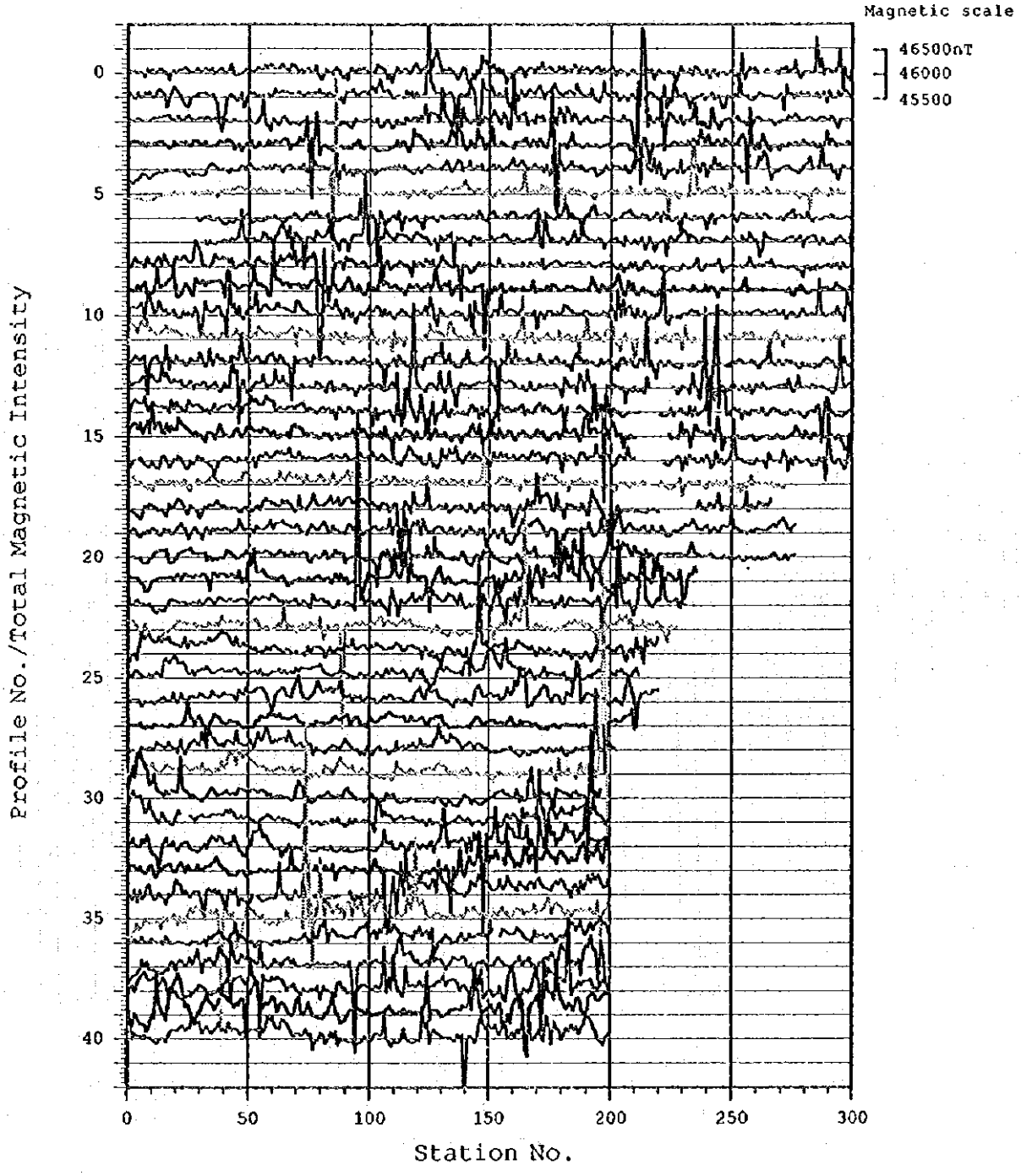

Fig. 2-2-4 Magnetic profiles, Central Shebenik Area

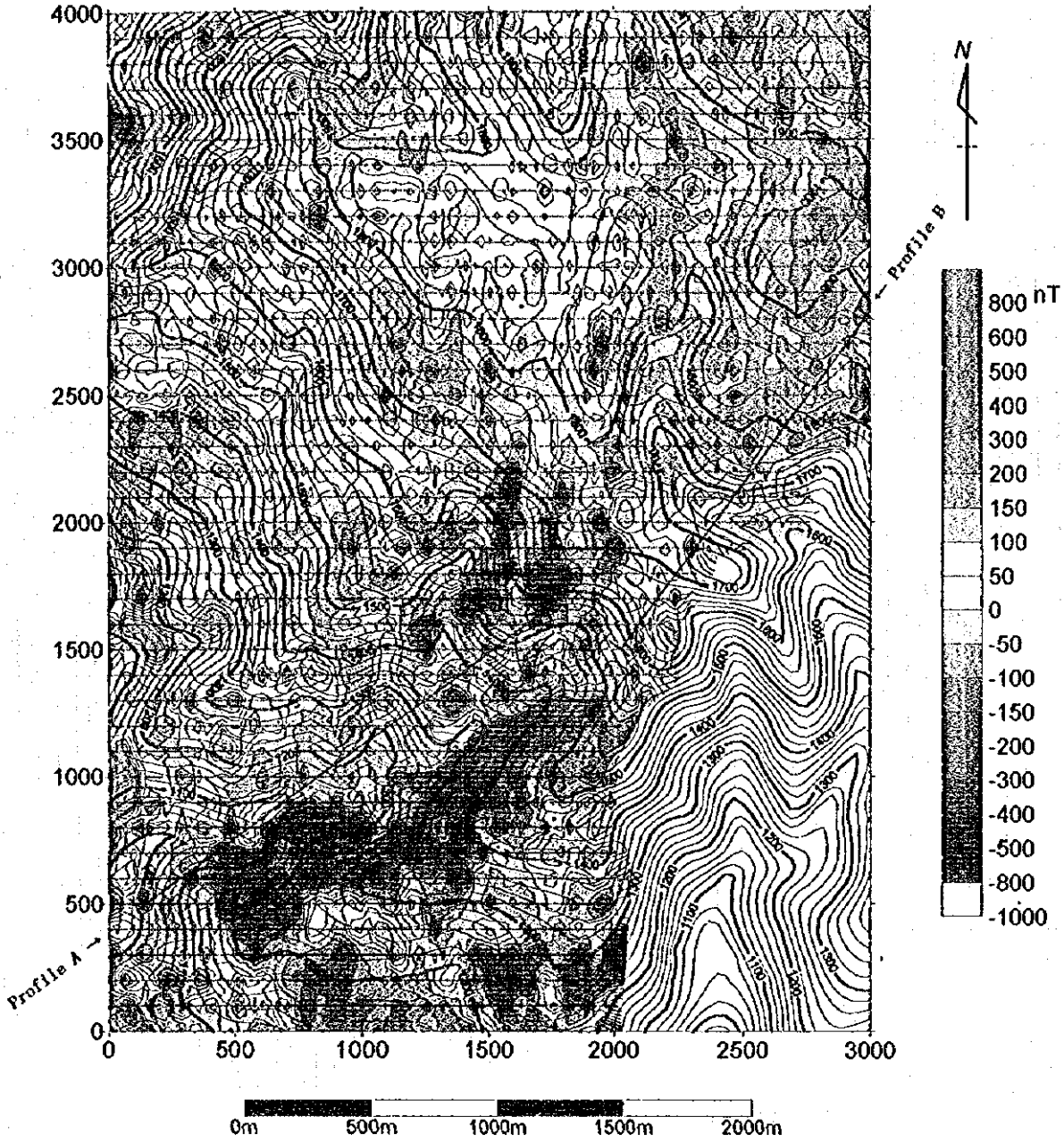

Fig. 2-2-5 Total magnetic intensity map (topography compensated), Central Shebenik Area

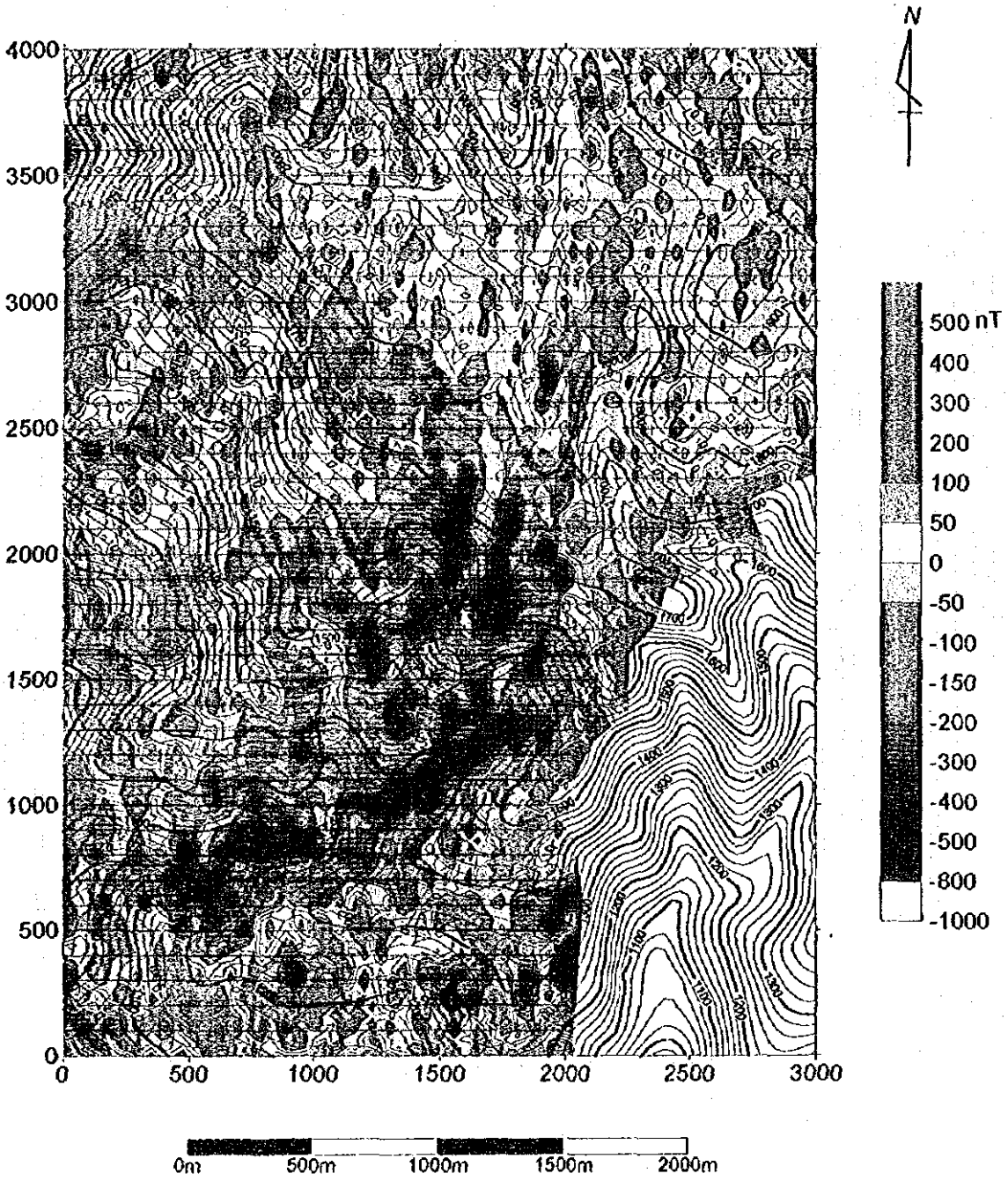

Fig. 2-2-6 Reduction to the pole map, Central Shebenik Area

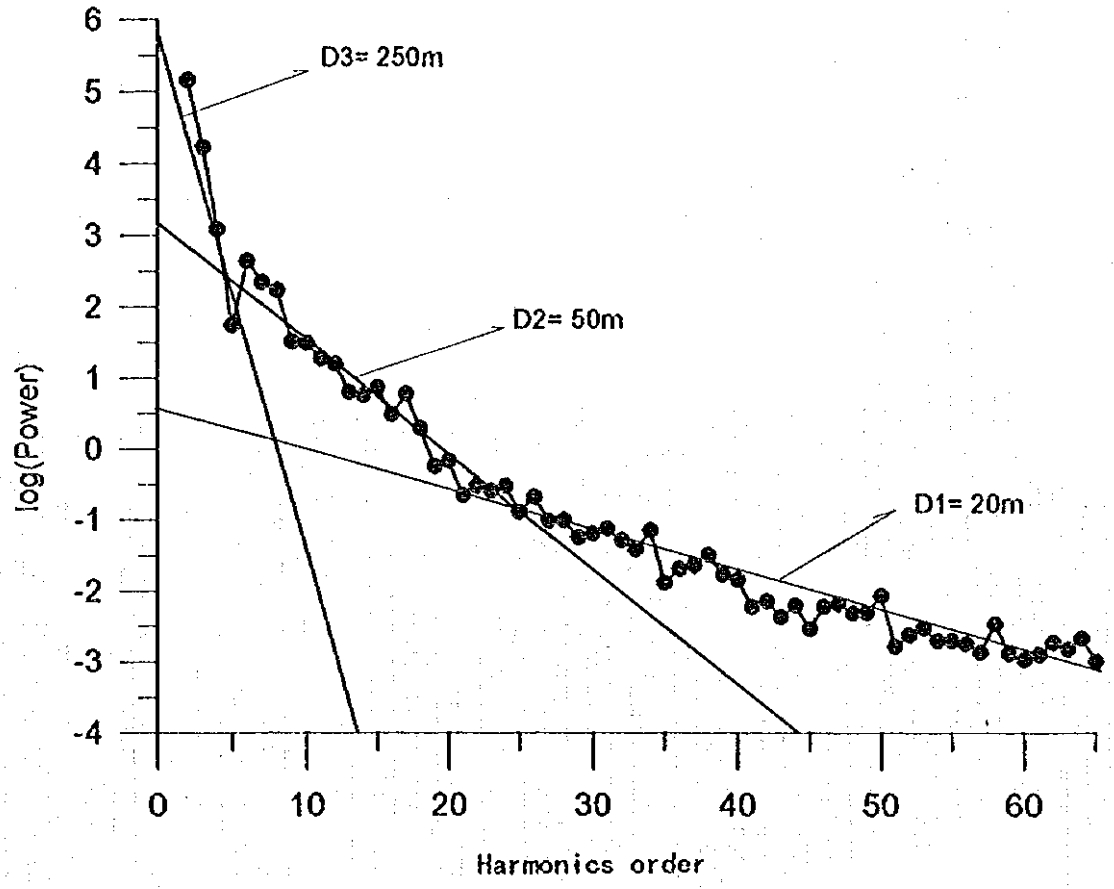

Fig. 2-2-7 Magnetic spectra, Central Shebenik Area

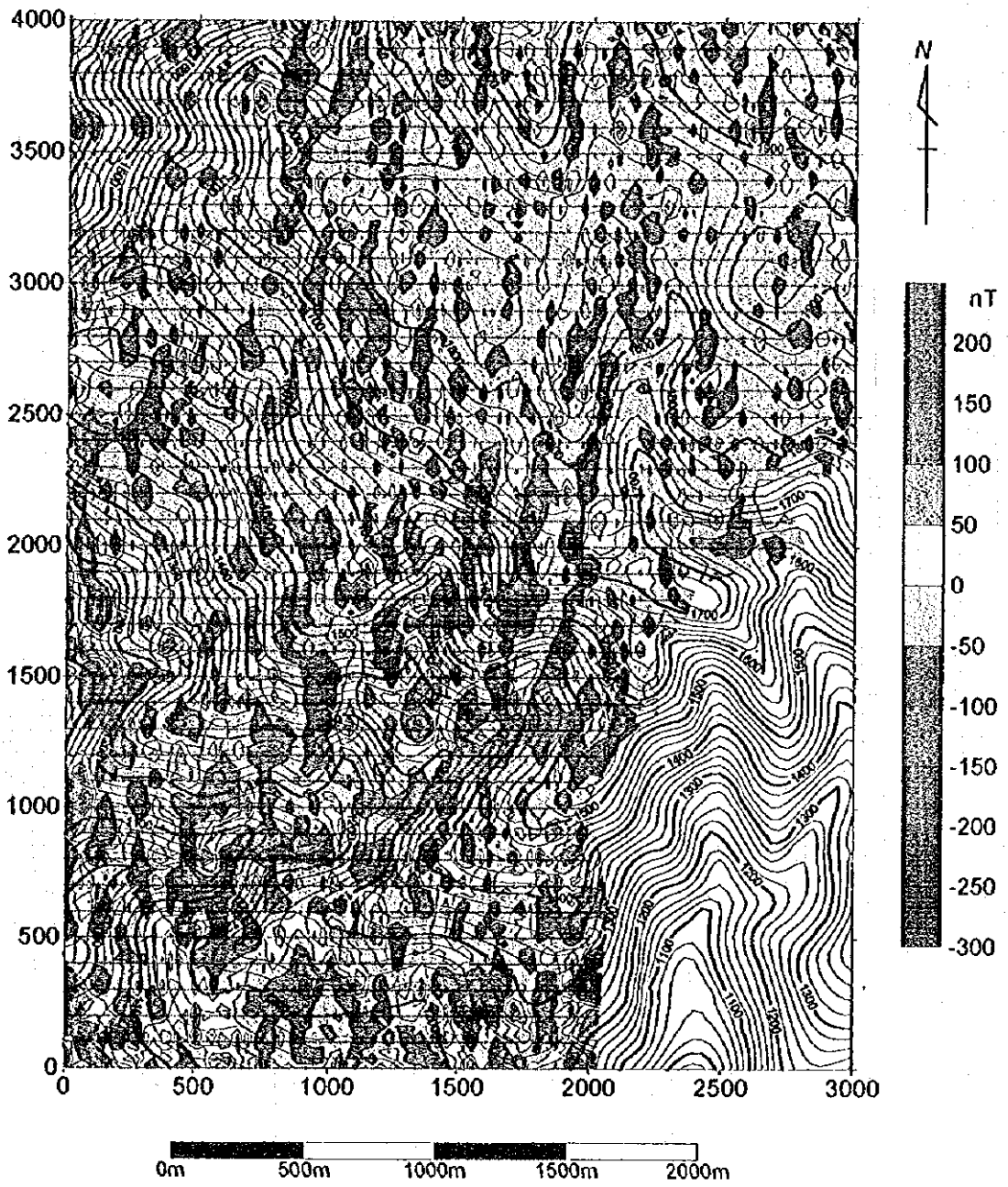

Fig. 2-2-8 Reduction to the pole map (shallow component extracted), Central Shebenik Area

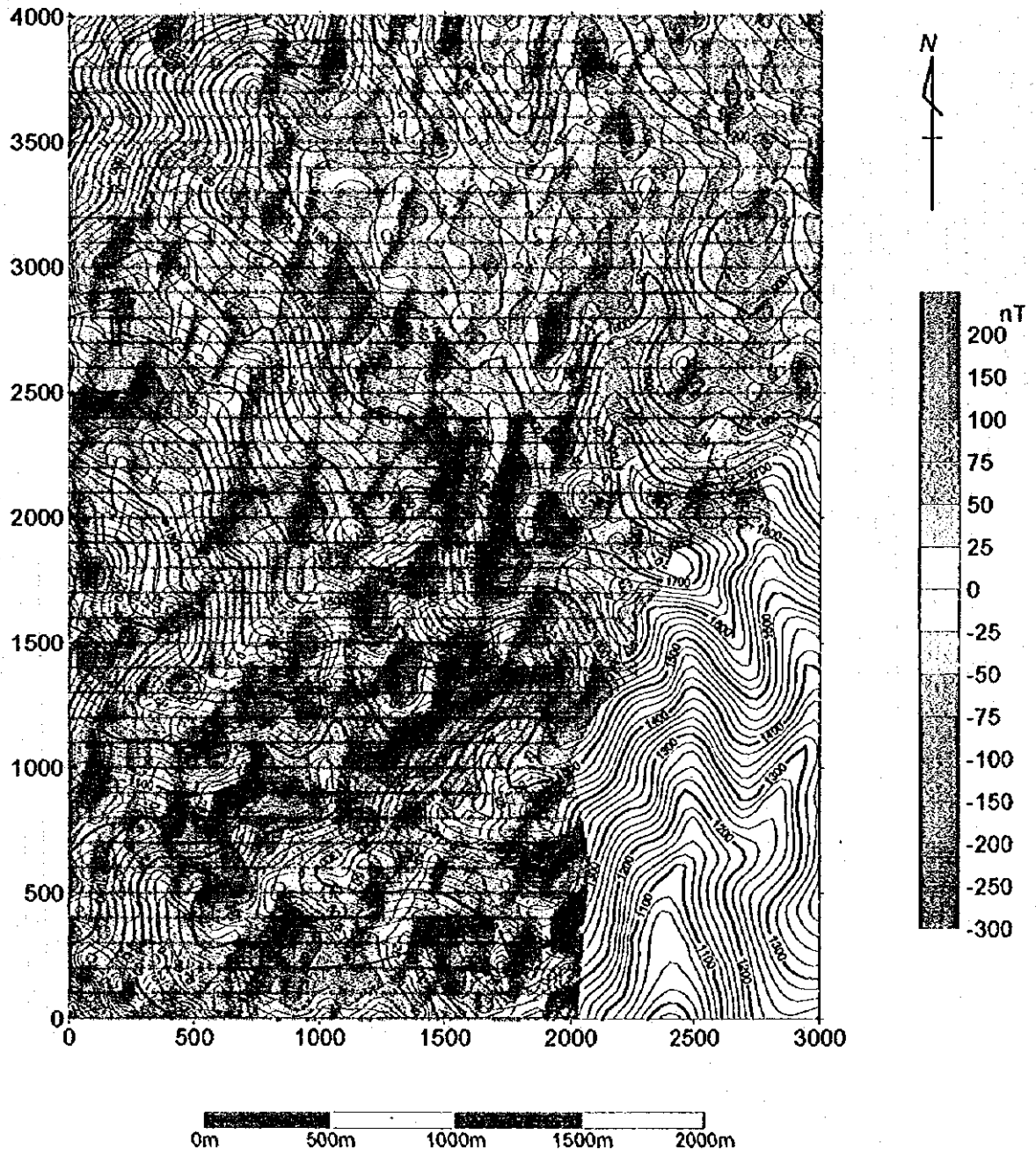

Fig. 2-2-9 Reduction to the pole map (middle component extracted), Central Shebenik Area

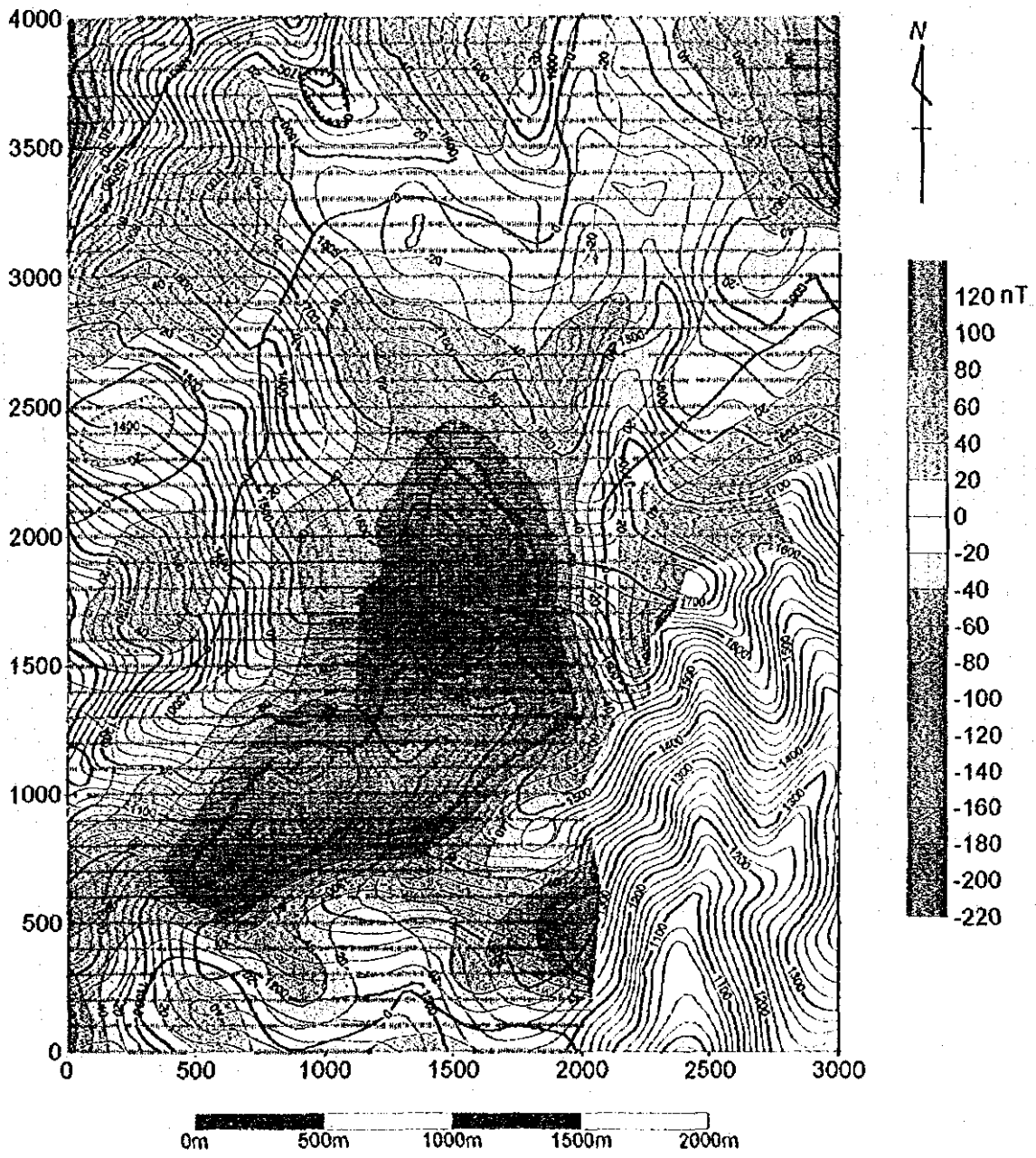

Fig. 2-2-10 Reduction to the pole map (deep component extracted), Central Shebenik Area

north and south sides thereof; and high magnetic anomalies in the N30°W direction on the eastern edge.

A good correspondence between magnetic anomalies in this depth range and the geological map is expected because of the fact that there is little influence of surface weathering at this depth. However, in this case there is no clear correspondence between magnetic anomalies and geology other than a rough coincidence of magnetic anomalies with weak-contrast trending in the N30°W direction in the northeast corner of the area with the DHSRL (dunite-harzburgite suite with remarkable layering) and the fact that low magnetic anomalies are frequently to be noted in the Dunite-rich zone of the MDHS (massive dunite-harzburgite suite).

Furthermore, because of the fact that a distinctive high magnetic anomaly trending in the N30°W direction is to be seen in the vicinity of the Ahu i Vetem and Lugu i Batres chromitite deposits in the northeastern corner of the southern half of the area and the fact that a pattern of distinctive high and low magnetic anomalies is to be seen in the vicinity of the Buzgare and other deposits distributed along the valley and its vicinity in the southern part of the area, four zones with anomalies analogous to that pattern were selected as significant magnetic anomaly zones. Moreover, a circular lineament of high magnetic anomalies was extracted in the southern half of the area extending from the Lugu i Batres deposit to the Ahu i Vetem deposit and on to the southwest corner of the area.

b-3) Reduction-to-the-Pole Map with Extraction of the Deep Component

In the reduction-to-the-pole map with extraction of the deep component (Fig. 2-2-10) a large low magnetic anomaly is distributed from along the valley in the southern part of the area to the middle of the northern half of the area, and high magnetic anomalies are distributed around it on the south, east and northwestern sides. Furthermore, a low anomaly is to be seen in the northeast corner of the area.

Although it is difficult to accurately estimate the geology at this depth (depths of more than 150 m), it is expected that there is a wide distribution of harzburgite accompanied by dunite.

It can be considered that the large low magnetic anomaly extending from the southern part of the area to the middle of the northern half is a reflection of the influence of the natural remanent reverse magnetization of rocks in view of the fact that, as will be discussed later, many of the rock samples collected in this large low magnetic anomaly zone showed reverse magnetization. However, one can also not deny the possibility that the terrain correction of total magnetic intensity was not sufficient for the survey points in and near the valley. It might be added that it is surmised that the low magnetic anomaly in the northeastern corner of the area are a reflection of the fact that the above-mentioned DHSRL may be found at depth in this region.

(3) Magnetic Susceptibility

Magnetic susceptibility was measured on 97 outcrops in the Central Shebenik area using the Kappameter KT-5. The locations of the outcrops are indicated in Fig. 2-2-11, the results of the measurements in Table 2-2-2, and the statistics in Table 2-2-3 and Fig. 2-2-12. The breakdown by rock type is: harzburgite at 61 outcrops, dunite at 49 outcrops, chromitite at 9 outcrops, serpentine at 1 outcrop and pyroxenite at 3 outcrops.

Since, as indicated in Fig. 2-2-12, not much of a difference was noted in the average value of magnetic susceptibility between the different rock types and, furthermore, there was a reasonably large dispersion of measured values within each rock type, it is believed that there is no significant

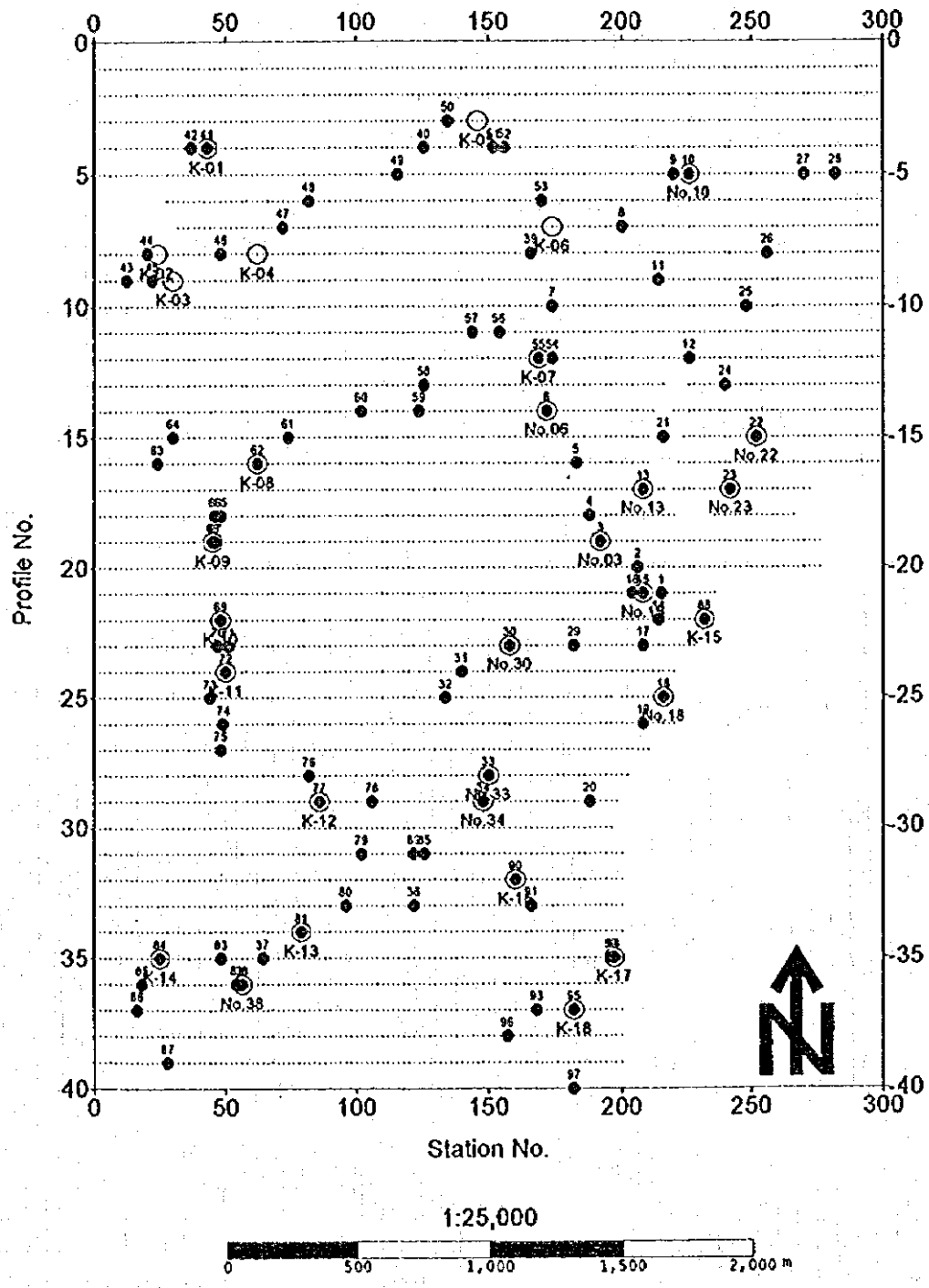

Fig. 2-2-11 Location map of oriented rock samples and susceptibility measurements, Central Shebenik Area

Table 2-2-2 Magnetic susceptibility, Central Shebenik (1/2)

No.	Location		Data1	Data2	Data3	Data4	Data5	Data6	Correction factor	Susceptibility $\times 10^{-3}$ SI	Description	Oriented sampling
	Profile	Station										
1	21	215	2.89	2.93	2.82				1.15	3.31	Hz	
			2.05	1.80	1.40	1.52	1.51		1.15	1.90	Hz	
2	20	206	3.02	3.25	2.90				1.15	3.52	Hz	
			6.49	8.08	4.95				1.15	7.48	Hz	
			6.27	10.20	9.64	9.91			1.15	10.36	Serpentinization	
3	19	192	9.68	9.35	9.86				1.15	11.07	Hz	No.3
4	18	188	6.35	4.99	3.82	6.36			1.15	6.19	Hz	
5	16	183	1.42	1.78	1.74				1.15	1.89	Hz	
6	14	172	3.40	4.59	3.49	3.32			1.15	4.26	Hz	
			2.66	2.81	2.75				1.15	3.15	Hz	No.6
7	10	174	1.46	1.76	1.63				1.15	1.86	Hz	
8	7	200	0.78	0.80	0.80				1.15	0.91	Hz	
9	5	220	0.83	0.85	0.87				1.15	0.98	Hz	
			1.98	1.99	1.92				1.15	2.26	Hz	
10	5	226	1.94	1.96	1.74				1.32	2.48	Du	
			2.22	2.28	2.43				1.15	2.66	Du	No.10
11	9	214	0.97	0.99	0.99				1.15	1.13	Hz	
12	12	226	4.13	4.28	4.75				1.15	5.04	Hz	
13	17	208	1.71	1.72	1.68				1.15	1.96	Hz	No.13
14	22	214	2.45	1.94	2.21	1.88			1.57	3.33	Cr	
			2.62	2.40	2.20				1.37	3.30	Cr	
			1.48	1.33	1.48				1.15	1.64	Cr	
15	21	208	1.77	1.72	1.82				1.15	2.04	Du	No.15
16	21	204	2.51	2.21	1.95	2.23			1.23	2.74	Cr	
17	23	208	3.75	3.56	3.72				1.23	4.52	Px	
18	25	216	1.81	1.79	1.84				1.15	2.09	Du	
			2.32	2.34	2.20				1.15	2.63	Du	No.18
19	26	208	1.07	1.12	1.03				1.15	1.23	Hz	
			1.61	1.62	1.79				1.23	2.06	Du	
			0.99	1.02	1.02				1.15	1.16	Hz	
20	29	188	1.33	1.05	0.99	1.05			1.15	1.27	Hz	
21	15	216	6.38	7.04	7.34	5.92			1.15	7.67	Du	
22	15	252	1.59	1.65	1.62				1.15	1.86	Hz	No.22
			1.04	1.08	1.01				1.15	1.20	Hz	
23	17	242	0.96	0.96	0.95				1.32	1.26	Hz	
			3.12	3.76	3.70				1.15	4.06	Du	No.23
			4.02	3.60	3.77				1.15	4.37	Du	
			2.46	2.55	2.55				1.15	2.90	Du	
			1.63	1.56	1.67				1.15	1.86	Du	
			2.27	2.28	2.20				1.15	2.59	Du	
			2.69	2.52	2.60				1.15	2.99	Cr	
24	13	240	2.13	2.12	2.15				1.15	2.45	Hz	
25	10	248	1.22	1.26	1.25				1.15	1.43	Hz	
26	8	255	0.75	0.81	0.78				1.15	0.90	Hz	
27	5	270	1.11	1.13	1.08				1.15	1.27	Hz	
28	5	282	1.21	1.17	1.08				1.15	1.33	Hz	
			2.61	2.63	2.53				1.15	2.98	Du	
			2.71	2.73					1.15	3.13	Du	
			1.06	1.14	1.06				1.15	1.25	Hz	
29	23	182	1.19	1.13	1.15				1.15	1.33	Hz	
30	23	158	1.40	1.43	1.49	1.34			1.15	1.63	Hz	
			2.27	2.24	2.37				1.15	2.64	Hz	No.30
31	24	140	2.59	2.50	2.77	2.65			1.15	3.02	Hz	
32	25	134	2.24	2.36	2.18				1.15	2.60	Du	
33	28	150	1.73	1.64	1.70				1.15	1.94	Hz	
			1.56	1.82	1.83				1.15	2.00	Hz	No.33
34	29	148	3.95	3.50	3.59				1.15	4.23	Hz	No.34
35	31	126	2.40	2.15	1.93	2.08			1.15	2.46	Hz	
36	33	122	2.72	2.51	2.77				1.15	3.07	Hz	
37	35	61	1.91	1.91	1.83				1.15	2.17	Cr	
			1.88	1.91	1.86	1.93			1.15	2.18	Cr	
			1.90	1.90	1.89	1.86			1.15	2.17	Cr	
38	36	56	1.05	0.94	1.29	1.05			1.15	1.24	Du	No.38
39	8	166	1.32	1.32	1.31	1.32			1.15	1.52	Du	
40	4	126	2.07	2.11	2.10	2.07			1.15	2.40	Du	

Table 2-2-2 Magnetic susceptibility, Central Shebenik (2/2)

No.	Location		Data1	Data2	Data3	Data4	Data5	Data6	Correction factor	Susceptibility $\times 10^{-3}$ SI	Description	Oriented sampling
	Profile	Station										
41	4	43	3.48	3.51	3.56	3.45			1.15	4.03	Du	
42	4	37	1.26	1.22	1.23	1.23			1.15	1.42	Du	
43	9	12	3.68	3.80	3.89	3.62			1.15	4.31	Du	
44	8	20	2.09	2.43	2.26	2.39			1.15	2.64	Du	
45	9	22	6.47	7.26	7.12	7.17			1.15	8.06	Du	
46	8	48	6.30	5.83	6.32	6.21			1.15	7.09	Du	
47	7	72	1.46	1.37	1.45	1.84	1.81		1.15	1.82	Hz	
48	6	82	2.61	2.78	2.93	2.85			1.15	3.21	Hz	
49	5	116	2.08	2.15	2.18	2.15			1.15	2.46	Du	
50	3	135	1.61	1.65	1.60	1.71			1.15	1.89	Du	
51	4	152	3.22	3.13	3.31	3.31			1.15	3.73	Du	
52	4	156	1.22	1.14	1.14	1.20			1.15	1.35	Hz	
53	6	170	4.07	4.54	3.84	3.91	3.73		1.15	4.62	Du	
54	12	174	12.50	11.60	12.80	13.90	15.60	12.10	1.15	15.05	Du	
55	12	169	2.86	2.71	2.80	2.80			1.15	3.21	Hz	K-7
56	11	154	2.55	2.60	2.66	2.87	3.34	2.58	1.15	3.18	Du	
57	11	144	1.31	1.20	1.27	1.11	1.15		1.15	1.39	Du	
58	13	126	1.17	1.19	1.31	1.38	1.36	1.38	1.15	1.49	Du	
59	14	124	1.55	1.57	1.51	1.59	1.59		1.15	1.80	Hz	
60	14	102	4.07	3.80	3.81	3.72	3.80		1.15	4.42	Du	
61	15	74	7.16	6.11	6.54	7.52	7.54		1.15	8.02	Du	
62	16	62	2.42	2.66	2.63	2.43			1.15	2.92	Hz	K-8
63	16	24	16.50	19.10	20.00	19.30	18.80		1.15	21.55	Du	
64	15	30	2.93	2.95	2.87	2.82	3.01		1.15	3.35	Hz	
65	18	48	1.51	1.51	1.80	1.71	1.53	1.19	1.15	1.77	Du	
66	18	46	2.64	2.33	2.38	2.35	2.30		1.15	2.76	Du	
67	19	46	1.18	1.17	1.17	1.19			1.15	1.35	Hz	
68	19	45	1.02	1.07	1.07	1.06			1.15	1.21	Hz	K-9
69	22	48	4.49	5.24	5.33	5.31			1.15	5.86	Hz	K-10
70	23	47	2.95	2.93	2.95	2.94			1.15	3.38	Du	
71	23	51	1.62	1.65	1.62	1.62	1.57		1.15	1.86	Hz	
72	24	50	1.26	1.30	1.35	1.25			1.15	1.48	Px	K-11
73	25	44	4.08	4.28	4.24	4.05			1.15	4.79	Hz	
74	26	49	3.94	4.02	3.96	3.95			1.15	4.56	Hz	
75	27	48	7.59	7.89	6.64	7.62	7.40		1.15	8.54	Du	
76	28	82	1.98	1.81	1.91	2.00			1.15	2.21	Hz	
77	29	86	2.89	2.83	2.92	2.89			1.15	3.31	Du	K-12
78	29	106	3.36	3.29	3.31	3.28			1.15	3.81	Du	
79	31	102	1.33	1.38	1.24	1.23	1.25		1.15	1.48	Hz	
80	33	96	1.16	1.12	1.15	1.16			1.15	1.32	Hz	
81	34	79	2.69	2.74	2.76	3.20	2.96		1.15	3.30	Hz	K-13
82	36	54	5.29	5.68	5.67	5.23			1.15	6.29	Hz	
83	35	48	6.58	6.78	6.77	6.93			1.15	7.78	Du	
84	35	25	5.96	5.87	5.97	5.97			1.15	6.83	Hz	K-14
85	36	18	5.11	4.87	5.96	4.54	4.55	4.62	1.15	5.68	Du	
86	37	16	13.60	13.70	13.70	13.60			1.15	15.70	Du	
87	39	28	15.00	14.90	15.10	15.00			1.15	17.25	Du	
88	22	232	3.77	3.19	3.20	3.23			1.15	3.85	Cr	K-15
			4.07	3.89	3.80	4.02			1.15	4.54	Du	
89	31	122	9.81	11.90	11.80	11.60	10.70		1.15	12.84	Du	
90	32	160	0.70	0.66	0.66	0.65			1.15	0.77	Px	K-16
91	33	166	2.48	2.35	2.27	2.22	2.25		1.15	2.66	Hz	
92	35	196	1.53	1.51	1.51	1.50			1.15	1.74	Hz	
93	37	168	6.00	6.25	6.49	6.25			1.15	7.18	Hz	
94	35	197	6.17	6.15	6.17	6.16			1.15	7.09	Hz	K-17
95	37	182	4.00	3.99	4.00	3.92			1.15	4.57	Hz	K-18
96	38	157	18.80	17.80	17.80	17.90			1.15	20.79	Du	
97	40	182	10.70	10.70	10.60	11.10			1.15	12.39	Du	
98	4	43									Hz	K-1
99	8	24									Hz	K-2
100	9	30									Hz	K-3
101	8	62									Hz	K-4
102	3	146									Hz	K-5
103	7	174									Hz	K-6

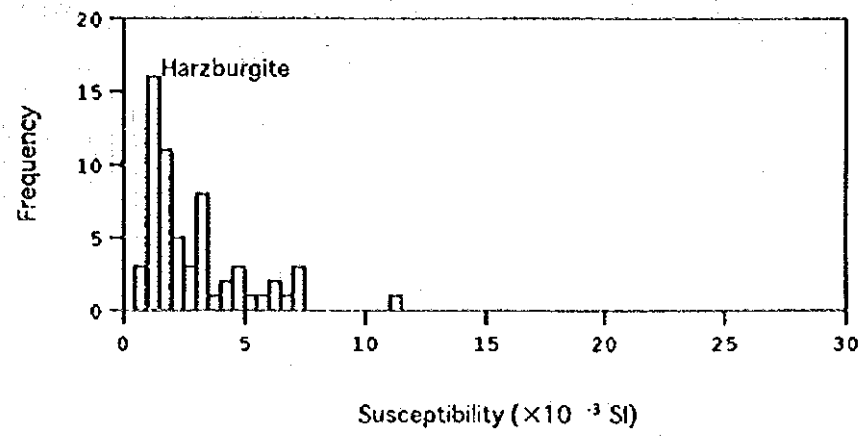

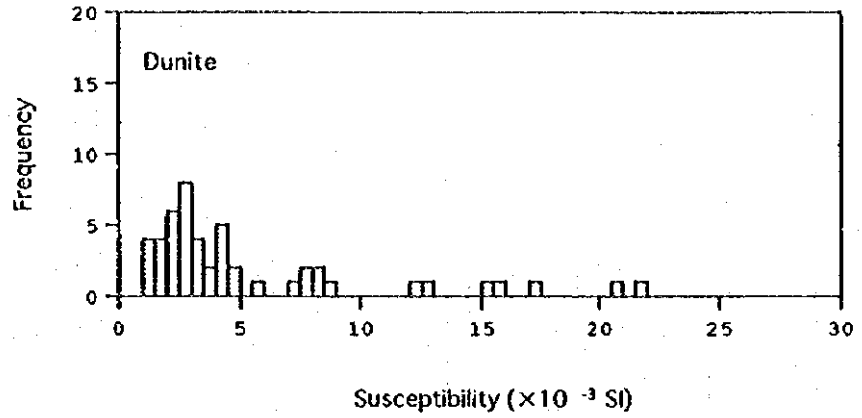

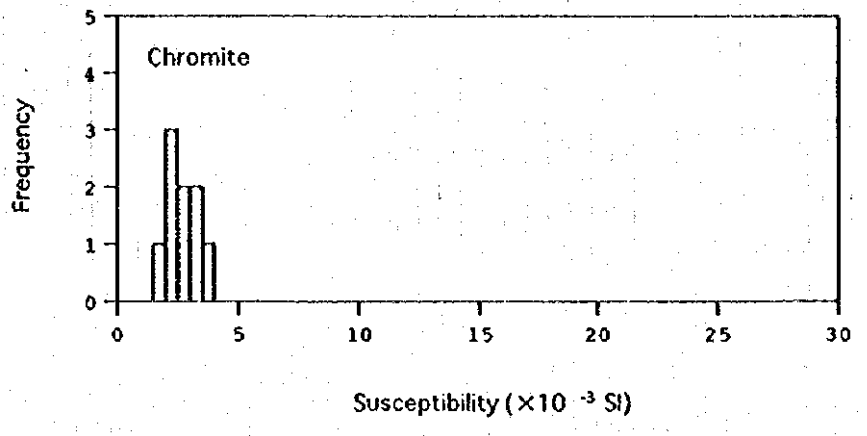

Fig. 2-2-12 Histogram of susceptibility, Central Shebenik Area

Table 2-2-3 Statistics of magnetic susceptibility of the Central Shebenik area

Description	Number of samples	Susceptibility ($\times 10^{-3}$ SI)				
		Minimum	Maximum	Median	Average	Std.Dev.
Harzburgite	61	0.90	11.1	2.00	2.92	2.05
Dunite	49	1.24	21.6	3.31	5.45	5.04
Chromitite	9	1.64	3.85	2.74	2.71	0.72
Serpentinite	1	—	—	10.4	—	—
Pyroxenite	3	0.77	4.52	1.48	2.26	1.99

Remarks; Std.Dev.: Standard Deviation

difference in magnetic susceptibility among the different rock types. However, as indicated in Table 2-2-3, the standard deviation for dunite was greater than for the other rock types, and some of the dunite samples had values greater than harzburgite and chromitite.

In view of the absence of significant difference in magnetic susceptibility among different rock types in the Central Shebenik area it would be difficult to explain the above-mentioned extreme low magnetic anomalies in the reduction-to-the-pole map in terms of induction magnetic fields attributable to differences in the magnetic susceptibility of the rocks.

(4) Natural Remanent Magnetization

Thirty oriented rock samples were collected for the purpose of studying the natural remanent magnetization of the different rock types distributed in the Central Shebenik area. Fig. 2-2-11 gives the sampling points along with the locations of the above-mentioned outcrops on which magnetic susceptibility measurement was made. Since one of the oriented samples was damaged during preparation in the laboratory, natural remanent magnetization and magnetic susceptibility were measured on the remaining 29 samples, of which 20 were harzburgite, 6 were dunite, 2 were pyroxenite and 1 was chromitite.

The results of the measurements are given in Table 2-2-4. As indicated in that table, all but one of the samples (No. 6: harzburgite) showed sufficiently high values for coercive force.

The orientation of natural remanent magnetization showed inverse direction of magnetization, i.e. opposite to the present geomagnetic field, in the case of five of the six dunite samples and about the same direction as the present geomagnetic field in the case of the sixth dunite sample. Of the 19 harzburgite samples, 5 showed opposite direction of magnetization, 11 the same direction as the present geomagnetic field, and 2 different direction from the present geomagnetic field, the relationship of the remaining harzburgite sample with respect to the geomagnetic field being unclear. The two pyroxenite samples and the single chromitite sample each showed magnetization of about the same direction as the present geomagnetic field.

Considering these results, it is noteworthy that dunite has a rather high probability of reverse magnetization (a probability of 5/7 = 0.714 if the chromitite sample is included) in comparison with the other types of rocks, the probability of reverse magnetization of harzburgite being only 5/19 = 0.263 and that probability declining still further to 5/21 = 0.238 if pyroxenite, which is considered to have been formed near the end of its activity, is included..

In view of the fact that the measurement samples were collected in a small area of only about 10 km^2, such differences in natural remanent magnetization orientation can be considered to be attributable to differences in the earth's magnetic field at the time of acquisition of magnetization and

Table 2-2-4 Magnetic susceptibility and remnant magnetization of the Central Shebenik area

No.	Sample Number	Rock facies	Susceptibility (SI)		Susceptibility (CGS)		NRM	Q	Core sample coordinates		Geographic coordinates		Coercively	Orientation of magnetization
			LF(0.46kHz)	HF(4.6kHz)	LF(0.46kHz)	HF(4.6kHz)	A/M		Declination	Inclination	Declination	Inclination	(Oe)	
			$\times 10^{-4}$	$\times 10^{-4}$	$\times 10^{-5}$	$\times 10^{-5}$	$\times 10^{-2}$							
1	K-1	Hz	3.70	3.70	2.95	2.95	16.80	12	22.0	30.5	23.5	30.5	100～700	●
2	K-4	Hz	1.11	1.11	0.881	0.881	8.08	20	36.1	31.5	37.6	31.5	100～600	●
3	K-5	Hz	1.69	1.69	1.35	1.35	11.30	18	42.9	-27.0	44.4	-27.0	200～700	○
4	K-6	Hz	1.02	1.02	0.811	0.811	4.76	13	22.0	34.3	23.5	34.3	100～700	◉
5	No.10	Du	2.79	2.79	2.22	2.22	20.00	20	-25.0	-48.1	37.4	-44.5	100～700	○
6	K-8	Hz	3.83	3.83	3.04	3.04	22.20	16	62.3	24.4	63.8	24.4	150～700	+
* 7	No.6	Hz	3.49	3.49	2.78	2.78	15.10	12	46.0	38.0	5.4	56.1	25～200	●
8	No.3	Hz	8.41	8.41	6.70	6.70	46.50	15	14.8	48.1	21.3	49.5	100～700	●
9	No.22	Hz	1.27	1.27	1.01	1.01	18.60	40	-79.0	22.7	62.4	-38.2	100～500	○
10	No.23	Du	2.03	2.03	1.61	1.61	12.60	17	-23.5	-45.0	39.6	-45.6	100～700	○
11	K-10	Hz	2.28	2.28	1.81	1.81	6.19	7	-106.4	-85.9	-104.9	-85.9	100～500	○
12	K-12	Du	3.97	3.97	3.16	3.16	6.82	5	133.2	-76.6	134.7	-76.6	100～500	○
13	No.30	Hz	2.31	2.31	1.84	1.84	112.00	132	149.8	-21.0	38.3	1.6	200～700	○
14	No.33	Hz	1.21	1.21	0.966	0.966	2.58	6	-76.0	3.3	30.9	-24.8	50～700	○
15	No.15	Du	1.96	1.96	1.56	1.56	5.47	8	-100.6	37.6	18.3	-63.6	100～700	○
16	No.18	Du	2.12	2.12	1.68	1.68	10.40	13	-135.0	0.8	14.1	-21.3	150～700	○
17	K-15	Cr	3.85	3.85	3.07	3.07	12.60	896	-2.0	58.6	-0.5	58.6	75～700	●
18	K-13	Hz	0.895	0.895	0.712	0.712	2.23	7	20.1	72.2	21.6	72.2	25～400	●
19	No.32	Du	1.27	1.27	1.01	1.01	5.71	12	127.0	18.8	3.4	45.3	25～500	●
20	K-16	Px	5.88	5.88	4.68	4.68	4.98	2	-11.4	40.1	-9.9	40.1	50～400	●
21	K-18	Hz	8.45	8.45	6.72	6.72	89.60	29	121.8	-1.1	123.3	-1.1	50～700	○
22	No.13	Hz	2.52	2.52	2.00	2.00	19.30	21	23.1	-4.0	72.9	1.2	50～700	○
23	K-9	Hz	1.17	1.17	0.93	0.93	3.70	9	33.5	22.1	35.0	22.1	100～700	+
24	K-7	Hz	1.94	1.94	1.54	1.54	14.50	20	46.6	44.3	48.1	44.3	100～700	◉
25	K-14	Hz	3.67	3.67	2.92	2.92	44.60	33	15.2	57.5	16.7	57.5	150～700	●
26	K-2	Hz	3.14	3.14	2.50	2.50	24.40	21	8.3	56.5	9.8	56.5	50～500	●
27	K-11	Px	3.17	3.17	2.52	2.52	47.30	41	10.8	59.4	12.3	59.4	50～500	●
28	K-17	Hz	6.65	6.65	5.29	5.29	84.60	35	-169.3	-64.3	-167.8	-64.3	100～600	○
29	K-3	Hz	6.20	6.20	4.93	4.93	31.60	14	13.7	62.0	15.2	62.0	100～500	◉

Notes (1) NRM : Intensity of Natural Remanent Magnetization; Q: Konigsberger ratio; Hz:Harzburgite; Du:Dunite; Cr:Chromite; Px:Pyroxenite
(2) LF,HF: Low Frequency(0.46kHz) and High Frequency(4.6kHz) of electric current were applied for inducing magnetic field on the samples
(3) * Coercivity was so weak that this sample was excluded from consideration.
(4)◉: nearly same orientation as the present geomagnetic field; ○: apparently different orientation from the present geomagnetic field
+: obscure orientation in the relation with the present geomagnetic field

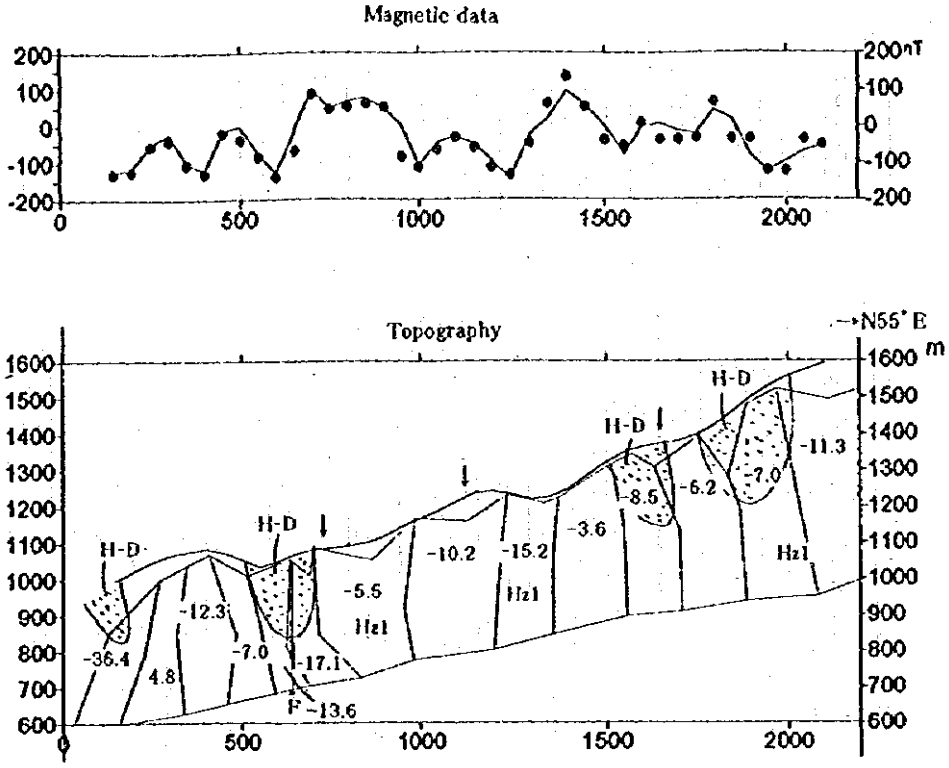

Profile A

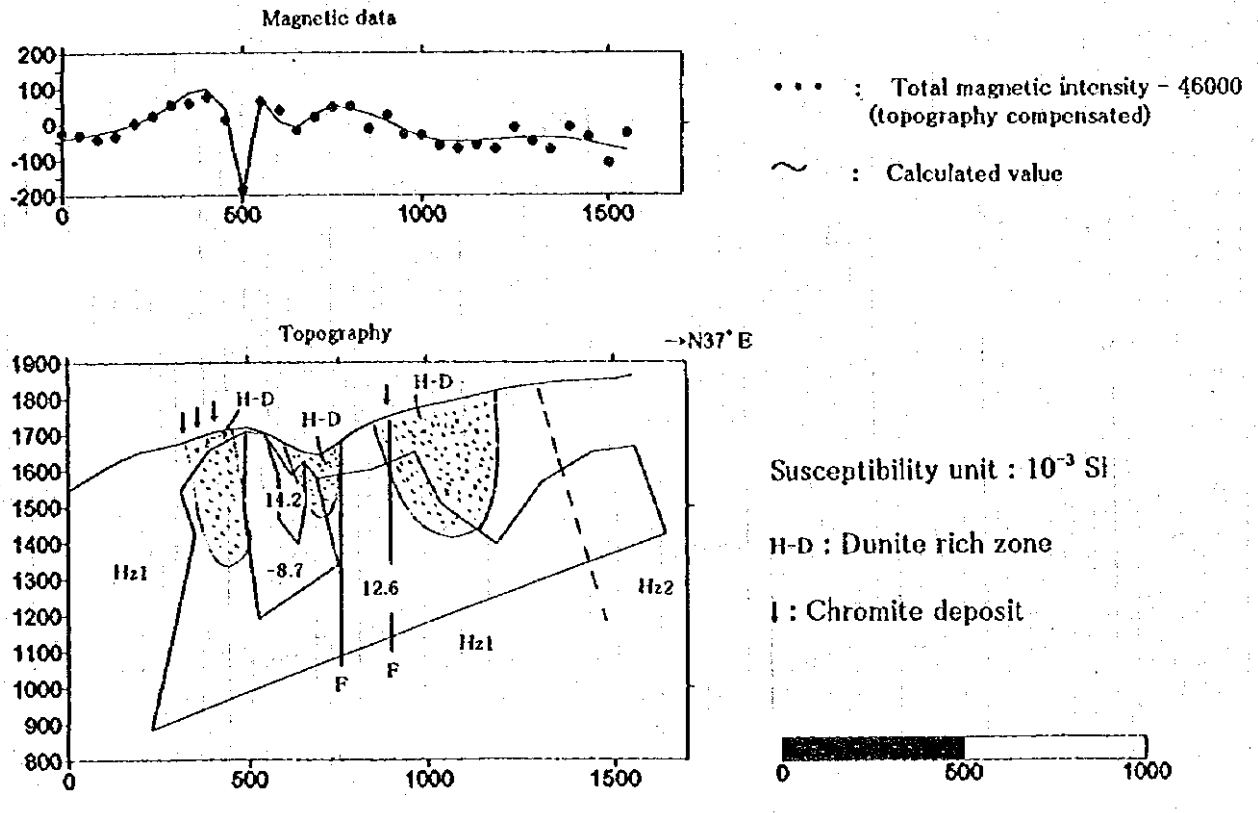

: Total magnetic intensity - 46000 (topography compensated)

: Calculated value

Susceptibility unit : 10^{-3} SI

H-D : Dunite rich zone

: Chromite deposit

0 500 1000

Profile B

Scale 1 : 20000

Fig. 2-2-13 Analyzed profiles, Central Shebenik Area

to transition due to faulting. Since, however, the measured samples do not include a datum plane of the time of magnetization such as a bedding plane, it is not possible to study the orientation of natural remanent magnetization of the samples on the basis of absolute orientation at the time of acquisition of natural magnetization. Furthermore, as the values of total magnetic intensity measured in the magnetic survey can be considered to be those of the resultant force of the induced magnetic field produced by the earth's magnetic field and the magnetic field that was produced by the natural remanent magnetization acquired when the rock was cooled to below the Curie point, it is difficult to separate these two.

As already mentioned, many magnetic anomalies were extracted from the Central Shebenik area on the basis of the results of measurement of total magnetic intensity. However, as mentioned in the section on magnetic susceptibility, no significant difference in magnetic susceptibility is to be noted between the different constituent rock types of the area: harzburgite, dunite and chromitite. Therefore one cannot explain such magnetic anomalies in terms of difference in rock types. Rather, it can be considered that they are a reflection of local differences in magnetic susceptibility, differences in the orientation of remanent magnetization due to fault transition, differences of the orientation in remanent magnetization according to rock type, etc. In particular, it is highly probable that low magnetic anomalies are reflections of rock bodies with reversed magnetization. Since dunite has a high probability of reverse magnetization, there is a high probability that those low magnetic anomalies correlate with dunite. The question of why dunite has an extremely high probability of reverse magnetization remains to be addressed.

(5) 2D Simulation on Profile

A model simulation was carried out with respect to two representative profiles passing through ore indications with rock body size and magnetic susceptibility as variable parameters. An optimum solution was sought by comparison with the values of total magnetic intensity. The positions of the profiles are indicated in the map of total magnetic intensity (Fig. 2-2-5), and the analysis profiles are given in Fig. 2-2-13. The negative magnetic susceptibilities in the analysis profile mean reverse magnetization.

In both profiles, it is necessary to give a relatively large negative magnetic susceptibility to low magnetic anomalies in the simulation. In particular, in profile A the position of the Dunite-rich zone confirmed in the geological survey is in close agreement with the position of the block assigned a relatively large negative magnetic susceptibility.

2-2-4 Results (Katjel area)

(1) Distribution of Total Magnetic Intensity

Fig. 2-2-14 gives the total magnetic intensity map after correction of diurnal variation, Fig. 2-1-15 (1) - (2) the profiles thereof, and Fig. 2-2-16 the total magnetic intensity map after terrain correction along with the confirmed scope of the Katjel deposit.

As shown in Fig. 2-2-14, the total magnetic intensity map is divided into a zone of high magnetic anomalies on the west side and a zone of low magnetic anomalies to the east, with control survey line M-2 roughly as the boundary between them. In the southern part of the low magnetic anomalies zone on the east side there are two points of high magnetic anomaly on the northwest extension of control survey line M-0, and there are comparatively high magnetic anomalies to the east side of the line connecting those two high magnetic anomalies. Furthermore, low magnetic anomalies are to be noted along the valley to the east of the middle of the survey area, but the low

magnetic anomalies along that valley are thought to be affected by the terrain. As for the direction of the magnetic anomalies, it is mainly N30°W.

Although no great change is to be noted in the magnetic anomaly distribution pattern in the total magnetic intensity maps after terrain correction (Fig. 2-2-16) and before terrain correction (Fig.2-2-14), the zones of high magnetic anomaly on the west side and in the southern part of the east side have less wide expression, and the low magnetic anomalies along the valley are expressed much more expansively, in Fig.2-2-16.

The scope of distribution of the ore body of the Katjel chrome deposit is from the eastern edge of the high magnetic anomaly zone in the west of the area to the low magnetic anomaly zone along the valley. The ore body strikes NW-SE and dips to the east, the west end of the ore body having a sharp inclination and which becomes more gentle towards the east.

(2) Filter Analyses

a) Reduction-to-the-Pole

Fig. 2-2-17 gives the reduction-to-the-pole map. Although there is some difference in the reduction-to-the-pole map because of the different color tones given the reduced values of magnetic intensity, the magnetic anomalies distribution pattern is very similar to that of the total magnetic intensity map.

b) Upward-Continuation Analysis

The power spectrum (Fig. 2-2-18) prepared in frequency analysis of the total magnetic intensity map was divided into three geomagnetic components corresponding to three layers with respective average depths of 6 m, 23 m, and 80 m. The depths 15 m and 50 m, roughly the median values of the average depths, were set as the depth boundary lines between those three layers, and upward-continuation analysis of the reduction-to-the-pole map was carried out on that basis.

Fig. 2-2-19 represents extraction of the shallow (up to a depth of 15 m) component from the reduction-to-the-pole map, Fig. 2-2-20 extraction of the medium-depth (15-50 m) component, and Fig. 2-2-21 extraction of the deep (depth greater than 50 m) component.

In the upward-continuation analysis maps expressing the shallow and medium-depth magnetic components indicated in Fig. 2-2-19 and Fig. 2-2-20 the wavelengths of magnetic anomalies are different, but as a whole the magnetic anomaly pattern is roughly the same, the predominant direction of extension being N30°W, with a magnetic anomaly in the direction N60°E in the southern part of the zone. The high magnetic anomaly at the northwest edge of the area is considered to be an indication of the laterite ultrabasic rock developed at the boundary between the ultrabasic rock and the limestone unconformably covering it. Furthermore, the steeply inclined western part of the Katjel deposit at a comparatively shallow depth appears to be expressed as a relatively low magnetic anomaly running in the NNW-SSE direction roughly along the M-2 control survey line.

As for the reduction-to-the-pole map representing the deep magnetic component that is given in Fig. 2-2-21, it shows a magnetic anomaly pattern that on the whole corresponds to the total magnetic intensity map. Several types of ore body have been identified. One type is almost vertical and is located at the boundary between the high and low magnetic anomalies. Immediately to the east of this boundary, mostly within the low magnetic anomaly, there are steeply inclined (dipping to the east) ore bodies and further to the east, gently dipping ore bodies are found near the center of the low magnetic anomaly. At the east end of the ore body have been confirmed up to the place of strongest low magnetic anomaly. Most of the Katjel ore bodies thus confirmed lie in the low magnetic anomaly

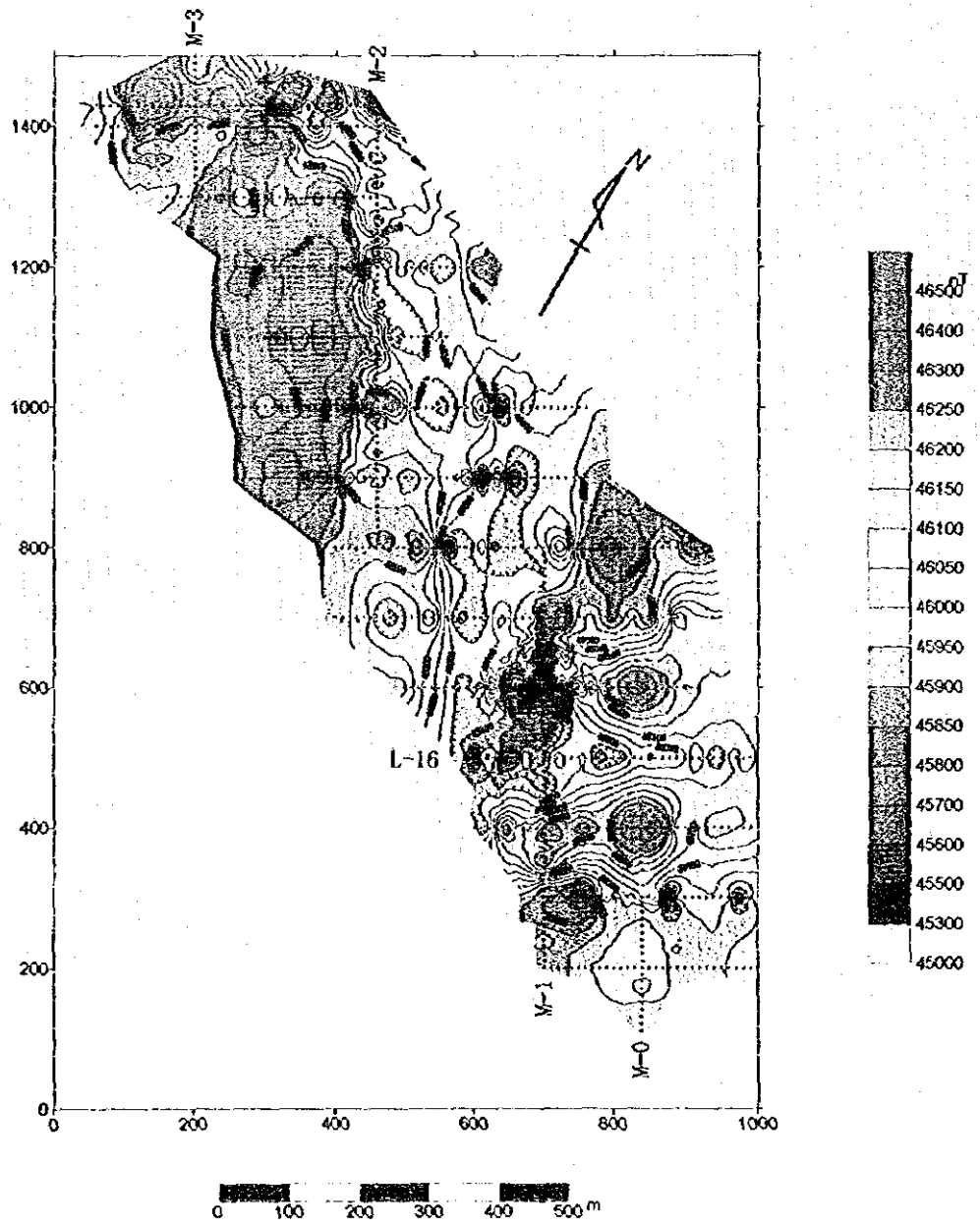

Fig. 2-2-14 Total magnetic intensity map, Katjel Area

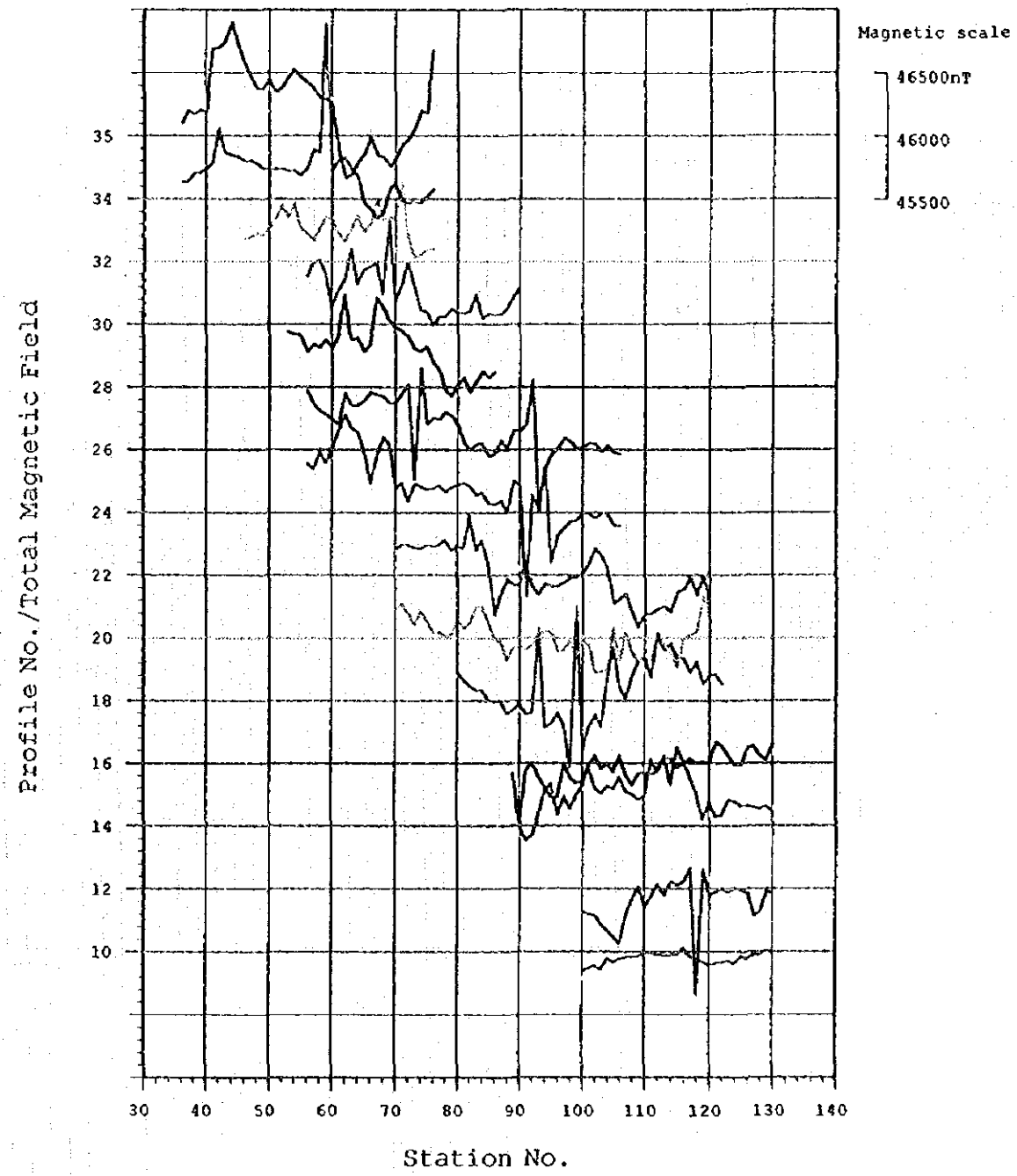

Fig. 2-2-15(1) Magnetic profiles, Katjel Area

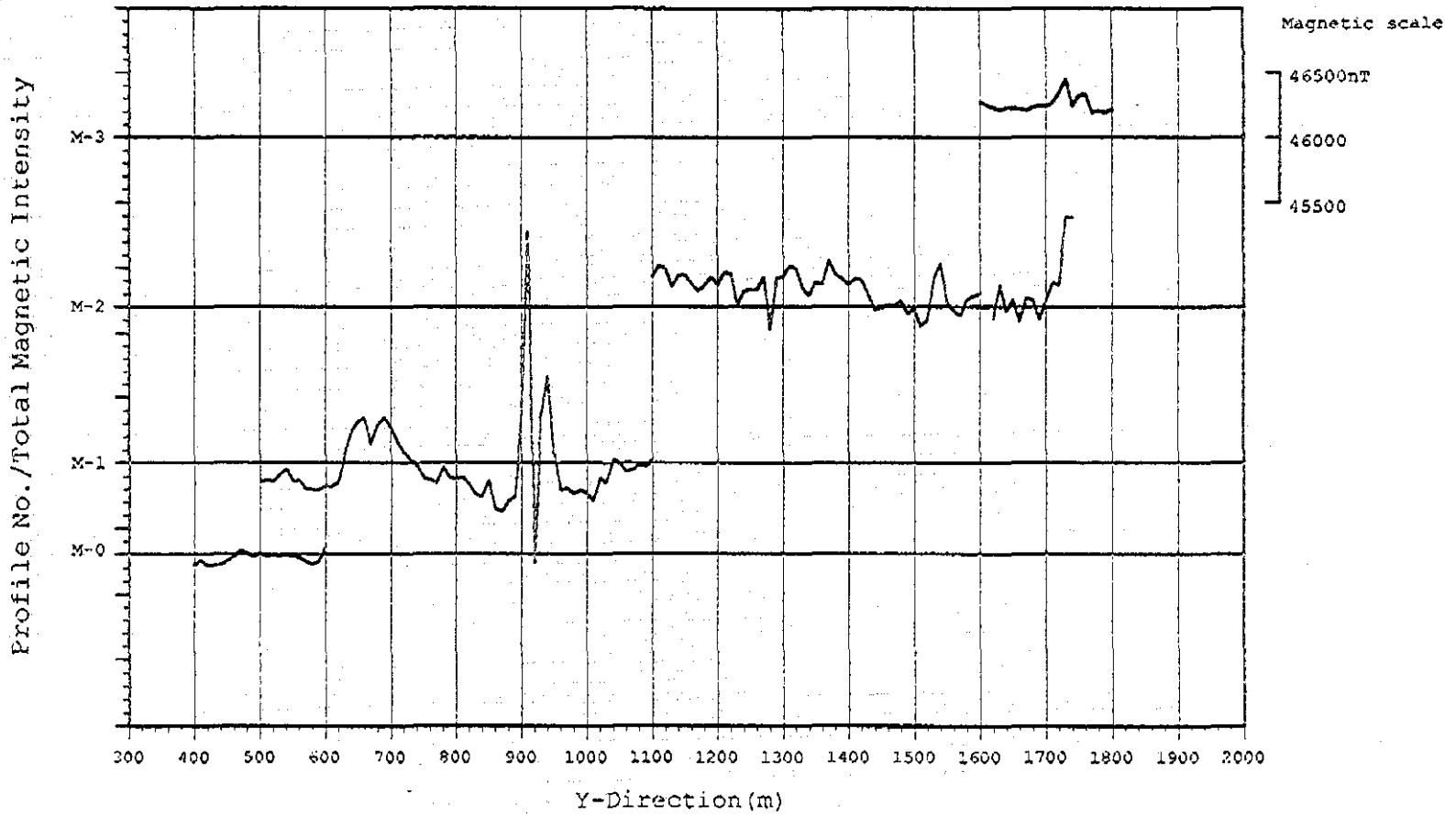

Fig. 2-2-15(2) Magnetic profiles, Katjel Area

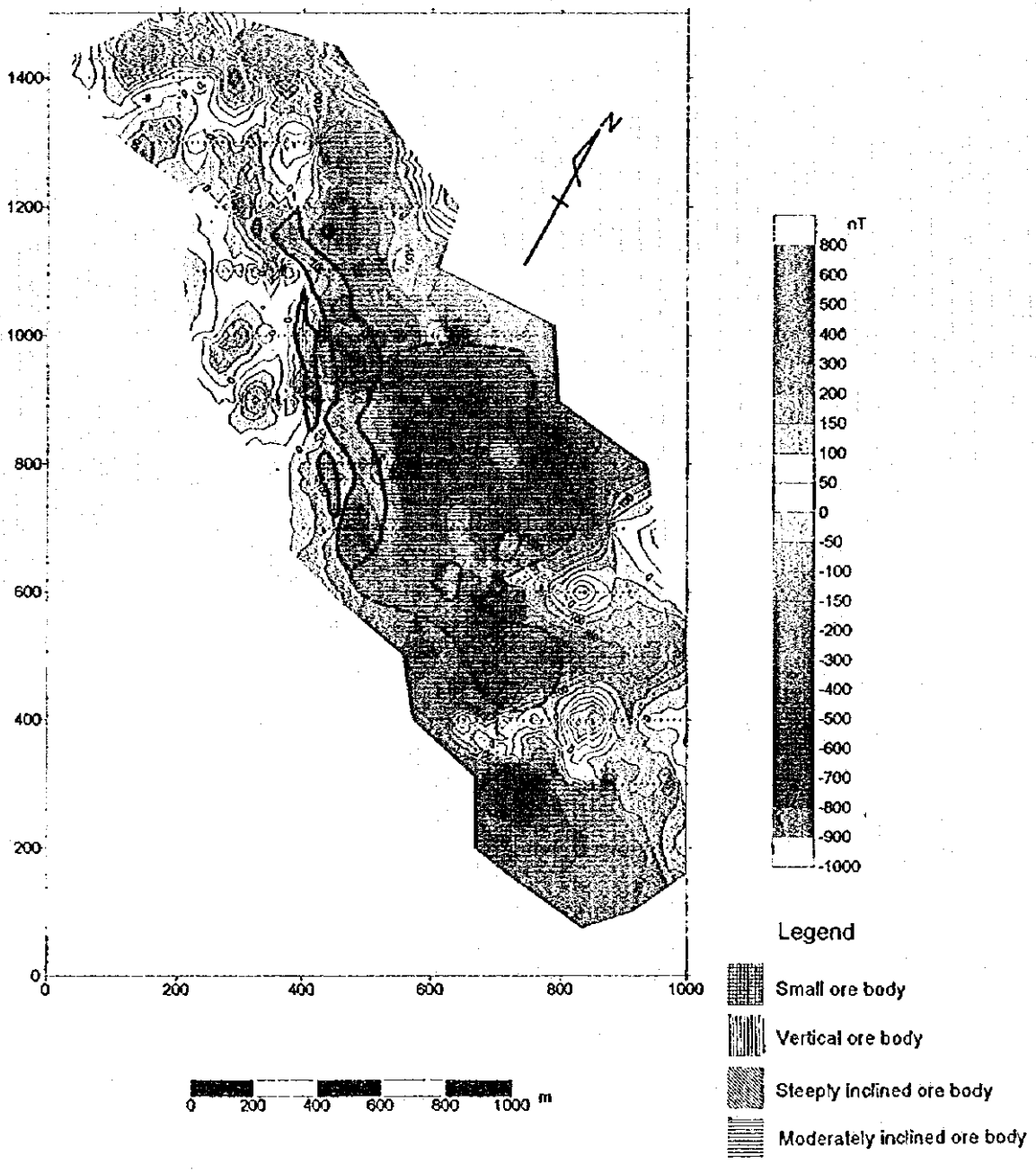

Fig. 2-2-16 Total magnetic intensity map (topography compensated), Katjel Area

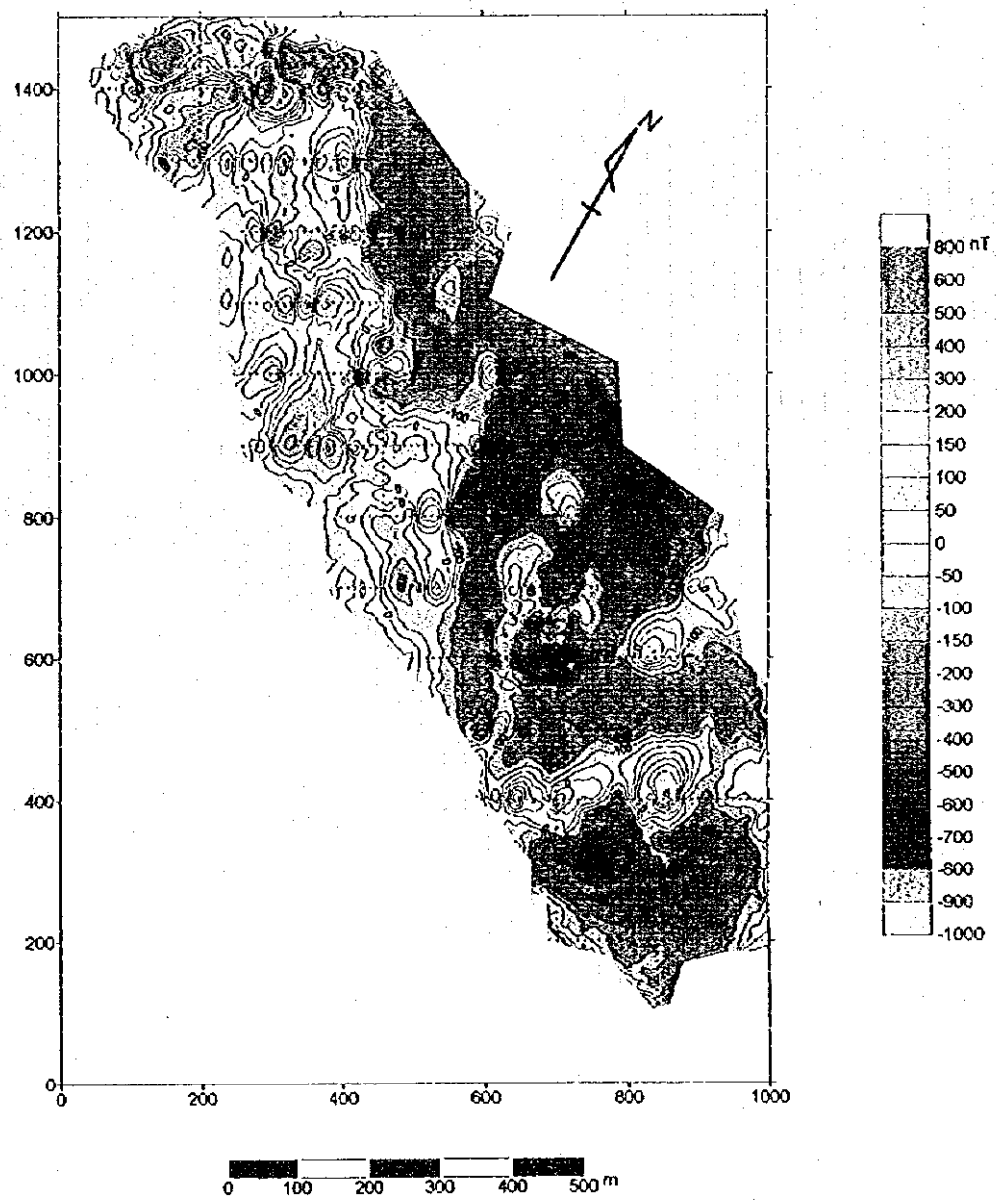

Fig. 2-2-17 Reduotion to the pole map, Katjel Area

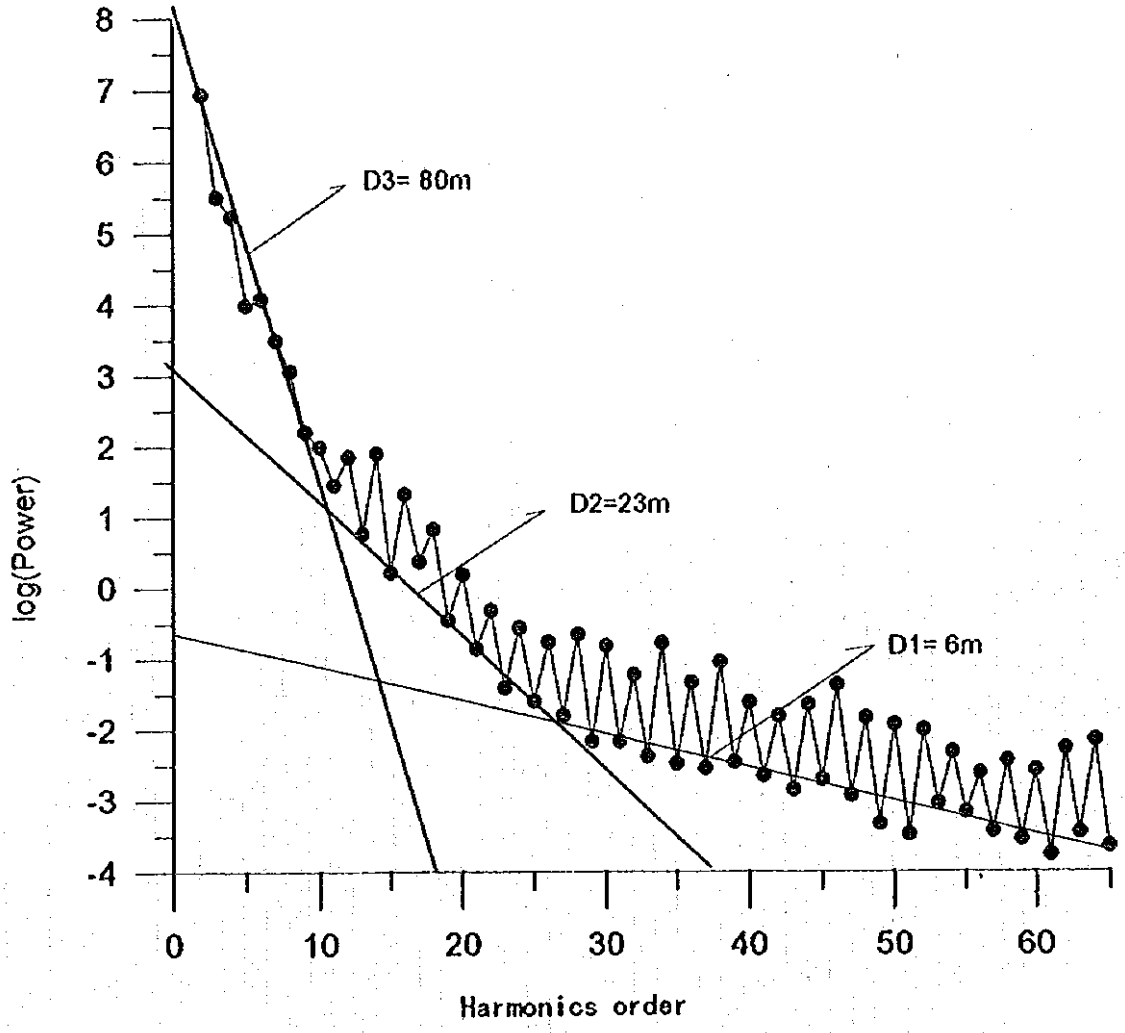

Fig. 2-2-18 Magnetic spectra, Katjel Area

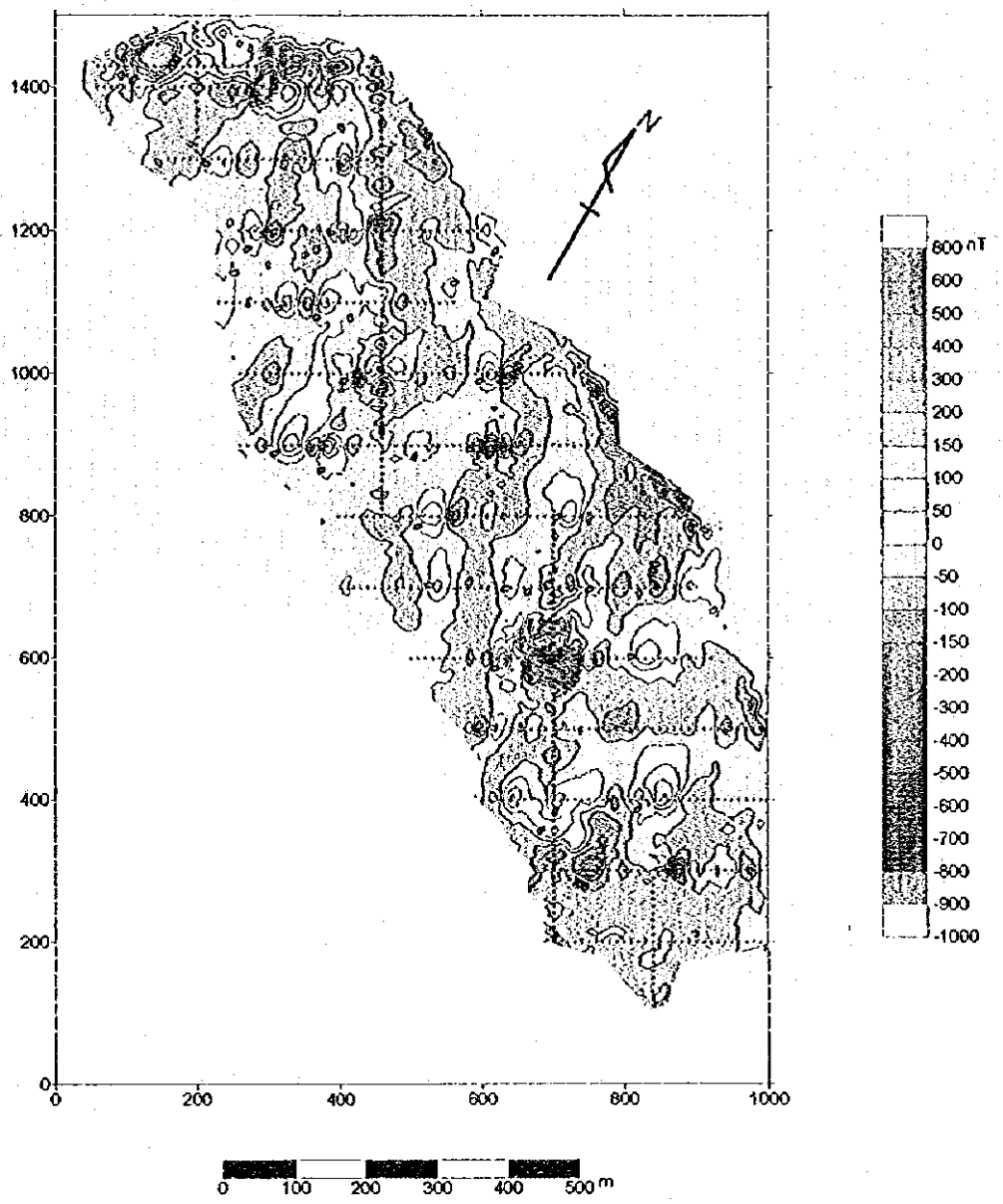

Fig. 2-2-19 Reduction to the pole map (shallow component extracted), Katjel Area

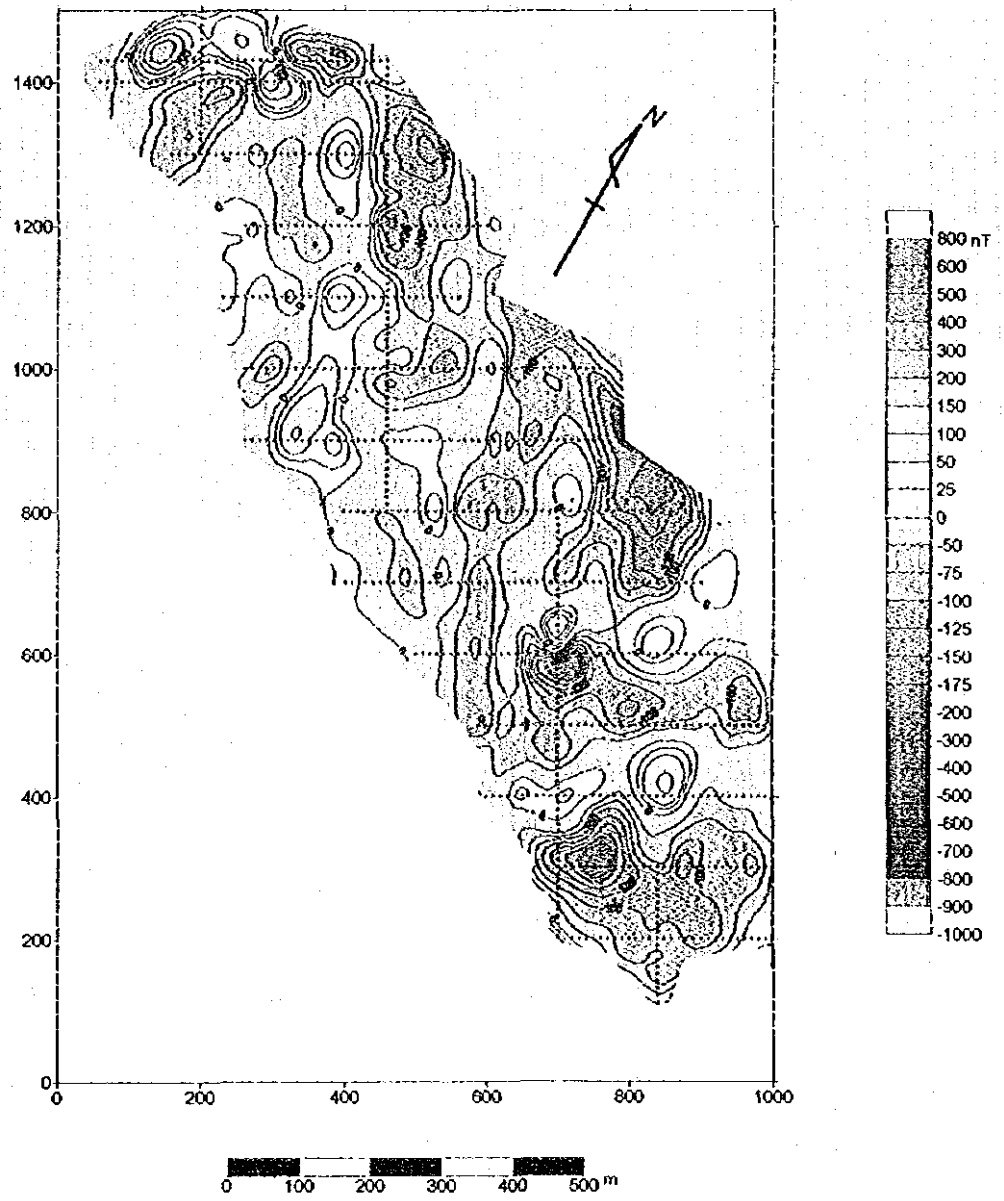

Fig. 2-2-20 Reduction to the pole map (middle component extracted), Katjel Area

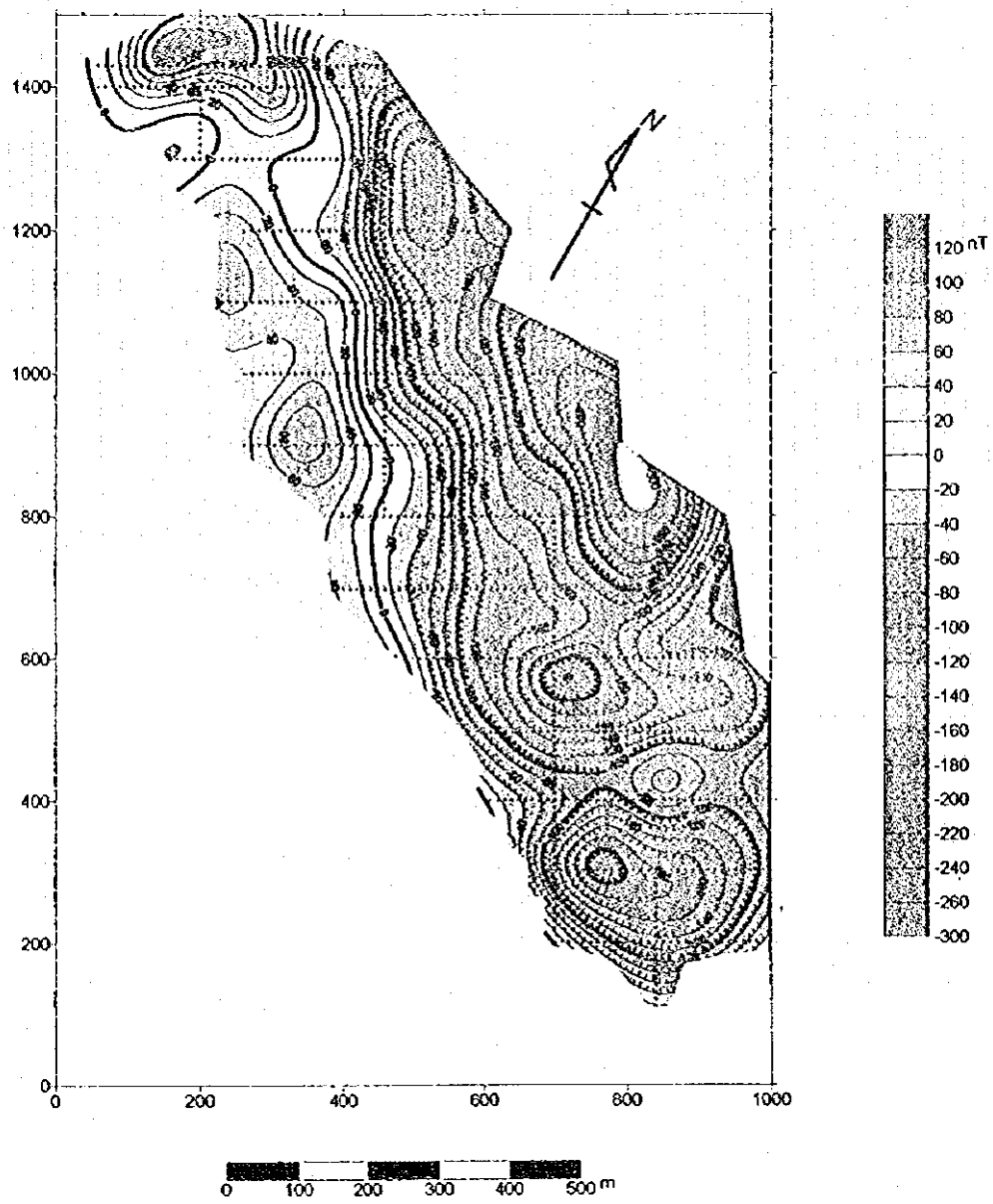

Fig. 2-2-21 Reduction to the pole map (deep component extracted), Katjel Area